ROBUST POSITION-BASED VISUAL SERVOING OF INDUSTRIAL ROBOTS

Xinyi Wu

A thesis
in
The Department
of
Mechanical, Industrial and Aerospace Engineering

Presented in Partial Fulfillment of the Requirements
For the Degree of Master of Applied Science (Mechanical Engineering)
Concordia University
Montréal, Québec, Canada

August 2020

CONCORDIA UNIVERSITY
School of Graduate Studies

This is to certify that the thesis prepared

By: Xinyi Wu

Entitled: Robust Position-based Visual Servoing of Industrial Robots

and submitted in partial fulfillment of the requirements for the degree of

Master of Applied Science (Mechanical Engineering)

complies with the regulations of the University and meets the accepted standards with respect to originality and quality.

Signed by the final examining committee:

_____ Chair
Dr. Mojtaba Kheiri

_____ Examiner
Dr. Lan Lin

_____ Examiner
Dr. Mojtaba Kheiri

_____ Thesis Supervisor(s)
Dr. Wen-Fang Xie

_____

Approved by _____
Dr. Martin Pugh Chair of Department or Graduate Program Director

_____
Dr. Mourad Debbabi Dean, Gina Cody School of Engineering and Computer Science

Date August 20, 2020

Abstract

Robust position-based visual servoing of industrial robots

Xinyi Wu

Recently, the researchers have tried to use dynamic pose correction methods to improve the accuracy of industrial robots. The application of dynamic path tracking aims at adjusting the end-effector's pose by using a photogrammetry sensor and eye-to-hand PBVS scheme. In this study, the research aims to enhance the accuracy of industrial robot by designing a chattering-free digital sliding mode controller integrated with a novel adaptive robust Kalman filter (ARKF) validated on Puma 560 model on simulation. This study includes Gaussian noise generation, pose estimation, design of adaptive robust Kalman filter, and design of chattering-free sliding mode controller. The designed control strategy has been validated and compared with other control strategies in Matlab 2018a Simulink on a 64bits PC computer. The main contributions of the research work are summarized as follows.

First, the noise removal in the pose estimation is carried out by the novel ARKF. The proposed ARKF deals with experimental noise generated from photogrammetry observation sensor C-track 780. It exploits the advantages of adaptive estimation method for states noise covariance (Q), least square identification for measurement noise covariance (R) and a robust mechanism for state variables error covariance (P). The Gaussian noise generation is based on the collected data from the C-track when the robot is in a stationary status. A novel method for estimating covariance matrix R considering both effects of the velocity and pose is suggested.

Next, a robust PBVS approach for industrial robots based on fast discrete sliding mode controller (FDSMC) and ARKF is proposed. The FDSMC takes advantage of a nonlinear reaching law which results in faster and more accurate trajectory tracking compared to standard DSMC. Substituting the switching function with a continuous nonlinear reaching law lead to a continuous output and thus eliminating the chattering. Additionally, the sliding surface dynamics is considered to be a nonlinear one, which results in increasing the convergence speed and accuracy.

Finally, the analysis techniques related to various types of sliding mode controller have been used for comparison. Also, the kinematic and dynamic models with revolutionary joints for Puma 560 are built for simulation validation. Based on the computed indicators results, it is proven that after tuning the parameters of designed controller, the chattering-free FDSMC integrated with ARKF can essentially reduce the effect of uncertainties on robot dynamic model and improve the tracking accuracy of the 6 degree-of-freedom (DOF) robot.

Acknowledgments

I would like to acknowledge my indebtedness and render my warmest thanks to my supervisor, Professor Wen-fang Xie, who guides me through my master study from time to time and encourages me to overcome the encountered difficulties. Her patient guidance and expert advice have been invaluable throughout all stages of this research work.

I would also wish to express my gratitude to Mr. Ehsan Zakeri for the technical discussions and valuable suggestions that have contributed greatly to the improvement of the thesis.

In addition, I would like to thank my colleage Dr. Pengcheng li and Mr. Zhang Ronghua for their help and experience share through my research path. Hearty thanks also go to my friends who accompanied me along these years: Miss. Ying Qi, Miss. Liu Mingshu, Miss. Yang Yiwen, Miss. Zhao Tong, Miss. Zhu Xinyi, Miss. Bahar Ahmadi and Mr. Ahmad Ghasemi and Mr. Mikail Shapoori. I am also grateful to everyone who has given me support, but I already have had keep in my mind. Special thanks are due to my family, my parents Mr.Wu Jisen and Mrs.Zhang Yizhuo. My grandmother Mrs. Yu Wenying, my aunt Mrs. Zhang Yi-jia for their precious support and concern through my journey of studying abroad in Canada.

To my beloved parents

Jisen Wu** and **Yizhuo Zhang

and my lovely grandmother and aunt

Wenying Yu** and **Yijia Zhang

Contents

List of Figures

List of Tables

Chapter 1

Introduction

1.1 Visual servoing

In industrial robotic field [3], some tasks such as drilling, welding large scale parts, assembling and fiber placement of composite manufacturing demand high accuracy positioning and trajectory tracking. Currently, the low accuracy issue is one of the important barriers to the development of industrial robots. The robot accuracy is defined as a measure of robot capability to attain a commanded position in terms of an absolute reference coordinate. Considering trajectory tracking, the accuracy can be defined as a measure of robot capability to track the prescribed trajectory with respect to the absolute coordinate frame. However, the concept of robot accuracy is also related to repeatability. Its definition says the measurement capability of robot returning to a previously memorized pose or a capability to repeatedly track the memorized trajectory. In real reality, the repeatability and absolute positioning accuracy are on the magnitude of $0.1mm$ and $1mm$ to $1cm$ respectively for the majority of robots.

Nevertheless, since the absolute positioning accuracy is frequently lower than the repeatability in terms of magnitude, low accuracy is usually considered as tedious challenging due to the fact that many factors affect the robot accuracy. Kochekali et al.[4] generalized them into six main categories: environmental (for instance, temperature changes), parametric (kinematic parameters, joint zero-reference offsets, influence of dynamic parameters, drive-train compliance, friction, and other nonlinearities, including hysteresis and backlash), measurement (resolution and nonlinearity of joint position sensors), computational (computer round-off and steady-state servo errors), and application (installation errors, and workpiece position and geometry errors). The analysis of those effects and corresponding elimination methods are discussed in the literature [5, 5–11]. In the practice, improving the accuracy of robots can be carried out in the following three ways: 1) calibrating robot with the help of complex mathematical algorithms [12, 13] by using high-accuracy metrology equipment [14]; 2) installing extra high-accuracy sensors at each robot joint [15] in Fig. 1.1 and 3) dynamically correcting/tracking the pose of the robot [1, 16–19].

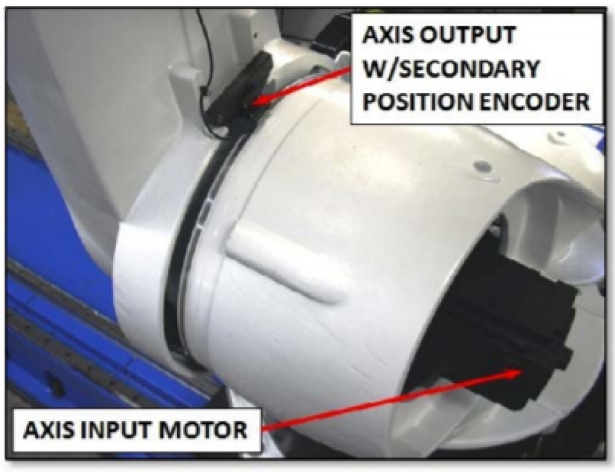

Figure 1.1: Secondary encoder

1.2 Overview on accuracy

The first solution to improve the accuracy of robots is through the calibration process, which is performed by measuring the pose of the end-effector in different configurations using sophisticated measurement equipment and identifying the calibration parameters [20]. Firstly, the mathematical model obtained by calibration is able to find the relation between the pose of the end-effector and the joint variables within tolerance. The robot calibration method includes identification of kinematic parameters and error compensation. The parameter identification process forms a simple measurement procedure using a cost-effective, instrumented, and articulated linkage with proper data collection. The measurement of end-effector positions can be present automatically.

As for error compensation, a computation scheme based on the nominal model different from the calibrated one is presented. In most industrial robots, the design algorithm allows the development of the closed-loop inverse kinematics solutions accessible which is widespread among on-line applications [21]. This paper [22] presented the concept of model completeness for kinematic identification models, which is defined as describing the model's capability of mapping joint positions into tool's pose for the chosen manipulator. The complete models should have a number of independent parameters. Since the end-effector pose is in general not available by measurement directly, the end-effector is manipulated by servoing joints into related positions. In order to get the desired pose, it is necessary to relate the tool's pose to joint positions. Many of these relations are combined with kinematic formulas to describe the motion mechanism. Even though there are several manipulator formulas, they are usually not accurate enough. Everett and Hsu attempt to improve the accuracy of these kinematic formulas by identifying these constant parameters. However, it is shown by example that model completeness does not guarantee its usefulness in identification algorithms. As mentioned before, a predetermined number of parameters to be identified

are suggested in terms of completeness. It is not sufficient to simply count the number of parameters changed by the algorithm since least squares or other optimal programs might assign values to dependent parameters. It is necessary to compute the rank of the Jacobian matrix. The identification might be considered complete when these matrices have sufficient rank. Zhang [23] proposed a new calibration method. The only required information for calibration is the planar pattern with different orientations. The camera and planar pattern are allowed to move by hand. However the motion should be previously known and the radial lens distortion is considered via modeling. It utilizes 2D measured information for the photogrammetric calibration and expressed 3D model.

As for self-calibration, rigid motion 3D information is adopted. Compared with classical techniques, this technique is kindly more flexible and user friendly. Compared with classical self-calibration, it develops the degree of robustness to large extent. It brings 3D computer vision to connect tightly from laboratory environments to the real application which is meaningful and a no-negligible milestone. In [12], a calibration of the ABB IRB 1600 robot considering all possible geometric errors using a laser tracker. The identification of 29 parameter errors using least square optimization. The maximum position errors therefore reduced from $2.158mm$ to $0.69mm$ after calibration. The robot calibration is offered by most of the main industrial robot manufacturers vendors. However, it is a costly and time-consuming service for the clients. The calibration can be performed on-site occasionally, but in most cases the robot needs to be returned to the manufacturer and their trained engineers who can operate 6D metrology measurement equipment. Apart from shipping and calibration service, the production stop can also be one of the shortcomings.

Considering that the industrial robots need calibration at least once a year, these procedures will impose a significant annual cost for the company. In addition to calibration services from robot manufacturers, there are some companies who provide software packages

for robot calibration. Dynalog has been operating exclusively in this field, the calibration package from Dynalog costs about \$50, 000. The software is capable of being conjugated with a 3D measurement device like a laser tracker. Rocal, offed by Nikon Metrology, is another calibration package based on the 6D measurement sensors [13]. Considering the total expense for an accurate measurement sensor and the software expense, this solution is feasible only for large companies who has hundred of robots needs calibration each year. Besides, filtering the robot programs before being uploaded to the robot of the third-party software in marketing for calibration is demanding, which performs automatically in case of manufacturer calibration [13]. However, robot calibration can only improve the accuracy under static or quasi-static conditions [24].

1.2.1 High-end Encoder Installation

The second solution is to install extra high-accuracy encoders at each joint of the robot to eliminate the effect of backlash, elasticity, and non-linearities in the gearbox [25]. In [26], the development of accurate robot technology has expanded the practical applications for articulated robots in air-frame assembly for both tracking and regulation. The secondary encoders integrating on each robot joint provide actual axis positions as opposed to inferred positions from motor encoders. This precise feedback through an optimized kinematic model is able to produce a high accuracy motion platform besides virtual stiffness. Global and on-part positioning under $0.25mm$ use long reach and heavy payload jointed arms. The corresponding required hardware for enhancement is minimal, retaining cost-competitive compared with standard systems. The range and flexibility of the arm are independent since it is not necessary for reaching accuracy via guidance. In this case, the articulated arm can be applied to a broader range of assembly, i.e. one-up assembly, two-sided drilling and fastening, automated fiber placement and material removal.

1.2.2 Dynamic Pose Correction

The third method is to use an external measurement device to guide the robot's end-effector to the desired pose dynamically. In this method, the external sensor provides the current pose of the robot on-line, and the obtained pose information is compared with the desired value through third-party software. Currently, the majority of the industrial robots are calibrated by laser trackers. Considering the economical expense, the most efficient method of robot calibration with the minimum costs is needed in the robotic industry. Among the major measurement instruments in industrial field, C-Track has the lowest price (less than \$50, 000) compared with the laser trackers and Nikon Metrology's optical CMM which cost more than \$100, 000 and \$70, 000 respectively. Besides, the reflectors for the laser tracker cost more than \$1000 each while the magnetic reflector stickers for the C-Track are cost-effective. Besides, the C-Track is more safe and user friendly compared with laser tracker which needs experienced operators. The C-track is able to measure the pose of all the targets simultaneously but the laser tracker can only measure one point each time step. Some factors like vibration, air turbulence, and temperature variation, humidity, and different operation affect the laser tracker measurement accuracy. In [12], the absolute accuracy of an ABB IRB1600 industrial robot is improved after extensive experimentation by using a 29-parameter calibration model. The error model considered all potential geometric errors including 25 geometric error parameters' identification through optimization and the pose parameters for the base and tool frames besides four error parameters corresponding to the compliance in joints 2 to 5. The least squares optimization technique is used to find the 29 error parameters that fit the measures best acquired with a laser tracker. By contrast with other similar works, the establishment of the robot's accuracy is performed with a very large number of measures around 1,000 throughout the robot's joint space. After calibration, the mean and maximum position errors of eight different measurement points on the end effector

were reduced from $0.968mm/2.158mm$ to $0.364mm/0.696mm$ respectively.

Considering the above-mentioned robot's accuracy enhancement methods, the robotic manufacturing companies such as GE Aviation and Coriolis Inc. are seeking for further research from academic research teams. Concordia University, ETS, and Creaform Inc propose using various photogrammetry measurement sensors to look at a cost-effective way to enhance the absolute accuracy of the industrial robots. C-Track is regarded as the feedback sensor to measure the pose of the robot end-effector and the dynamic pose correction is applied to the robot controller simultaneously. This method does not rely on high-end encoders. Also, it does not need to intrusively modify the built-in kinematic model of the robot during the controller. With the support of FRQNT, the team in Concordia University has developed real-time positioning and path tracking algorithm for an industrial robot (Fanuc M20-iA) using the Creaform 3D measurement sensor (C-Track). Several noise reduction methods have been developed for the pose date from C-track such as RMS [20] and adaptive Kalman Filter [16]. Also, the team has developed PID position-based visual servoing with stability proof to enhance the dynamic performance of industrial robots. However, the developed noise reduction and the pose-based visual servoing controller cannot handle the large uncertainties in the robot and the disturbances from the environment. This thesis research tries to explore an effective noise reduction method to obtain precise pose information and a robust PBVS controller to handle large uncertainties and disturbances.

1.3 Research Objectives

This research goal is to enhance the overall accuracy of the industrial robots via designed control algorithm and Kalman filters to reduce the disturbance from the noise and uncertainties of the system. Motivated by the adaptive Kalman filter that is proposed to obtain smooth pose estimation and to eliminate the effects caused by image noise, vibration, and

other uncertain disturbances resources. This research aims at enhancing the robustness of this control system and eliminating the noise and uncertainties of the robot physics model and the measurement. To achieve the objectives, a robust PBVS scheme is in demand to filter out the noise in the measured robot's pose data and to realize the fast and accurate trajectory tracking performance of the industrial robots.

1.4 Contribution of This Thesis

1.4.1 Pose Estimation

The main contribution of this research is designing an enhanced robust PBVS approach for industrial robots. The proposed method utilizes the ARKF for smooth estimation of the robot pose and a chattering-free fast SMC (CFSMC) as the controller. The designed adaptive robust Kalman filter (ARKF) exploits the advantages of adaptive covariance estimation method for **Q** along with a state variables-dependent tuning method for **R**.

1.4.2 ARKF

ARKF enjoys the robust estimation mechanism of state variables covariance **P** mentioned in the literature [27]. The combination of all these above-mentioned techniques makes the proposed ARKF method a fairly precise, smooth, and robust filter for robots' end-effectors' pose estimation. Note that the adaptation mechanism used in ARKF makes its performance optimal since it corrects the deviation of the estimated **P** from its theoretical one emanated from existing model dynamic uncertainties [27]. Both simulation and experimental tests demonstrate the superiority of the proposed ARKF over the classical KF and the reported AKF method in the pose estimation of industrial robots. This paper "Adaptive Robust Kalman Filter for Vision-based Pose Estimation of Industrial Robots" has been presented in

ICCC 2019 IEEE 5th International Conference on Computer and Communications (ICCC 2019) with Ei Compendex and Scopus index.

1.4.3 CFSMC

The CFSMC exploits a nonlinear reaching law which increases the convergence speed and tracking precision. Substituting the switching function with a slope generates continuous output and thus eliminates the chattering. This substitution, however, leads to a boundary layer around the sliding surface that affects the tracking accuracy [28]. The boundary layer analysis along with stability proof of the CFSMC is also investigated in this thesis.

1.4.4 Simulated Validation

To evaluate the performance of the proposed method, simulation tests on the PUMA560 robots are conducted. Analyzing the results demonstrate the proposed method outperforms other well-known approaches in terms of chattering level, tracking accuracy, and convergence speed. There is another paper "Robust position-based visual servoing of industrial robots utilizing chattering-free sliding mode control method" to be submitted.

1.5 Thesis Outline

This thesis is organized as follows. Chapter 1 aims at introducing the problem statement, research goal, and background information for this research. Chapter 2 is about the literature review on visual servoing, sliding mode control method and the error enhancement methodologies combined with controller and Kalman filter. Chapter 3 introduces the pose estimation solution for the removal of the noise in the measurement sensor. An adaptive robust Kalman filter is proposed and a noise identification experiment has been carried out.

Chapter 4 aims at demonstrating the design procedure of the chattering-free fast sliding mode controller and its performance has been validated through simulation in MATLAB Simulink. Chapter 5 illustrates the comparison of the afore-mentioned controller and analysis of the tracking performance of the proposed CFSMC. Chapter 6 summarizes the research work and gives future work related to this research.

Chapter 2

Literature Review

Robustness plays an important role in the practical visual servoing systems. The handling uncertainty when modeling systems is the first and foremost procedure to achieve accurate and robust visual servoing. Camera displacement error due to image noise has been investigated using the noise boundaries in the previous works. Also, error covariance propagation has already been developed to model the uncertainties of different visual servoing system components. However, these works were either open-loop or not fully successful under when the robot system is subjected to large uncertainties and disturbances.

2.1 Visual Servoing

Visual servoing (VS) is to use the visual measurement from a visual sensor as the feedback to guide the robot [29].Visual servoing (VS) is a mature technology which has been widely applied in robotic and control engineering fields [30–32]. In robotics, VS regularly utilizes visual definition instead of the low-precision technique of manually teaching in Cartesian space coordinates by CAD models of the workplace [33]. Low accuracy always being an issue in industrial applications of robots. When a robot tool-tip pose is calculated d based on the

robot kinematics and the measured joint positions sensed by the encoders, the pose error will arise due to the existing uncertainties in the robot physical model [34]. By processing the information of the robot and environment acquired from a vision system and designing a proper controller, VS can handle the uncertainty issue and the accuracy of the robot manipulation therefore increases [31, 32].

It has been used in the industrial robots to control the pose of the robot's end-effector with respect to a target object or target features. VS can be categorized into two basic branches: image-based visual servoing (IBVS) and position-based visual servoing (PBVS). While the former takes advantage of image planes' features as feedback to generate the control command directly, the latter reconstruct the 3-dimensional (3D) end-effector pose from the 2-dimensional (2D) image plane features [35] for control. The PBVS has a significant advantage over IBVS: it can directly act on workspace variables, which means the controller can be designed based on the dynamic behavior of the end-effector motion variables [3]. However, it is highly sensitive to the calibration errors of the vision system subject to the uncertainties and noise [3, 35]. It is noted that the images captured by an optical system are always contaminated by the noises, whose properties may vary from one position to another of the industrial robots or with different velocities [16] due to translation from 2D image to 3D pose in a Cartesian frame [35], and intrinsic noises of the captured image introduced by the low light of the environment and/or fading issues [36].

2.1.1 PBVS of Industrial Robots

As for PBVS, the reconstruction of the 3-dimensional (3D) robot's pose from the 2-dimensional (2D) image features [35] and utilizing the 6-DOF pose variables in the controller are carried out. Therefore, the PBVS holds a noticeable advantage over IBVS: the controller can be designed based on the dynamic behavior of the end-effector motion variables in the workspace

[3, 37]. However, it is highly sensitive to the error of the vision system calibration associated with the uncertainties and noises [3, 35]. Accordingly, a desirable PBVS process relies on a competent controller along with an efficacious method for filtering the restructured pose signals in order to approximate robot pose precisely. The images captured by a visual system are always contaminated by noises, whose characteristics may vary in different positions and velocities of the industrial robot end-effector [16, 35, 36].

2.1.2 Principles of Visual Servoing

Visual servoing is commonly proposed to deal with the general case of full 3D motion. It uses related position and orientation of the object inside the field-of-view (FOV) with respect to the camera frame and to form the six-elemental pose vector. Both of two broad classes: position-based visual servo control, and image-based visual servo control methods can handle the full 3D motion case. The relative position and orientation of the target object with respect to the camera frame is used to form the six-element POSE vector. X, Y, Z used for the position, and using roll, pitch, and yaw angles for orientation. The pose vector is denoted as follows:

$$\boldsymbol{W} = [X, Y, Z, \phi, \alpha, \psi]^T \tag{2.1}$$

where the relative position of the object frame with respect to the camera frame is defined by X, Y, Z in each orthogonal direction of coordinate respectively. The relative orientation of the object frame in respect of the camera frame is defined by the roll, pitch and yaw angles of coordinate via ϕ, α, ψ respectively.

The object feature points are mapped into image plane and measurement of those feature points are used for the robot control. In PBVS, the measurement image plane points are used to constitute the POSE values. And the control design is therefore to generate control

command according to the comparison of these estimated Poses and the desired Poses. The most common method used in IBVS is by controlling robot motion to control the camera and to guide the image plan feature measurements to the desired destination. In some cases, it also uses the definition of feature characteristics relation. For IBVS, it is usually involved with an image interaction matrix, which relates the changing rate of image plan feature coordinates to the changing rate of POSE parameters. Through normal robot Jacobian, the robot joint rate can then calculated with the kinematic relationship between the camera and the endpoint of the robot manipulator [38].

Many researchers are working on the tracking of objects moves at 2D plane [3, 35]. Since the object moving in a 2D plane, the desired POSE trajectories should be transferred into image plane feature coordinate trajectories which are tedious and causing time-delay for real implementation. Note that the range of the object is assumed to be known. The adaptive control methods normally cannot handle unpredictable changes and uncertainty of image interaction matrix and therefore the large change of control system loop gain is needed. However, the PBVS allows the direct and intuitive specification of desired trajectories in the end-effector Cartesian coordinate frame. That is the extra procedure compared with IBVS, i.e. the POSE estimation. According to the POSE estimation results, we can get a more accurate value which is close to the true POSE of end-effector and the controller design will achieve high precision. The object's feature characteristics are in demand in both PBVS and IBVS for POSE estimation and specification of path planning. There has been a comprehensive research on IBVS [35, 39]. By contrast, only a few researchers focus on the PBVS method in the robotics [40, 41].

The paper [38] proposes a 3D POSE estimation strategy considering planar motion in VS design. It improves the normal method by defining an integrated 3D relative POSE estimation approach instead. The overall 3D visual servo control is designed based on the

POSE estimation. The ability of eliminating occlusion of features is also improved without abrupt control. An extended Kalman filter(EKF) is used in this control loop which solves the photogrammetric equations to transform the 2D image plan feature point coordinates to the POSE parameters. The recursive and statistical combination of redundant measurement information demonstrates the advantages of the filtering method for POSE estimation. The control design according to the POSE estimates takes the Cartesian POSE vector trajectories as the reference input. The control error is therefore defined in the end-effector frame. There are transformation relationships among the end-effector frame, the robot base frame, and joint coordinate frame through the robot forwards and inverse kinematics. It adopts PD controllers in the joint space control for the visual servo loop and the control signal regulates the joint positions in the joint position servo loops. In summary, it is a dual loop with a multi-sample rate system.

When the robot is working in a manufacturing environment, it is surrounded by noises and existing uncertainties which will lead to poor performance and low accuracy and even failure of robot operation and undesired trajectories. In general, there is an open-loop kinematic transformation relationships utilized to calculating the accuracy end-point pose in a fixed world coordinate frame while the object work-piece must be positioned in the same coordinate frame. The errors will fail those predefined tasks. Hence, an advanced controller is in demand to handle large errors and uncertainties.

However, the robot control strategy based on the immediate measurement of the relative pose of work-piece with respect to the robot end-point aims at reducing or eliminating the errors throughout the whole process in the conventional robot manufacturing. It also realizes the online programming and operation based on the moving object. [42] presents a control loop design with the experimental verification based on the visual servoing. This design is in eye-in-hand configuration and is based on the measurement of image plane coordinates of

known object feature points. The relative POSE of the object with respect to the camera is therefore determined. The estimated POSE values and their velocities based on Kalman filter are used in the closed-loop trajectory control.

2.2 Source of Errors and Noise Under Measurement

An error is the difference between the observed value and the true value that usually unobserved and generated by the DGP. A residual is the difference between the observed value and the predicted value (by the model). The residual is the difference between the true value and the model being employed to describe it. Noise is that part of the residual which is in-feasible to model by any other means than a purely statistical description. Note that such modeling limitations also arise due to limitations of the measurement device (e.g. finite bandwidth resolution). Error is the component of the residual that remains after accounting for the noise according to the above definitions: a) noise and error are uncorrelated.b) residual may be reduced by either reducing noise or by reducing error.c) these definitions are compatible with the intuitive statements that noise does not introduce bias.

Nowadays, the product quality, expense, and productivity have attracted extensive attention worldwide. In this case, the offline programming based on simulation and motion control has been essential. Considering accuracy, the robot motion control and the simulation according to real robot demand the accurate dynamic robot model, especially for the design of advanced modern robot controllers such as computed torque or velocity controller. Hence, the controller performance directly depends on the extent of model accuracy. If a robot model simulated without a dynamic robot model, it can not provide meaningful and realistic execution time estimates.[43]. For example, in the case of spot welding operations, where the time required to stop the robot end-effector at the different spot welding places depends on robot dynamics. In order to obtain the accurate robot models and indications

on their accuracy, confidence, validity, the experimental parameter identification is required. The dynamic model parameter provided by robot manufactures is not sufficient enough and even not given.

It is also impossible to measure the physics parameters directly since the complex assembling of most robots. In the real specific designed experiment, the identification of the robot can estimate the robot model parameters from measurement data. During the design procedures of identification experiment for a robot manipulator, the sufficient excitation is required so as to offer timely and accurate parameter estimation in the presence of measurement noise and actuator disturbances. The statistical properties of the measurement noise been bringing about due to the coherent parameter estimation. Those consistent error estimation methods consider random disturbances on both input and output measurements.[44]. In [45], Xi proposes a common space-time stereo framework that unifies and generalizes triangulation-based depth extraction methods and using the total least square(TLS) method for the identification of robot parameters.

Another method is the generalized total least squares(GTLS) which allows corrections between the noise on the elements of the regression matrix and is able to calculate errors and random variables covariance matrix. However, the nonlinearity relationship of the regression matrix on joint angle measurements makes it difficult to obtain a covariance matrix. The maximum-likelihood estimator as a consistent estimator even though the model is highly nonlinear in parameter or measurements which means if a complicated nonlinear friction model is included in the robot model, this method is the optimal solution than TLS and GTLS.

2.2.1 Strategy of Eliminating Errors and Noise

To address the aforementioned imperfection, several techniques have been suggested [37, 46–48], the most widely-used of which is employing a Kalman Filter [37, 48]. For the nonlinear equation definition of relative POSE values with respect to multiple feature points measured on the image plane, the solution is the iterative method which can be extremely time-consuming if the sampling rate is high when doing dynamic vision servoing. Kalman filter is widely used in industrial field for its dynamic estimation of system state and redundant output measurements [42]. KF and its derivations have been employed in many research studies in the context of PBVS [16, 37, 49]. In [49], an adaptive KF (AKF) for robot pose estimation is presented whose noise co-variances were adjusted online. The adaptation rules are based on the forgetting factor technique which contributes smooth parameter tuning.

2.2.2 Photogrammetry Sensor C-track

If using the regular camera as the control loop sensor offing feedback signal, the processing of image and pose estimation algorithm will be time-consuming. Besides, the accuracy of the estimated pose is sensitive to the camera's parameters. The correlated time delay is the challenging part of online pose correction. Therefore, a sensor with dynamic pose information will be the solution to those problems.

Stereo vision is the data fusion of two views of the scene taken from known different feature points so as to resolve depth ambiguity. The location of feature points in one view should match the location of the same feature points in the other. This correspondence problem is in the presence of error. The missing parts is another non-negligible problem. If we only use this stereo camera sensor for measurement and a feature point is only visible in one of the views, its depth cannot be known. This matching normally can be done on a few feature points. For example, the region's centroids, corner features, or fine features like

surface texture, projected random texture pattern [50].

In [51], the stereo-vision system receives left and right image from the two CCD cameras installed on the robot head. Image distortion is removed by calibration and camera intrinsic parameters such as focal length and the principal point are therefore obtained, which are used on 3D range data computation. In [52] an approach to stereo visual servoing on which vision is used to measure error is proposed. The error is the visual distance between a robot manipulator and the pre-defined position in the sensor coordinates which is the feedback signal throughout the robot end-effector PBVS design. Murray and James [53] present a method for reducing stereo vision inequality images to two-dimensional map information. They reduce errors by segmenting inequality images based on continuous disparity surfaces to prevent stereo mismatches. Stereo vision processing and map updates are effectively reduces at 5 Hz and the robot moves at the speed of 300 cm/s.

Optical coordinate measurement machines(CMMs) use an image-based triangulation method for calculating the model of robot pose. They are able to dynamically tracking the object model. The C-track equipped with high-quality optical element and especial lighting and can measure all the reflectors within the operating range. In order to track the entire model of the object, the C-track determines the location of the HandyPROBE and emerges continuous image acquisition and transmission, the lighting of reflectors and the arrangement exchange with the computer configuration and storage of correlated parameters at the rate of maximization $29Hz$. The accuracy of C-track 780 in this research is up to 0.025mm, 0.050mm with $3.8m^2$, 0.055mm with $7.8m^3$. It weighs 5.5kg and operating temperature between 15 to $40°C$.

2.2.3 Kalman Filter

To address the aforementioned shortcomings of the PBVS, i.e. the effects of the existing noise on the estimated pose of the robot's end-effector, numerous methods such as analytical solutions i.e. Kalman Filter and the numerical stochastic solutions have been suggested [5, 46, 47, 54, 55]. However, the latter has been more attractive to the researchers than the former analytical methods [48]. The reason is that analytical solutions such as perspective 3-point-problem or 4-point-problem [46, 47] need a piece of profound mathematical knowledge and are to solve, whereas numerical methods are more convenient to apply and can bring about a rather optimal solution [48].

Applying Kalman filtering for pose relative POSE estimation has many advantages. First, Kalman filter can solve the nonlinear photogrammetric equations in each time step which is of vital importance in the case of a high-sampling rate compared with the relative motion method. Second, Kalman filter is able to provide appropriate statistical data fusion from different sensors. Third, Kalman filter implements temporal filtering so as to improve dynamical estimation. The fourth advantage is that since Kalman filter predicts the state at the next time it can be used as a windowing technique in image processing. Last and most relative is that, the Kalman filter also proposes the esimates of POSE velocities as it is commonly used throughout control system design. If the Kalman filter method is used to solve the relative POSE estimation problem, the dynamical model of the system and output equation should be defined in advance. In many cases, the motion of the work-piece is unknown even if the model of robot end-point dynamic motion is usually known.

Therefore, a constant velocity is assumed in modeling the relative dynamic motion. In each time step, the relative velocity is not much changed or slowly from time to time and remains constant. Considering the disturbance noise, there exist small errors during modeling. The state vector can be defined as $\mathbf{w} = [X, \dot{X}, Y, \dot{Y}, Z, \dot{Z}, \phi, \phi, \alpha, \alpha, \psi, \psi]^T$, and let γ be

the disturbance white noise vector which means zero Gaussian distributed with covariance matrix Q. The discrete system dynamical model is therefore represented as

$$\mathbf{w}_k = A\mathbf{w}_{k-1} + \gamma_k \tag{2.2}$$

where A is the state transition related to the system model with the diagonal elements of 1 and sampling interval T

$$A = \text{diag}\begin{bmatrix} 1 & T & \\ & & :\cdots\cdots \\ 0 & 1 & \end{bmatrix} \tag{2.3}$$

another system output model marked as B is utilized to link the output variables with defined system states. Those outputs are presented in the image plane feature point locations. Noted that the output equations are the nonlinear photogrammetric functions. The output equations are of the form

$$\mathbf{z}_k = G\left(\mathbf{w}_k\right) + \mathbf{v}_k \tag{2.4}$$

where v always assume to be zero-mean Gaussian white noise with covariance matrix R. In a camera system by calibration, the covariance matrix R elements can be obtained from experiments on this visual servoing system. Also, other sensor outputs such as robot joint encoders can be included to determine the POSE state throughout the combination. In[42], KF and its derivations, as one of the most efficacious methods for filtering noisy signals and observing the state variables have been employed in many researches [56–59]. The KF method carries out the filtering in two stages: the prediction of the real signal out of noisy signal based on the dynamic model of the system and the correction of the predicted signal based on the covariance of the measurements errors of the system output $\mathbf{R}$ and stated variables $\mathbf{Q}$ associated with the existing noises [60]. Therefore, the quality of the filtering largely depends on the accuracy of the system's dynamics, the error covariances $\mathbf{R}$ and $\mathbf{Q}$.

To improve the performance of the KFs, a lot of modifications and techniques have been suggested, such as, adaptive Kalman filter(AKF), robust Kalman filter(RKF), and extended or uncented Kalman filter(EKF or UKF) [16, 27, 39, 49, 59].

The standard KF uses the linear dynamic model of the system for the variables estimation, which results in an inaccurate estimation when the dynamic model of the system under observation is nonlinear. To cope with this issue, extended KF (EKF) has been suggested. EKF is the nonlinear version of standard KF which uses the linearized model of the nonlinear dynamic model around the current estimated point rather than using a predetermined linear dynamic model [48]. Consequently, its estimation is more accurate than those of the standard KF. Several researchers have employed EKF for the pose detection of robots [61, 62]. Another method is unscented Kalman filter which is the same as EKF except that it uses unscented transformation (UT) for estimating the covariance matrices, which results in more accurate estimation and hence, lower error in nonlinear estimation [63]. UKF has also been employed for pose detection in [64]. Although EKF and UKF tackle the problem with nonlinearity of the estimation, setting the appropriate components of the $\mathbf{R}$ and $\mathbf{Q}$ matrices still remains unaddressed. Therefore, adaptive Kalman filters (AKF) are presented in order to solve the mentioned issue. Several methods for adaptive Kalman filters have been used to estimate the pose of industrial robots [16, 27, 49, 65]. The most well-known one is based on the limited memory and/or forgetting factor covariance estimation and state variables covariance estimation correction [16, 27, 49].

In the AKF with limited windowing memory, the estimation of covariance matrices, i.e. $\mathbf{Q}$ and $\mathbf{R}$, is carried out by using the numerical covariance of the previously collected data. However, the numerical computing of the covariance or averaging is cumbersome, hence, a limited windowing memory method is employed [65]. A similar procedure takes place for the forgetting factor AKF, except for the fact that instead of collecting a number of data

in a window, a forgetting factor method is employed [49]. Another AKF, known as robust KF (RKF), has been presented to address the estimation error of $\mathbf{P}$ due to the uncertainties of the model's dynamics. In this method, a correction coefficient is adaptively computed to correct the estimated $\mathbf{P}$ based on the comparison between the theoretical and estimated $\mathbf{P}$. Since this method aims to correct the estimated covariance matrix $\mathbf{P}$ towards the real covariance matrix $\mathbf{P}$ adaptively, it is also called to be an adaptive optimal KF (AOKF) [27]. The mentioned advantages of the RKF makes it a good candidate to be employed for VS and that is the reason why a lot of research work has been conducted using this method [6, 66].

2.2.4 Kalman Filter-based Pose Estimation

In computer vision field, pose estimation is to determine the pose of a camera in terms of an object's coordinate frame according to image information. It is also known as an extrinsic calibration problem with its solution which plays a crucial role in many computer-vision applications, such as object recognition [67], intelligent surveillance [10], and robotic visual servoing (RVS) [68]. Estimation of the camera displacement (CD) between the current and desired pose for RVS [69, 70] is also relevant.

However, this study will be on pose estimation for visual servoing of the robotics system in which the relative pose between camera and object in real-time control of robot motion [68]. In RVS, the control error will be calculated in the image space, Cartesian space, even hybrid spaces [68, 71, 72]. However, partial estimation of the pose vector is required for image-based and hybrid visual-servoing schemes [73, 74], an important class of visual-servoing methods. The position-based visual-servoing (PBVS) scheme requiring full pose estimation to calculate Cartesian error of the relative pose between end-effector and object [38]. Those major difficulties in pose estimation are related to the requirements of the robustness of pose

estimation effectively [75].

The solutions to pose estimation problem usually focus on using sets of 2-D–3-D correspondences between physics features and their projections on the image plane. Even though high-level geometric features, such as lines and conics, have been proposed, point features are used for pose estimation thanks to their wide available in many objects [76]. Solutions for three points [11], and 4 to higher points [77] have been presented. Nevertheless, exact and closed-loop solutions are only available for three or four non-collinear points [46]. Such method is simple to implement but often encounters the difficulty of point matching during crowded environments. Moreover, point-based solutions are not robust and demonstrate highly sensitive to noise in image coordinates [78]. For three-point solutions, it has been shown that the point configuration and noise in the coordinates of points can affect the output errors [11]. It has also been demonstrated that when the noise level exceeds a knee level, least-squares-based methods, which are usually used for points solutions, becoming unstable and result in huge errors[79]. Addition of more points would enhance pose-estimation robustness with the cost of increased computational expense. Nonlinear, iterative, and/or recursive methods are then recommended for more than four points as well as high-level features.

The least-square problem can be formulated by the iterative approaches. It offers the robustness and accuracy for the control system, which depends on the initial condition of the pose estimation [80, 81]. In most cases, iterative methods rely on nonlinear optimization techniques, such as the Gauss–Newton method [67]. In order to simplify the problem, there are approximation method proposed via the perspective camera model simplification, such as relaxing the orthogonality constraint on the rotation matrix [81, 82]. The survey on both superior approximation pose-estimation methods is found in the papers [5, 46]. In summary, this class of methods demonstrates convergence problems and does not clearly explain the

orthonormal structure of rotation matrices [83].

Furthermore, those noisy visual-servo images will result in poor pose estimation with this class of techniques [84] hence requiring temporal filtering. There is a class of recursive methods on temporal-filtering methods. Kalman-filtering techniques are used to address robustness and efficiency issues. Owing to 3-D pose time rate forming a 12-D state vector to be estimated online, those class of these filtering methods e.g. particle filters model the true distribution in real time [85]. A 3-D pose estimation with Kalman filter (KF) for robotic visual servoing has been realized in [38]. Photogrammetric equations using KFs are constructed by projecting the object features into the camera frame and then mapping them onto the image plane. A KF is then applied to provide a recursive solution of those pose values.

Due to the non-linearity of filter output model in the system states, an extended KF is proposed where the output equations are linearly approximated about the current state. KF is applied in RVS due to several advantages which are recursive implementation, statistical ability combine redundant information for instance features or measurement sensors, temporal filtering, the possibility of using a lower number of features, and the possibility of changing the measurement set without interrupting the operation [38, 68]. For example, an EKF-based platform has been proposed in [75] range sensor integrated with a vision sensor for robust pose estimation. Additionally, an EKF implementation facilitates dynamic windowing of the features of interest by providing an estimation of the next time-step feature location which means only small window areas are allowed to be processed for image-parameter measurements and results in a significant reductions in image-processing time. It has been shown that practically, an EKF providing near-optimal estimation[38].

Despite those advantages, there exist a few issues during the application of EKF to pose estimation in robotic visual servoing. Firstly, a known object model is usually assumed to

be available. Some model-free approaches based on Euclidean reconstruction have been proposed for pose estimation [38, 74], which are typically relying on the fundamental, essential, and homography matrix estimation in [38, 86]. Despite some strategies on [74], it is still sensitive to outliers. Additionally, the majority of these require several images for reconstruction and hence are more appealing for post-production applications [87]. The assumption of th object model is not a major issue in many industrial setups owing to computer-aided-design (CAD) models of the objects. For uncertain environments with an unknown model of the object, an EKF-based approach for real-time estimation of and target model combined pose has been proposed in [88, 89].

Secondly, although KF provides an optimal solution with the assumption of zero-mean Gaussian noise, the EKF formulation can not guarantee optimal results. Actually, linearization can generate unstable filters when the assumption of local linearity is not satisfied [90]. Through previous work, taking a sufficiently high sampling rate to impose linearization accuracy through the sampling period is suggested [38]. Nevertheless, RVS-system bandwidth limits the sampling rate of filtering in the real applications. As it is shown in [65], an EKF-based system will easily diverge with fast and nonlinear trajectory dynamics or with a relatively high-sampling rate.

Thirdly, the statistics of the measurement and dynamic noise are known and remain constant in advance. Poor measurement and dynamic models and poor noise estimates probably degrade the system performance and causing the filter divergence. Particularly, although the measurement noise-covariance matrix is tuned through experiments, it is difficult to tune dynamic covariance matrix [84]. The reason of this phenomenon is that dynamics of the object motion with respect to camera frame would not be predicted accurately in the dynamic environment. Fourth and foremost, the convergence of EKF large relies on the initial state estimate setting and tuning of filter parameters. In many RVS applications, such

as the assembly industry, the initial pose of the object with respect to the camera is able to be approximated. However, sufficiently good pose estimates cannot be initially available in unstructured and uncertain environments. The paper [59] will contribute to the formulation of the EKF method to address two of the aforementioned issues.

The adaptive EKF (AEKF) with a fixed setting of image features has been proposed for the first time in [65] to update the dynamic-noise covariance matrix and to address the issue of varying uncertain dynamic noise. The AEKF-based approach extended in [91] has a variable set of image features when improving servoing robustness. Despite the adaptation capability of AEKF to unsuspected noise statistics, the presented AEKF methods do not offer robustness and accuracy of pose estimation under uncleared filter initialization or camera calibration, especially when tracking a fast and nonlinear trajectory. Tuning EKF noise-covariance matrices is addressed in the aforementioned AEKF-based approaches [65, 91] and tuning or initialization of other EKF parameters and mechanisms to enhance output linearization for RVS did not matter compared with the overall system performance.

In order to address tuning of other filter parameters and to achieve its initialization, an initial proposal for iterative EKF (IEKF) in RVS has been provided in [92]. In fact, Lefebvre et al. [93] have studied several modifications of KFs for general nonlinear systems, such as the central difference filter (CDF), unscentedKF (UKF), and divided difference filter (DDF) as the linear regression KFs (LRKFs). The comparison study shows that EKF and IEKF outperform LRKFs even if the trial and error tuning is required. The result of their study shows that IEKF outperforms EKF credit to the measurements to linearize the measurement function, while in EKF and LRKFs, the measurement is not adopted with the same purpose. However, the lack of an adaptive noise estimation mechanism would degrade the performance of IEKF. The iterative AEKF (IAEKF) for RVS is also proposed to address the existing limiting problem of IEKF and AEKF.

2.3 Controller Design for PBVS

Most reported visual servo systems do not perform as expected. The most obvious characteristics are slowness of motion and lag in terms of target motion, and often causing jitter or shakiness. Computer vision holds a number of significant disadvantages when used as a feedback sensor such as relatively low sample rate, and significant latency like one or more sample intervals, and quantization of crude. These characteristics present a challenge for the design of high-performance motion control systems and they are not insurmountable. Latency, as the most significant dynamic characteristic and its sources including transmitting delay of pixels from the camera to vision system, image processing algorithms, communications between vision system commanding computer, control algorithm software, and communications with the robot.

In fact, problems of delay in visual servo systems were first noted over 15 years ago [94]. If the target motion is constant, the prediction can be used to compensate for latency. However, a low sample rate results in poor disturbance rejection and long reaction time to unmodeled motion. Grasping objects on a conveyor belt [95] are however ideal applications for prediction. Franklin [96] suggests that the sample rate of a digital control system should be between 4 and 20 times of the desired closed-loop bandwidth. For the case of a 50Hz vision system, this implies that a closed-loop bandwidth between $2.5Hz$ and $12Hz$ is achievable. Very few reported systems can achieve this. One can draw the conclusion that the whole area of dynamic modeling and control design has, to date, been largely overlooked [34].

2.3.1 PD Controller on Industrial Robots

Many advanced industrial manipulators especially those from CRS Robotics Ltd., Applied AI, Inc., etc.[97–99] are controlled by using only proportional–derivative (PD) or PID controllers. This PD type of robot controller can be dated back to [100, 101]. The design

procedure of the controller comprises PD control with gravity compensation and the PD control with the desired gravity compensation term. Those researchers demonstrate that a PD-type robot controller can be used to stabilize the joint positions of rigid robot manipulators asymptotically. Nevertheless, the controller design according to the gravitational loading vector of the robot dynamics, where those uncertain parameters of manipulator dynamics are essential to meet the desired control objective.

The adaptive form of these controllers can be found at [102, 103] which require a prior known structure of the gravitational loading vector. It is very difficult to meet the challenges of the online operation. In fact, PD design may cause a steady-state filtering error with the gravitational loading vector, which can be deduced by tuning the proportional and derivative gains or adding integration parts. In [104–106] it is shown the local stability proof of the PID-based robot controller without the knowledge of the robot dynamics. The control design parameters can be chosen to achieve the desired tracking objective which depends on the robot manipulator dynamics [104–107].

In order to eliminate the gravitational loading vector from the controller structure, a new control strategy is introduced in [108, 109]. The controller is developed through proportional and differential feedback with proportional integral components via the linear sum of velocity and saturation position error. Basically, the fundamental method is to use the energy-shaping technique and passivity theory. This method is able to achieve the desired tracking only if the designer can choose suitable design parameters by using the Lyapunov second method. In fact, the controller parameters of these controllers need to satisfy complex inequalities that maybe not popular for industrial applications. In [110], Rocco proposed the Lyapunov-based PID controller in which the local stability property of the closed-loop system is established. The author shows that the overall design is just a simple PD controller design. This is because the integral gains used in PID design are smaller than PD control gains. Actually,

the implementation of the PD or PID controller is difficult to realize owing to the fact that it requires velocity signals in addition to joint position signals.

Practically, the advanced robotic systems do not offer velocity sensors due to the constraints of weight and cost. To obtain velocity signals, the communal practical method is to differentiate the position measurements obtained from encoders. The measurement of joint position is also contaminated by noise [97–99]). Consequently, the performances of the PD and PID controller are limited since practically the noise is amplified with the increase of the values of controller gains. To reduce the amplification of noise, the cut off frequency of the filter should be chosen by a trial-and-error method based on the derivative control gains containing measurement noise of the sensor and the filtered derivation of the velocity signals [97, 98]. However, it may work for some applications, such as a simple approximation which is often not sufficient with polarized velocities. Furthermore, the quantization effect of the noisy velocity signals usually bring about undesirable oscillations at joint. This may render the control system unstable. Last but not least, there is a lack of theoretical proof for such a solution which has been applied in existing industrial robot controllers.

In [111], a linear estimator is proposed to reproduce the unknown velocity signal in PD-based industrial robot controllers. At the beginning of the design procedure, a PD term with nominal robot model dynamics is proposed in which the unknown velocity signals estimated via the linear estimator output. The Lyapunov method is used to construct necessary conditions in order to guarantee the asymptotic stability of the closed-loop error model dynamics. This condition sets the bound on the filtering error trajectory of the closed-loop system. Secondly, the nominal model dynamics are removed from the control design to formulate an independent PD model type feedback method. It is shown in the analysis that the filtering error bound can be made randomly small by increasing the minimal eigenvalue of the control gains. With a given set of initial conditions, the region of the PD-based state

feedback design is estimated.

Then, the control outside the estimated region is saturated in order to get bounded control input. The linear estimator is utilized after that so as to generate unknown velocity signals and to develop the law of PD-based output feedback control. The bounded control allows increasing the speed of the observer dynamics without compromising the transient tracking performance for the user. With the adoption of such an asymptotic analysis of the singularly perturbed closed-loop model, it is proven that the observer and filtering error variables are finally bounded. Besides, their bounds can be limited to a small neighborhood of the origin through observer–controller gains.

2.3.2 Sliding Mode Controller on Industrial Robots

In recent years, the control of uncertain processes has attracted great interest in the research community[112, 113]. Among the robust control methods, the sliding mode control has attracted high attention due to its high simplicity and robustness. The essence of SMC techniques is that the controlled system trajectories converge to the designed sliding surface. The system performance is expected on the sliding manifold in order to obtain the control of the designed system with authority to dominate the uncertainties and disturbances acting on the system. The control will promptly react to any declination from the prescribed behavior of the system back to the sliding manifold. One of the advantages of this approach is that the sliding behavior is robust to model uncertainties and disturbances which would not let the system state to escape outside from the chosen manifold.

Even though the presence of aforementioned robustness advantages, the implementation of SMC techniques still holds an obvious drawback since the finite switching frequency of real control devices. The high-frequency components of the system could affect parasitic resonant modes so that the system trajectories from the ideal ones. In general, the system and the

actuators will definitely result chattering phenomenon, which is a high frequency motion that effect the state trajectories oscillating about the sliding manifold briskly. The chattering phenomenon and the discontinuous control constitute two main reasons for criticisms of sliding modes in variable structure systems and these drawbacks are much more evident when dealing with mechanical systems.

In spite of the above-cited drawbacks, VSS with SlidingModes (SM) have been considered often in the technical literature for the robust control of mechanical systems [28, 40, 114–120]. The sign function of the discontinuous control is approximated by the saturation function in order to avoid chattering. In this case, the system motion is bounded within a boundary layer of the sliding manifold [121–123]. However, if the parasitic dynamics is not accurate in the dynamic model, the approximation of the discontinuous control may scarify the robustness of disturbance rejection properties in SMC [124]. Since the chattering phenomenon is caused by both the switching delays and parasitic system dynamics.

Another solution for this chattering phenomenon is to implant an asymptotic state observer in the controller. In this case, [125, 126], a different approach to avoid chattering is proposed to augment the controlled system dynamics by adding integrators at the input. If the discontinuous signal is consistent with the highest derivative controlled by the plant, the latter result is continuous. Also, the smoothness is related to the considered derivative order. This procedure is referred to as higher-order SM implementing higher-order sliding modes, dynamic SMC, and terminal SM [124, 127–129] respectively. Even though the usage of differentiators has been assumed to be a regular inspection. The theoretical development of output feedback is considered [130].

In practice, the behavior of those devices needs to be considered for real implementation due to the prescience of the measurement noise, whose negative effects on the closed-loop performance rapidly increase along with the number of differentiation stages. Those research

activities are devoted to develop online differentiators which are less sensitive to the noise propagation as well as control algorithms for non-linear uncertain systems. Hence, the number of differentiation stages are reduced. In the real situation, many differentiation algorithms based on second and higher order sliding modes have been presented [125, 127, 131] which shows a non-eligible compromise between accuracy and noise-immunity.

The second research topic of 2-SM controllers, to deal with the cases where the relative degree between the constraint output of which the system motion meets the desired performance specification and the discontinuous control. The main challenging part lies in solving differential inequalities of a higher order. The comparison principle in non-linear control theory including Lyapunov stability theorems in general does not work in the high relative degree case. In this paper [119], various 2-SMC algorithms are presented to solve several classes of second-order differential inequalities. The proper tuning of parameters are identified influence some qualitative of transient properties [119, 125].

2.3.3 Chattering Free SMC on Industrial Robots

The initial propose of the sliding-mode control is to design a control law with varying structures of control then let the trajectory of the system state goes to a certain predefined sliding surface, although an appropriate switching of the control structures such that the system state will stay there. However, the digital implementation of the sliding-mode control has a chattering problem. The chattering phenomenon occurs when the control input switches discontinuously cross the boundary which involves high control activity and may excite high-frequency dynamics [132]. To eliminate chattering, various methods such as sliding-mode controller with boundary layer (SMCB) [133], fuzzy sliding-mode controller (FSMC) [134], the sliding-mode controller (SMC) with the sliding sector [135] has been proposed. In all these researching works, the fundamental goal is to smooth the control action across the

sliding surface while preserving the classical variable-structure control law. In order to improve the system response of the traditional SMC and SMCB, However, chattering still may occur under certain operating conditions [122]. There is a new chattering-free sliding mode controller with fast-response behavior has been proposed and implemented in paper [122].

Different from the traditional SMC or SMCB adopting a switching control term, the proposed SMCS utilizes a continuously varying term instead. It also takes the distance of the system state from the sliding surface into account. In this case, the proposed SMCS has the superiorities of chattering-free behavior. By contrast with SMCB, it holds the controllable max steady-state error and ease of adaptability, reduced hitting time and better robustness. Sliding-mode control has been widely used for the nonlinear system [136]. Nowadays, a growing number of modern advanced control systems are implemented with computers, the study of SMC in the discrete-time domain. The discrete-time SMC has been an important topic in SMC literature [137]. The main feature of discrete-time SMC (DSMC) compared with continuous-time SMC (CSMC) relies on that the switching frequency of DSMC is bounded [138].

In this case, the study of DSMC attracted the attention of many researchers and can be divided into two categories. The first direction is that obeying the design procedure of CSMC and meanwhile, the switching term is still preserved. The design of DSMC law directly based on discrete-time systems. Although there is no switching term in the reaching law based DSMC, the generation of an over-large control effort is also processed. Therefore, the main problem is find a suitable method to guarantee a smaller boundary layer area especial for the sliding mode movement. According to this, some improved DSMC methods have been therefore proposed, such as disturbance observer-based DSMC.

However, these improved DSMC methods belong to the equivalent-control-based DSMC. In [139], Bhat, Sanjay, and Sprovide provided a new DSMC design method which is based on

non-smooth control. The advantage of such non-smooth control lies in its good performances such as better robustness. In this new kind of DSMC, avoiding the chatting phenomenon and the generation of large control, a non-smooth term or continuous function is therefore employed instead of the switching term, and a reaching process is added. Under the proposed DSMC, a strict theoretic analysis shows the same accuracy for the sliding mode motion that may be obtained as the equivalent-control-based DSMC which provides a higher precision than that of traditional reaching law-based DSMC. The related example is funded in [123] to show the potential of such a proposed method.

2.4 Summary

In this chapter, a comprehensive literature survey on the key components of PBVS has been carried out. On the pose estimation topic, this chapter presents the analysis of the modeling errors and strategies of eliminating errors and measuring noise. The main focus is on the techniques based on Kalman filter. On the topic of controller design, this chapter presents a complete survey on the schemes based on the PD controller and sliding mode controller. The subsequent chapters will develop an adaptive robust Kalman filter (ARKF) and a fast chattering-free SMC for PBVS.

Chapter 3

Pose Estimation

In this chapter, an adaptive robust Kalman filter (ARKF) for precise and robust pose detection of industrial robots is presented. The proposed ARKF exploits the advantages of adaptive estimation method for states noise covariance (Q), least square identification for measurement noise covariance (R), and a robust mechanism for state variables error covariance (P). In the simulation of PUMA 560, the comparison between the proposed ARKF and other well-known Kalman filters such as adaptive Kalman filter (AKF) and standard Kalman filter (SKF) shows the superiority of the ARKF in terms of root mean square (RMS) and Variance (Var) of filtered errors. The ARKF outperforms the above-mentioned methods both in smooth filtering and in signal tracking. Simulation results reveal the superior tracking performance of the ARKF when the robot is subjected to the measurement noises and uncertainties.

3.1 Robustness

There are many essential requirements on control system such as tracking availability, rejecting the external disturbances through measurement, and process noise. It is of vital

importance to analyze the system performance with a previous understanding of the aforementioned indexes. There always exist a compromise between the robustness and system performance. Robustness is the capability to describe the extent that the system can sufficiently reject external disturbance. It simplifies the design procedure via extremely simplified models which plays a key role in system design. The dynamics variation captured by the models can be used for analysis. However, some dynamic phenomena may be ignored when building a system model such as time delay due to the difficulty of high order modeling. The transfer functions are used to describe linear variation and adopted to correspond to dynamic variation including time delay. It is also worthy of seeking a numerical method to determine to what extent the feedback system performs.

3.2 The Sensitivity Function

The parameters of varying during the control process. Thus, it is necessary to set the controller parameters with the capability of insensitive to process dynamics. The characterization of the extent of sensitivity is through the sensitivity peak M_s as follows,

$$M_s = \max_{0 \leq \omega < \infty} |S(j\omega)| = \max_{0 \leq \omega < \infty} \left| \frac{1}{1 + G(j\omega)C(j\omega)} \right| \tag{3.1}$$

where $G(s)$ and $C(s)$) are the transfer function of plant and controller with negative, and S is the sensitivity function. The sensitivity function suggests how the disturbances are influenced by feedback and how sensitive the closed-loop system is to small perturbations of process dynamics. The structure of the feedback controller is another essential element. The sensors in the error feedback system only obtain the error signal while in the other feedback systems both the reference and output are measurable. Therefore, it is automatic to separate command signals from robustness and disturbance attenuation via 2-DOF controller. The

feedback signal is for processing disturbance and robustness. The feedforward signal is to take a response to generate the control signal. In the error feedback system, the feedback signals need further estimation. In order to enhance the accuracy of the industrial robot control system, we have to get the accurate pose of the object, i.e. end-effector's pose in this research. However, in the real situation, there are several sources of noise such as robot intrinsic noise, sensor instruments measurement noise due to its limitation. Hence, the distribution of those kinds of noise can be obtained by measuring the data time series in the experiments.

3.3 Gaussian Noise and Adaptive Robust Kalman Filter Functions

In this section, the design procedure of the ARKF for pose detection is presented. First, SKF is introduced in a discrete time domain. Then, the modifications on the SKF towards adaptation and robustness will be stated.

3.3.1 State Variables of the End-effector's Pose

The position and orientation of the end-effector of a six degree-of-freedom (DOF) robot is represented by 6 variables, i.e.,x, y, and z, the translational variables in the Cartesian ground frame, r, p, and w, the Euler angles in the mentioned frame(see Fig 3.1 [1]). Accordingly, the vector of state variables q of the end-effector in Kalman filter is usually denoted as follows,

$$q = \begin{bmatrix} x & y & z & r & p & w & \dot{x} & \dot{y} & \dot{z} & \dot{r} & \dot{p} & \dot{w} \end{bmatrix}^{\mathrm{T}} \tag{3.2}$$

where q is the vector of state variables consisting pose variables and their velocities.

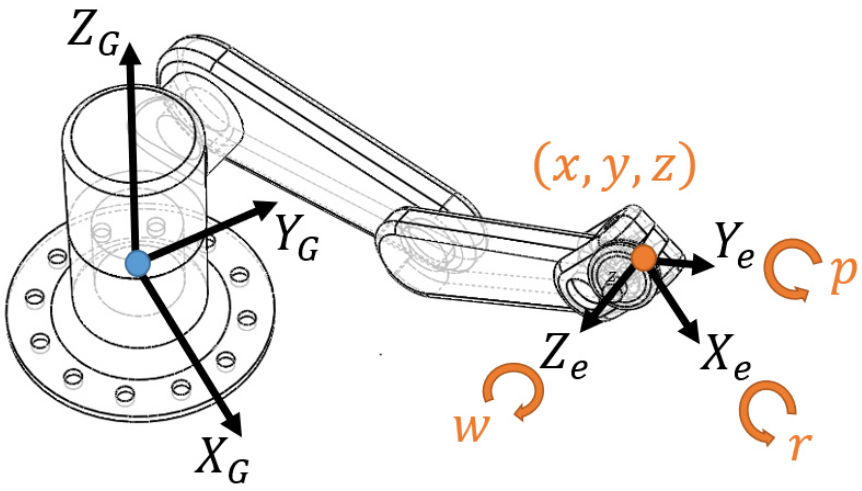

Figure 3.1: The pose variables in the ground frame [1]

3.3.2 Standard Kalman Filter for Pose Detection

The task of a KF is to estimate the pose q as $\hat{q}$, which is the real signal vector without noise. SKF normally filters a noisy signal in two stages: prediction and correction. For prediction, SKF relies on a pre-determined dynamic model of the system, through which it predicts the current state based on the previous data. The prediction relations the first stage is shown as follows [140],

$$\begin{aligned} \hat{q}_{k|k-1} &= \mathbf{A}\hat{q}_{k-1|k-1} \\ \mathbf{P}_{k|k-1} &= \mathbf{A}\mathbf{P}_{k-1|k-1}\mathbf{A}^{\mathrm{T}} + \mathbf{Q}_{k-1} \end{aligned} \tag{3.3}$$

where $\hat{q}$ is the estimated state vector of the robot pose q, $\mathbf{W}$ is the covariance matrix of the state variables error, and $\mathbf{Q}$ is the covariance matrix of the noise in the state variables. Note that subscript k indicates the time instant. Matrix $\mathbf{A}$, a 12×12 matrix of the state transition (system model), with the diagonal elements of 1, and $\mathbf{A_{(i,i+6)}}(i = 1, \ldots, 6)$ equals the sampling interval T_s [16]. After obtaining the prediction of the state vectors, one has to correct the prediction using the following relations [49],

$$\begin{aligned} \hat{q}_{k|k} &= \hat{q}_{k|k-1} + \mathbf{K}_k \left(d_k\right) \\ \mathbf{P}_{k|k} &= \mathbf{P}_{k|k-1} - \mathbf{K}_k \mathbf{B} \mathbf{P}_{k|k-1} \end{aligned} \tag{3.4}$$

where d_k and $\mathbf{K}_k$ are the residual and Kalman filter gain respectively, which are obtained as,

$$\begin{aligned} d_k &= o_k - \mathbf{B}\hat{q}_{k|k-1} \\ \mathbf{K}_k &= \mathbf{P}_{k|k-1}\mathbf{B}^{\mathrm{T}} \left(\mathbf{B}\mathbf{P}_{k|k-1}\mathbf{B}^{\mathrm{T}} + \mathbf{R}_{\mathrm{k-1}}\right)^{-1} \end{aligned} \tag{3.5}$$

where, o_k is the vector of noisy signals of the robot end-effector's pose, acquired from vision measurement system, $\mathbf{R}$ is the 6×6 measurement noise covariance matrix and $\mathbf{B}$ is the output matrix transformation considered as,

$$\mathbf{B} = \begin{bmatrix} \mathbf{I}_{6\times6} & \mathbf{O}_{6\times6} \end{bmatrix} \tag{3.6}$$

3.3.3 Adaptive State Noise Covariance (Q) using Forgetting Factor

Setting the entries' values of $\mathbf{Q}$ is a demanding task, and improper tuning leads to an undesired performance in filtering [141]. Therefore, one way to handling this issue is to update the entries of $\mathbf{Q}$ adaptively. The numerical estimation of $\mathbf{Q}$, i.e., $\widehat{\mathbf{Q}}$, using previously collected data, whether by taking advantage of averaging limited memory windowing or forgetting factor, has been employed widely in many research works [16, 65]. In this paper, the forgetting factor method is employed for evaluating $\widehat{\mathbf{Q}}$ due to its slighter numerical computation. As a matter of fact, forgetting factor is used for computing the expected value for $\widehat{\mathbf{Q}}$ in [49],

$$\widehat{\mathbf{Q}}_k = \mathrm{E}\left[\mathbf{K}_k d_k d_k^{\mathrm{T}} \mathbf{K}_k^{\mathrm{T}}\right] \tag{3.7}$$

$$\widehat{\mathbf{Q}}_k = \gamma \left(\mathbf{K}_{k-1} d_{k-1} d_{k-1}^{\mathrm{T}} \mathbf{K}_{k-1}^{\mathrm{T}} \right) + (1-\gamma) \left(\mathbf{K}_k d_k d_k^{\mathrm{T}} \mathbf{K}_k^{\mathrm{T}} \right) \tag{3.8}$$

In the relation above, γ is the forgetting factor which takes a value between 0 and 1.

3.3.4 Identification of Noise Covariance (R) using Least Square Method

Matrices $\mathbf{Q}$ and $\mathbf{R}$ need to be appropriately tuned for KF for having acceptable performance. Since $\mathbf{R}$ is the covariance matrix of the measurement noises, it is possible to estimate its entries by taking numerical samples. Following this idea, in the case of VS, one possible task is to get the data from the visual system when the robot is in a stationary status and to estimate $\mathbf{R}$ as $\widehat{\mathbf{R}}$. However, it has been observed that $\mathbf{R}$ entries vary when the end-effector moves from one point to another with different velocities, causing the delay, blur, vibration in the acquired images by camera. To cope with this problem, the following adaptive Kalman filter method was suggested by Tingting et al [16]:

$$\widehat{\mathbf{R}}_k = \widehat{\mathbf{R}}_{s_k} + \widehat{\mathbf{R}}_{v_k} \tag{3.9}$$

where, $\widehat{\mathbf{R}}_{s_k}$ is the covariance of noise measurement evaluated when the robot is stationary, and $\widehat{\mathbf{R}}_{v_k}$ is the additive covariance of noise measurement emanated from the moving end-effector's variables shown as the following relation.

$$\widehat{\mathbf{R}}_{v_k} = \mathrm{diag}\left([\mu_1 |\dot{x}(k)| \quad \mu_2 |\dot{y}(k)| \quad \mu_3 |\dot{z}(k)| \quad \mu_4 |\dot{r}(k)| \quad \mu_5 |\dot{p}(k)| \quad \mu_6 |\dot{w}(k)| \right) \tag{3.10}$$

where μ_1 to μ_6 are positive constant weights estimated based on the influences of the variables' velocities [16]. In this relation, although the effect of the velocity is taken into account, the effect of the location and orientation of the end-effector is being neglected. Therefore,

in this paper, a novel method for computing $\widehat{\mathbf{R}}$ is suggested which considers both effects of the velocity and pose, i.e., the state of the end-effector. However, $\widehat{\mathbf{R}_\mathbf{s}}$ and $\widehat{\mathbf{R}_\mathbf{v}}$ are calculated differently as follows,

$$\begin{aligned} \widehat{\mathbf{R}}_{s_{k_{i,i}}} &= \mathbf{C}_i \times q_{k_{(1:i)}} \\ \widehat{\mathbf{R}}_{v_{k_{i,i}}} &= \mu_i \times \left| q_{k_{(s+1)}} \right| \end{aligned} \tag{3.11}$$

where $\mathbf{C}_i$ is the regressors vector, whose entries are computed by applying the least square error (LSE) identification method [142] based on the collected data from several tests on the stationary robot(see Figure 3.2-a). Furthermore, μ_i is considered to be dependent on the position and orientation variables as follows,

$$\mu_i = \mathbf{D}_i \times q_{k_{(1:6)}} \tag{3.12}$$

where $\mathbf{D}_i$ is the regressor vector, whose entries are calculated by using the same method employed for $\mathbf{C}_i$, and using the collected data from several tests on the robot moving with constant speed (see Figure 3.2-b). Note that both $\widehat{\mathbf{R}_\mathbf{s}}$ and $\widehat{\mathbf{R}_\mathbf{v}}$ are diagonal matrices.

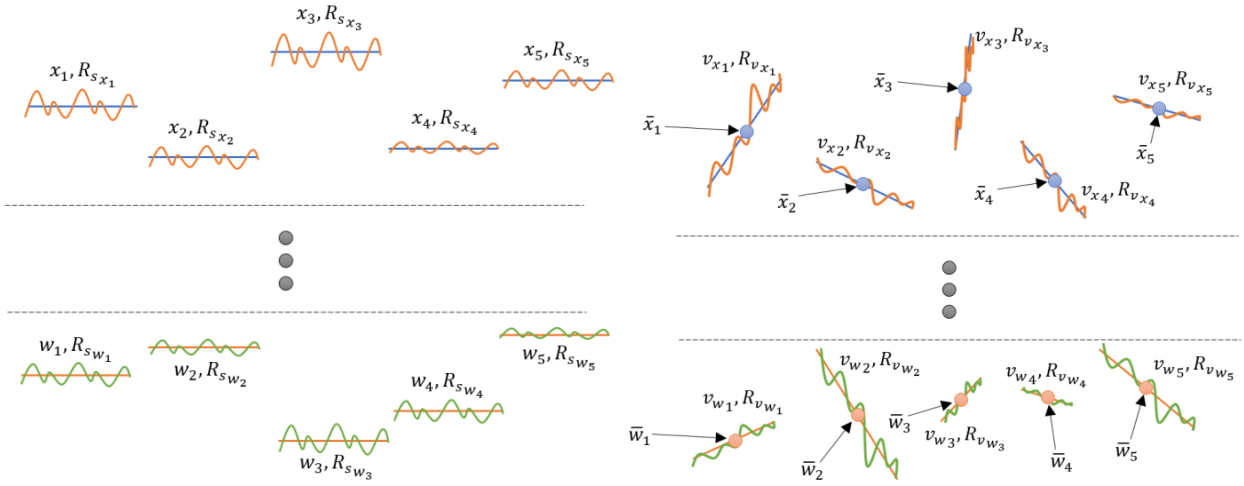

Figure 3.2: Least square identification; a) constant position and orientation b) constant velocity

3.3.5 Robust Correction of the State Error Covariance (P)

Properly tuning of $\mathbf{Q}$ and $\mathbf{R}$, whether by adaptive updating or by identification, leads to improving the performance of the KF significantly. However, the existing uncertainties in dynamic model considered for KF result in inaccurate estimation of $\mathbf{P}$ and hence cause destructive effect on the filtering process. To tackle this issue, an adaptive robust correction method is suggested, in which the estimate $\mathbf{P}$ and the theoretical evaluated $\overline{\mathbf{P}}$ are compared and a correction factor α compensates the inaccuracy of $\mathbf{P}$. The compensated $\mathbf{P}$, namely $\widehat{\mathbf{P}}$ is obtained as follows [27],

$$\widehat{\mathbf{P}}_k = \frac{\mathbf{P}_k}{\alpha_k} \tag{3.13}$$

where α_k is obtained using the following switching mechanism:

$$\alpha_k = \begin{cases} 1 & \text{tr}\left(\overline{\mathbf{P}}_k\right) < \text{tr}\left(\mathbf{P}_k\right) \\ \frac{\text{tr}(\mathbf{P}_k)}{\text{tr}\left(\overline{P}_k\right)} & \text{otherwise} \end{cases} \tag{3.14}$$

In the relation above, $\overline{\mathbf{P}}$ is obtained as the follows [27],

$$\overline{\mathbf{P}}_k = \text{E}\left[d_k d_k^{\text{T}}\right] \tag{3.15}$$

which can be represented by:

$$\overline{\mathbf{P}}_k = \omega\left(d_{k-1} d_{k-1}^{\text{T}}\right) + (1-\omega)\left(d_k d_k^{\text{T}}\right) \tag{3.16}$$

In the relation above, γ is the filter coefficient which takes a value between 0 and 1. Additionally, it is worth to mention that, in order to avoid the chattering problem in adapting α the forgetting factor and smoother adaptation, technique is also applied to this adaptive

rule which leads to deriving the following relation.

$$\alpha_k = \beta\left(\alpha_{k-1}\right) + \left(1-\beta\right)\left(\alpha_k\right) \tag{3.17}$$

ω is the weighting coefficient which takes a value between 0 and 1.

3.4 Results and Discussion

In this section, the performance of the proposed method, i.e. ARKF is compared to other well-known methods such as SKF and AKF with limited-memory windowing technique, and the results are presented both by plotting the test and by computing several numerical indicators, experimentally, and in simulation. The numerical indicator that are considered for comparing the simulation results includes root mean square (RMS) and Variance (Var) of the end-effector's pose's errors. Note that in the simulation test, a PUMA 560 is implemented in Matlab/Simulink and the pose of the robot is contaminated by the noise (see Fig. 3.7 A PBVS with a PID controller is adopted to control the pose of the PUMA 560 robot to follow the desired one. In the experimental test, the C-Track from Creaform Inc. is adopted to obtain the end-effector's pose information of a FANUC robot (see Fig. 3.5).

3.4.1 Simulation Results

As mentioned before, a PUMA 560 with noisy output is implemented for the simulation test. The desired input for the robot is chosen as a spiral path in 3D space and sinusoidal path

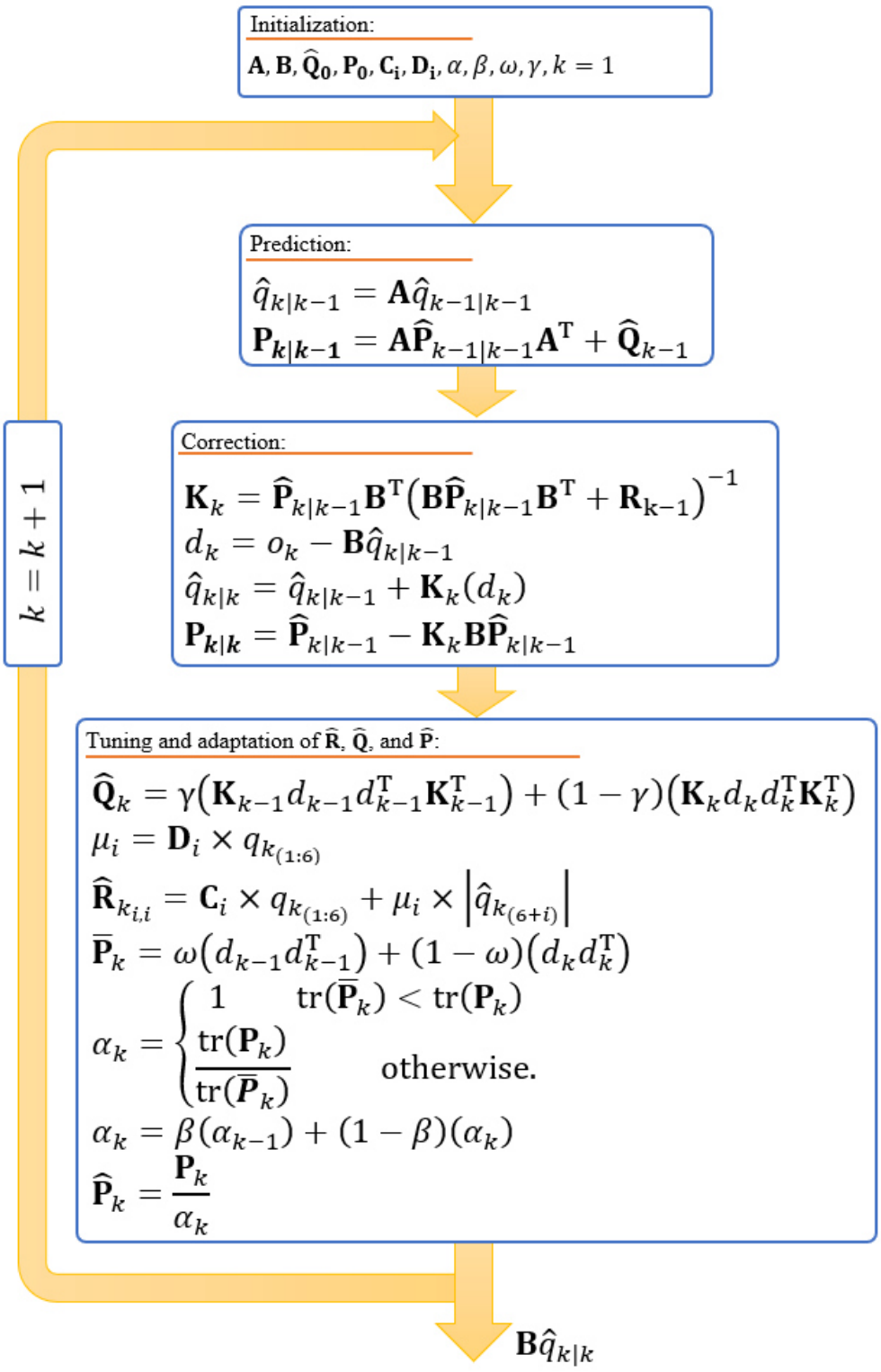

Figure 3.3: Flow chart of ARKF algorithm

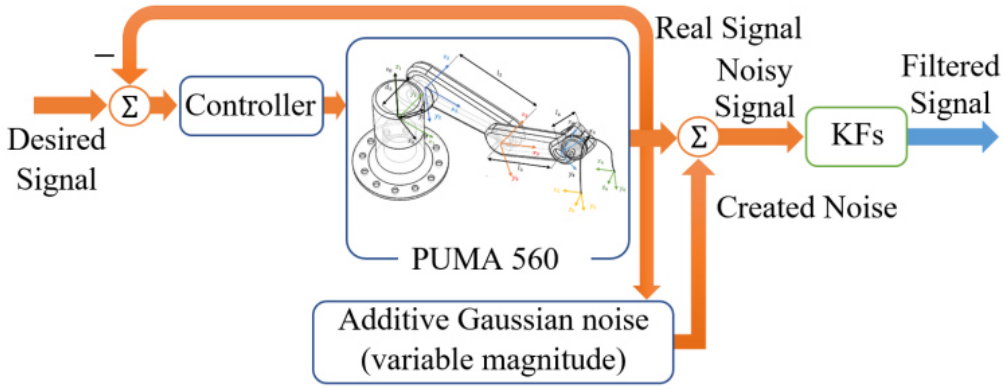

Figure 3.4: Simulation and experiment for testing the ARKF; a) Simulation's schematic.

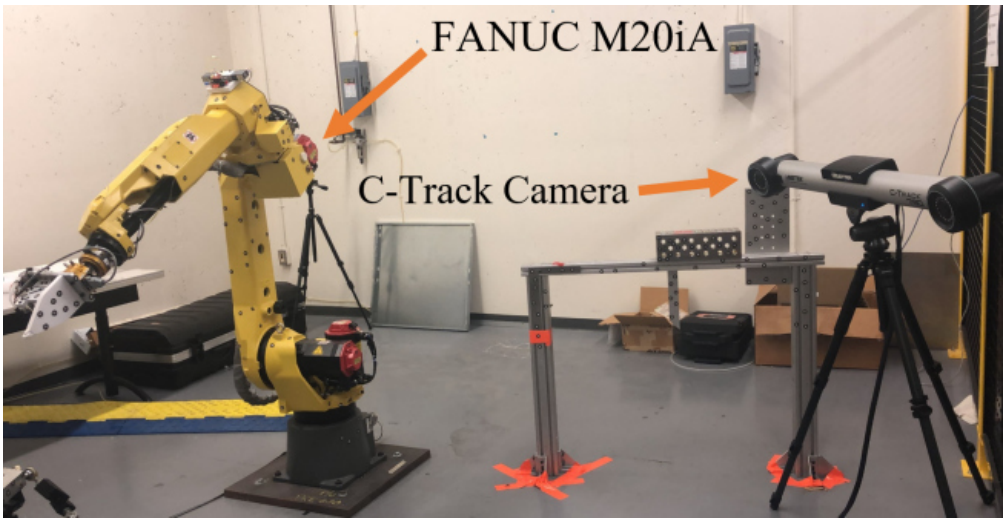

Figure 3.5: Simulation and experiment for testing the ARKF: b) Experimental setup.

for the end-effector orientation (angles) as presented in the following relation.

$$\begin{aligned} x_d &= 0.3 + 0.1\sin(t) \\ y_d &= 0.3 + 0.1\cos(t) \\ z_d &= 0.01t \\ r_d &= \tfrac{\pi}{6}\sin(t) \\ p_d &= \tfrac{\pi}{6}\cos(t) \\ w_d &= \tfrac{\pi}{6}\cos\left(t + \tfrac{\pi}{6}\right) \end{aligned} \tag{3.18}$$

The simulation results of applying ARKF, AKF, and SKF are presented in Fig. 3.6. In this figure, it is evident that the ARKF has a better performance than other KF methods in terms of smoothness and filtering errors for all state variables. The SKF have filtered the noise compared to the AKF in a smoother manner. However, it fails to track the signals properly compared to the AKF, and there exist a significant delay and error in its predictions for almost all end-effector's pose variables. In addition to simulation results' plots, the mentioned numerical indicators are evaluated and presented in Table. 3.1. According to this table, it can be seen that the values of Var and RMS indicators for all state variables are lowest for ARKF, which means the ARKF filters the noise in the signals smoother and with lowest filtering error than those of the other methods do. Overall, ARKF and AKF outperform the SKF both by comparing the values of RMS and by values of Var.

Indicator	Method	Filtered signal's error					
		e_x	e_y	e_z	e_r	e_p	e_w
RMS	SKF	7.3165	7.6855	7.8694	1.7927	1.3263	0.7434
	AKF	3.2322	1.0326	1.0153	0.9680	0.9196	0.4317
	ARKF	2.6039	0.8471	0.2615	0.8434	0.6951	0.3782
Var	SKF	51.7836	55.6627	58.0549	3.0671	1.6792	0.5381
	AKF	10.4533	1.0669	1.0305	0.9371	0.8455	0.1857
	ARKF	6.7613	0.7160	0.0684	0.6959	0.4835	0.1411

Table 3.1: RMS and Var indicators' values for the simulation test on PUMA 560

3.4.2 Experimental Results

In the experimental test, a multi-step desired signal is considered for the input of a Fanuc M20iA industrial robot and while the robot is tracking the desired signal, the pose of the robot is captured consistently by a C-track 780 dual camera in 29 frames per second (FPS). The noisy signals, captured by the camera, are filtered by the mention KFs and their results are illustrated in Fig. 3.7. As shown in the plots, the ARKF outperforms other KF methods

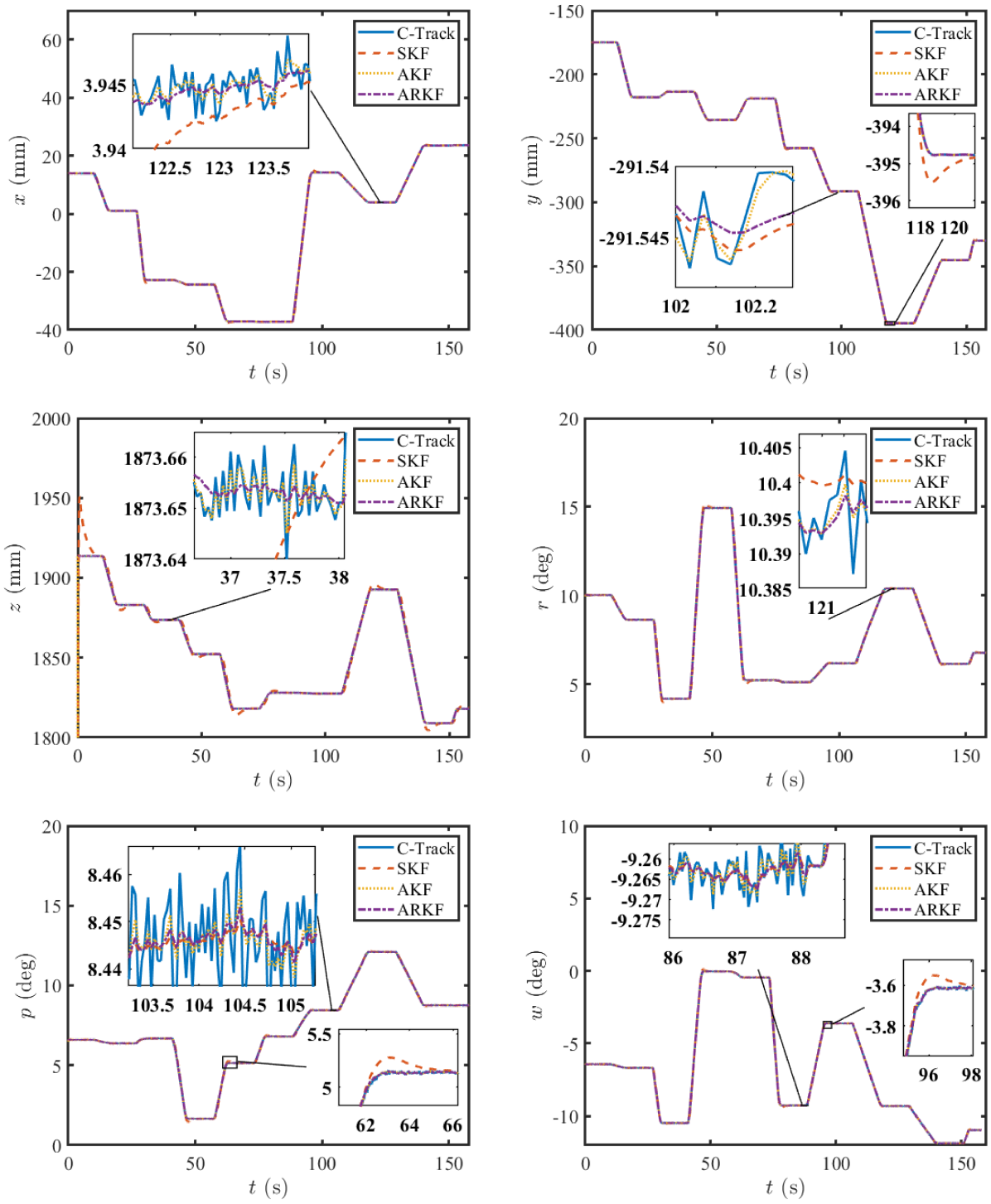

Figure 3.6: Experimental test on FANUC M20iA; a) filtering noisy signal x; b) filtering noisy signal y; c)filtering noisy signal z; d) filtering noisy signal r; e) filtering signal p; f) filtering signal w.

both in terms of smoothness and filtering errors for all state variables. It shows that the ARKF has filtered the noisy signals with higher precision than those of the other methods do. Compared with SKF, AKF tracks the signal with a lower lag. However, in terms of smoothness, the SKF is superior to AKF. These plots show that the SKF has the highest lag in tracking the signals and longest converging time specially after a high rate change in the steps' values.

3.5 Summary

In this chapter, an adaptive robust Kalman filter (ARKF) for pose estimation of industrial robots' end-effectors is proposed. The method takes advantage of an adaptive estimation method for Q, automatic least square identification for R and a robust mechanism for P. The simulation tests demonstrate that the proposed ARKF is able to reduce the effects of noise on the pose estimation signal effectively and has a superior performance to the other KF methods in terms of smoothness and filtering errors for all state variables. However, compared with SKF, AKF tracks the signal with a smaller lag. SKF has better smoothness than AK but with the largest lag and longest converging time especially when the rate change occurs.

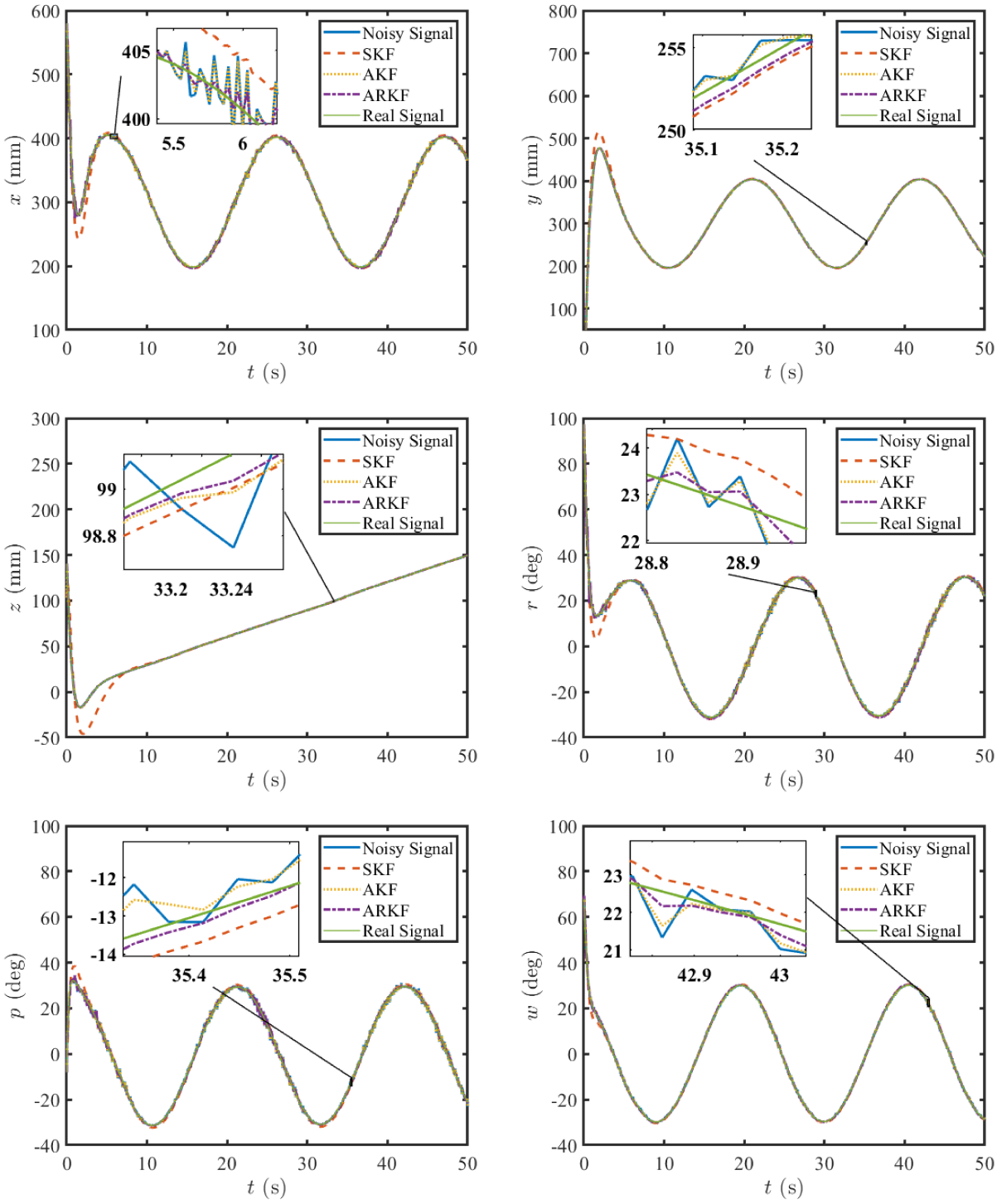

Figure 3.7: Simulation test on PUMA 560; a) filtering noisy signal x; b) filtering noisy signal y; c)filtering noisy signal z; d) filtering noisy signal r; e) filtering signal p; f) filtering signal w.

Chapter 4

Controller design

In this chapter, a novel robust position-based visual servoing (PBVS) approach for industrial robots is presented. This method combines a chattering-free fast digital sliding mode controller (FDSMC) with an adaptive robust Kalman filter (ARKF) to exploit their beneficial features. This combination results in improving the robustness and tracking performance of the robot. First, an eye-to-hand vision system (C-track) is used to detect the pose of the robot. Then, ARKF is applied to filter out the noises in the detected pose signals. These filtered signals then are fed to the FDSMC. FDSMC exploits a fast-nonlinear reaching law that provides not only robustness against uncertainties in dynamics and kinematics of the robot, but also high tracking accuracy and faster convergence speed. Furthermore, this reaching law is continuous which results in a chattering-free control process. The sliding surface of the FDSMC is also considered to be a nonlinear one, which contributes to faster convergence and decreasing the filtering error. The stability proof of the FDSMC is investigated and quasi-motion in the generated boundary layer is also analyzed.

4.1 Industrial Robot

In our research lab, we focus on the research of FANUC M20iA serial industrial robot. Since the identification techniques for modeling the FANUC M20iA is experience required and time-consuming. We use the PUMA560 robot model instead, which is an RRRRRR type robot, similar as FANUC M20iA both with 6-DOF and is regarded as one of the mature industrial robot for research and education purpose with the known mathematics description method of kinematics and dynamic parameters from previous researchers' work, to simplify the process of testing the control methodology for FANUC M20iA in order to enhance its accuracy. The controller design and entire PBVS control system response depend on both the kinematic and dynamic model of the plant which is PUMA560 in the simulation environment. Hence, modeling the PUMA560 is the first design procedure preparation. Model of robot with n-DOF can be derived by utilizing the Lagrange-Euler method as follows [143].

$$\tau = M(\theta)\ddot{\theta} + V(\theta, \dot{\theta}) + G(\theta) \tag{4.1}$$

$$\begin{aligned} \dot{x} &= A(x) + B\tau \\ y &= Cx \end{aligned} \tag{4.2}$$

$$\text{where } x = \begin{bmatrix} x_1 \\ x_2 \end{bmatrix} = \begin{bmatrix} \theta \\ \dot{\theta} \end{bmatrix}, A(x) = \begin{bmatrix} x_2 \\ M^{-1}(x)[V(x) + G(x)] \end{bmatrix}, B = \begin{bmatrix} 0 \\ M^{-1}(x) \end{bmatrix} \tag{4.3}$$

with the assumption of robot kinematic structure, the position of the tool center tip(TCP) in industrial robot manipulators is generalized from the measured joint coordinates. Errors do exist once the assumed kinematic structure differs from that of the actual manipulator.

Table 4.1: Parameters of PUMA 560 robot (Denavit-Hartenberg notation).

Link i	m $[kg]$	r_x $[m]$	r_y $[m]$	r_z $[m]$
1	0	0	0	0
2	17.4	-0.3638	0.006	0.2275
3	4.8	-0.0203	-0.0141	0.070
4	0.82	0	0.019	0
5	0.34	0	0	0
6	0.09	0	0	0.032

Table 4.2: Inertia parameters of the PUMA 560 robot. [2]

Link i	I_{xx} $[kg \cdot m^2]$	I_{yy} $[kg \cdot m^2]$	I_{zz} $[kg \cdot m^2]$	$I_{xy} = I_{yz} = I_{zx}$ $[kg \cdot m^2]$
1	0	0.35	0	0
2	0.13	0.524	0.539	0
3	0.066	0.086	0.0125	0
4	0.0018	0.0013	0.0018	0
5	0.0003	0.0004	0.0003	0
6	0.00015	0.00015	0.00004	0

Such errors may from manufacturing tolerances in link length or link distortion due to heavy load. Due to the factual tolerances during manufacturing, these invalid assumptions will reduce robot accuracy.

4.1.1 Accuracy and repeatability

Accuracy defined as the error between the measurement and command pose of the robot. Practically, the inverse kinematics must be solved for the required joint coordinate when robot moving to the desired position, even the servo system moves very accurately to the computed joint coordinates, the discrepancies between the assumed kinematic model when the designed controller and the actual robot will cause noneligible positioning errors at the TCP. Accuracy typically varies over difference workspace and could be improved by calibration which means identify the kinematic parameters for the particular robot is also demanding.

Repeatability refers to the error that a robot returns to a previously taught point. Generally, repeatability performed better than accuracy, which depends on the quality of joint servo performance. In order to exploit this capability, points must be manually taught which is time-consuming and takes the robot "strike". For example, the AdeptOne manipulator has a quoted repeatability of 15μm but accuracy of 76μm. The comparative of low accuracy and difficulty exist in applying repeatability are the main of the vindication for visual servoing [26, 50].

4.1.2 Manipulater Kinematic Parameters

Kinematics is the science of motion without regard to the forces that cause it. Once studies the position, the velocity, the acceleration, and all higher-order derivatives of the position variables with respect to time or any other variables should consider its kinematics. Hence, the study of the kinematics of manipulators refers to all the geometrical and time-based properties of the motion. The relationships among motion, force and torque cause them to establish the dynamics[144].

In this research, we use PUMA560 for the kinematic and dynamic controller design and analysis. Although the PUMA560 robot is classical compared with modern standards having poor performance. Its mechanical design such as revolute structure, geared servo motor drive, and nested control loops, independent axis control, remain typical over many modern industrial robots. The kinematic parameters of a robot are important in computing the forward and inverse kinematics of the manipulator. The kinematic constants for the PUMA560 are given in Table 4.2. These parameters are derived from several sources [145, 146]. Intrinsically, some variation exists in the link lengths and offsets provided by several previous researchers [147]. Those variations in parameters could gradually impact the design or manufacture of the robot or may be counted as errors. Hence, the kinematic parameters are of

Table 4.3: DH table of the PUMA 560 robot

Link i	α_i [°]	a_i $[m]$	d_i $[m]$	θ_i range [°]
1	190	0	0	-160 to 160
2	0	0.4318	0	-225 to 45
3	-90	0.0203	0.15005	-45 to 225
4	90	0	0.4318	-110 to 170
5	-90	0	0	-100 to 100
6	0	0	0	-266 to 266

vital importance both in kinematics and manipulator dynamics calculations. The kinematic parameters arose on the dynamic equations of motion according to the link transformation matrices 4.1.2.

$$i-1_{\mathbf{A}_i} = \begin{bmatrix} \cos\theta_i & -\sin\theta_i\cos\alpha_i & \sin\theta_i\sin\alpha_i & a_i\cos\theta_i \\ \sin\theta_i & \cos\theta_i\cos\alpha_i & -\cos\theta_i\sin\alpha_i & a_i\sin\theta_i \\ 0 & \sin\alpha_i & \cos\alpha_i & d_i \\ 0 & 0 & 0 & 1 \end{bmatrix} \tag{4.4}$$

4.1.3 Dynamic Model and Manipulator Control of PUMA560

The manipulator dynamics is about the equations of motion. The manipulator moves as the input of actuator applied torques as well as external forces. The main concern related to manipulator dynamics is inverse dynamics. It is used on solving the manipulator's equations of motion under the given motion in order to define the generalized force. In typical manipulator control, for instance, the standard Unimate controller, the torques due to inertial coupling, Coriolis, centripetal and gravity effects are treated as disturbances. Furthermore, although each axis is independently controlled, gearing helps reduce the coupling of some

dynamic effects, and the magnitude of disturbance torques from the motor. In the conventional robot regulation and tracking problem, its quality directly depends on the robustness of each axis servo. From the manipulator's equations of motion, inertial parameters and state of the manipulator, and the assigned joint torques are therefore available. The torque demand for each actuator is

$$Q = \mathbf{M}(q)\left\{K_v\left(\dot{q}_d - \dot{q}\right) + K_p\left(q_d - q\right) + \ddot{q}_d\right\} + \mathbf{C}(q,\dot{q})\dot{q} + \mathbf{F}(\dot{q}) + \mathbf{G}(\mathbf{q}) \tag{4.5}$$

where K_p and K_v are the position gain and the velocity gain or damping term respectively. The inverse dynamics are included in the control loop and must be evaluated every servo interval.

4.2 Robot Modeling and Problem Statement

Let the forward and inverse kinematics of a six-DOF industrial robot be as,

$$\begin{aligned} X &= \mathrm{FK}(\Theta) \\ \Theta &= \mathrm{IK}(X) \end{aligned} \tag{4.6}$$

where X is the robot pose, Θ is the vector of robot joints' angels and FK(.) is forward kinematic function IK(.) is inverse kinematic function that takes X and returns Θ. Additionally, the kinematic relation at the velocity level maps the joint velocities to the pose velocities as follows,

$$\dot{X} = \mathrm{J}(\Theta)\dot{\Theta} \tag{4.7}$$

where $J(\Theta)$ is the Jacobian matrix that can be derived using the following relation:

$$J(\Theta) = \frac{\partial(\mathrm{FK}(\Theta))}{\partial\Theta} \tag{4.8}$$

Note that there always exist uncertainties in kinematic relations associated with the physical parameters of the robot. Considering these uncertainties, i.e. $\dot{X} = \mathrm{J}(\Theta)\dot{\Theta}$, Eq. 4.7 can be rewritten as,

$$\dot{X} = \left(J_{\mathrm{n}}(\Theta) + \Delta_J(\Theta, t)\right)\dot{\Theta} \tag{4.9}$$

where $J_n(\theta)$ is the nominal Jacobian and Δ_J is the uncertainty of the Jacobian. In order to control the pose of the robot, its end-effector position and orientation must be measured. To this end, the data can be obtained by using the C-track and the designed ARKF. However, the detected pose signals are contaminated with noise emanated low regulation of the cameras, low light of the environment or fading issues [36]. Schematic of a six-DOF industrial robot (PUMA-560) equipped with a camera with an ETH configuration is depicted in Figure 4.1. The main problem of position-based visual servoing of the mentioned system is to design a control scheme that is robust against the vision system noisy signal and the existing uncertainties. A competent controller should also be fast and accurate. The solution to this control problem is investigated in the following section.

The dynamics and kinematics a series six-DOF industrial robot are modeled as the following pair of relations [3]:

$$\begin{aligned} &\left(\mathbf{M_n}(q) + \boldsymbol{\delta}\mathbf{M}(q)\right)\ddot{q} + \left(\mathbf{C_n}(q,\dot{q}) + \boldsymbol{\delta}\mathbf{C}(q,\dot{q})\right)\dot{q} + \left(G_n(q) + \delta G(q)\right) + D(q,\dot{q},t) = \tau \\ &\dot{X} = \left(\mathbf{J_n}(\mathbf{q}) + \boldsymbol{\delta}\mathbf{J}(\mathbf{q})\right)\dot{q} + d(q,\dot{q},t) \end{aligned} \tag{4.10}$$

where $X \in R^6$ is the robot's pose and $q \in R^6$ is the vector of robot joint angels, $\mathbf{M_n}(q) \in R^{6\times6}$ is the nominal inertia matrix, $\mathbf{C_n}(q) \in R^{6\times6}$ is the nominal matrix of centrifugal and Coriolis forces, $\mathbf{G_n}(q) \in R^6$ is the nominal vector of gravitational torques, $D(q,\dot{q},t) \in R^6$ is the vector

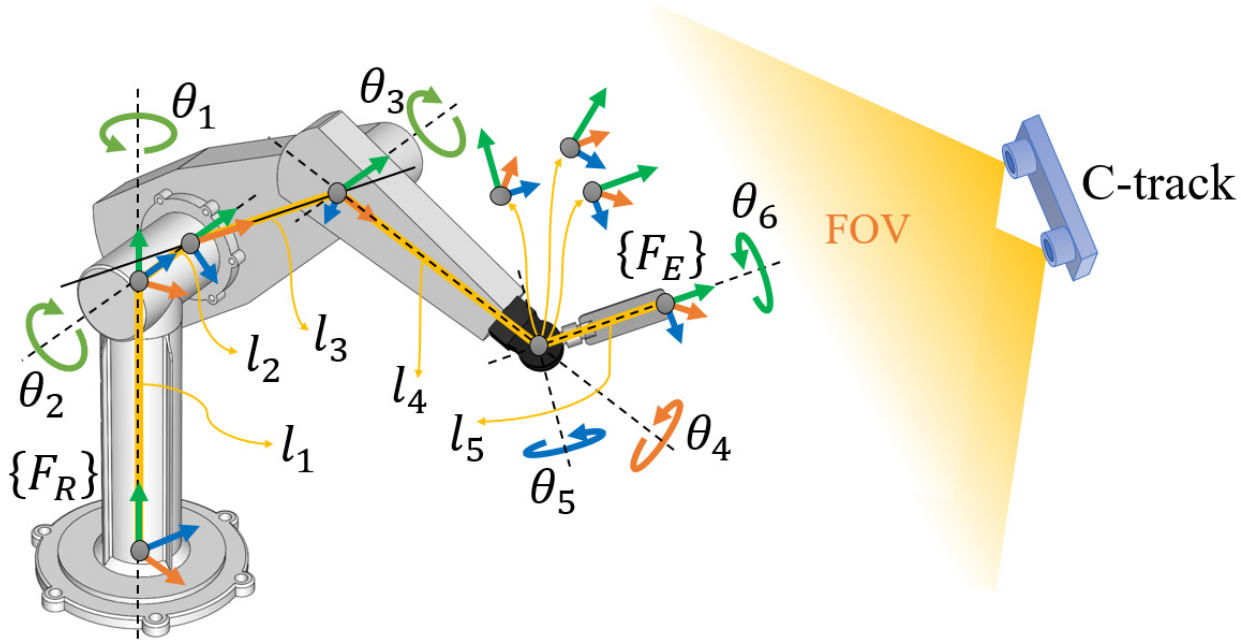

Figure 4.1: Schematic of a six-DOF industrial robot (PUMA 560) equipped with a camera with an ETH configuration

of external disturbances exerted to the system dynamics, and $\tau \in R^6$ denotes the system input (the controller output). $\mathrm{J_n(q)} \in R^{6\times6}$ is the nominal Jacobian matrix which relates that of velocity of the robot pose to the robot joints, $d(q, \dot{q}, t) \in R^6$ is the external disturbance which affects the kinematics. $\boldsymbol{\delta}\mathbf{M}(q) \in R^{6\times6}, \boldsymbol{\delta C}(q, \dot{q}) \in R^{6\times6}, \delta G(q) \in R^6$ and $\boldsymbol{\delta}\mathbf{J}(q) \in R^6$ are the matrices and vectors written in compact forms denoting the uncertain parts of the dynamics and kinematics of the robot system. The pair relations of Eq. 4.10 can be rewritten in compact forms as follows:

$$\begin{aligned} \ddot{q} &= f_n(q, \dot{q}) + \mathbf{g_n}(q)\tau + \Delta_q \\ \dot{X} &= \mathbf{J_n}(q)\dot{q} + \Delta_X \end{aligned} \tag{4.11}$$

where,

$$\begin{aligned}
&\Delta_q = (\mathbf{M}(q))^{-1}(-\boldsymbol{\delta}\mathbf{M}(q)\ddot{q} - \boldsymbol{\delta}\mathbf{C}(q,\dot{q})\dot{q} - D(q,\dot{q},t)) \\
&\Delta_X = \boldsymbol{\delta}\mathbf{J}(q)\dot{q} + d(q,\dot{q},t) \\
&f_n(q,\dot{q}) = (\mathbf{M_n}(q))^{-1}(-\mathbf{C_n}(q,\dot{q})\dot{q} - G_n(q)) \\
&\mathbf{g_n}(q) = (\mathbf{M}(q))^{-1}
\end{aligned} \tag{4.12}$$

The presented relations are derived to be used in controller designing. However, as discussed in Section 4.1, the derived controller will be discretized to be implementable on digital computers and devices. Therefore, it would be more convenient to design the controller in discrete dime domain in the first place [148]. To this end, the dynamics and kinematics of the robot should be converted to discrete time models. Using forward finite-difference technique for first and second derivatives, i.e.,

$$\dot{x}(t) \equiv \frac{x_k - x_{k-1}}{T} \tag{4.13}$$

and

$$\ddot{x}(t) \equiv \frac{x_{k+1} - 2x_k + x_{k-1}}{T^2} \tag{4.14}$$

where T is the sampling time, k is the sampling index. Hence Eq. 4.11 and can be discretized to the following relations:

$$\begin{aligned}
\tfrac{q_{k+1}-2q_k+q_{k-1}}{T^2} &= f_n(q_k, q_{k-1}) + \mathbf{g_n}(q_k, q_{k-1})\tau_k + \Delta_q \\
\tfrac{X_{k+1}-2X_k+X_{k-1}}{T^2} &= \left(\tfrac{\mathbf{J_n}(q_k)-\mathbf{J_n}(q_{k-1})}{T}\right)\left(\tfrac{q_k-q_{k-1}}{T}\right) + \mathbf{J_n}(q_k)\left(\tfrac{q_{k+1}-2q_k+q_{k-1}}{T^2}\right) + \dot{\Delta}_X
\end{aligned} \tag{4.15}$$

The main target of position-based visual servoing of the mentioned system is to increase the accuracy of the industrial robot by using C-track and designing a control scheme that is robust against the vision system noise and the existing uncertainties. The solution to this control problem is investigated in the following section.

4.2.1 Adaptive Robust Kalman Filter

To implement the KF the measurement equations of the end-effector of a six-DOF industrial robot are usually considered as follows [37].

$$\begin{cases} \eta_k = \mathbf{A}\eta_{k-1} + w_{k-1} \\ X_k = \mathbf{B}\eta_k + v_k \end{cases}, w_{k-1} \sim \mathrm{N}(0, \mathbf{Q}), v_k \sim \mathrm{N}(0, \mathbf{R}) \tag{4.16}$$

where, $\eta = \begin{bmatrix} X^{\mathrm{T}} & \dot{X}^{\mathrm{T}} \end{bmatrix}^{\mathrm{T}} \in R^{12}$ is the vector of state variables, $w \in R^{12}$ is the vector of state noise with the covariance matrix Q, $v \in R^6$ is the measurement noise vector with the covariance matrix R, and $X_k \in R^6$ is the vector of noisy signals of the robot pose acquired from vision system. Matrix $\mathbf{A} \in R^{12\times12}$ matrix of the state transition with the diagonal elements of 1 and $\mathbf{A}_{i,i+6}(i = 1, \ldots, 6)$ equal to the sampling interval T_s, and $\mathbf{B} = \begin{bmatrix} \mathbf{I}_{6\times6} & \mathbf{0}_{6\times6} \end{bmatrix}$ is the output matrix transformation [16]. Note that subscript k indicates the time instant. The standard KF handles a noisy signal into two stages: prediction and correction. Using Eq. 4.17 and Eq. 4.18, KF predicts the current state based on the previous data [140].

$$\hat{\eta}_{k|k-1} = \mathbf{A}\hat{\eta}_{k-1|k-1} \tag{4.17}$$

$$\mathbf{P}_{k|k-1} = \mathbf{A}\mathbf{P}_{k-1|k-1}\mathbf{A}^T + \mathbf{Q}_{k-1} \tag{4.18}$$

$$\hat{\eta}_{k|k} = \hat{\eta}_{k|k-1} + \mathbf{K}_k\left(d_k\right) \tag{4.19}$$

$$\mathbf{P}_{\boldsymbol{k|k}} = \mathbf{P}_{k|k-1} - \mathbf{K}_k\mathbf{B}\mathbf{P}_{k|k-1} \tag{4.20}$$

where $\hat{\eta}$ is the estimation of η, P is the covariance matrix of the errors of the state variables. After obtaining the predictions of the state variables, one has to correct the prediction using Eq. 4.19 and Eq. 4.20 [49]. d_k and K_k are the residual and Kalman filter gain respectively, and are obtained as,

$$d_k = X_k - \mathbf{B}\hat{\eta}_{k|k-1} \tag{4.21}$$

$$\mathbf{K}_k = \mathbf{P}_{k|k-1}\mathbf{B}^{\mathrm{T}}\left(\mathbf{B}\mathbf{P}_{k|k-1}\mathbf{B}^{\mathrm{T}} + \mathbf{R}_{\mathrm{k-1}}\right)^{-1} \tag{4.22}$$

Accordingly, the filtered signal of the robot pose can be obtained as $\hat{X}_k = \mathbf{B}\hat{\eta}_{k|k}$. Setting the entries of Q is a demanding task. Besides, their improper tuning may result in undesired filtering [49]. Therefore, a solution to this problem is to update the entries of Q adaptively. Based on the forgetting factor technique, ARKF presented in [37] suggests that $\hat{Q}$ which is the estimation of Q, can be adaptively updated using the following relation.

$$\widehat{\mathbf{Q}}_k = \gamma\left(\mathbf{K}_{k-1}d_{k-1}d_{k-1}^{\mathrm{T}}\mathbf{K}_{k-1}^{\mathrm{T}}\right) + (1-\gamma)\left(\mathbf{K}_k d_k d_k^{\mathrm{T}}\mathbf{K}_k^{\mathrm{T}}\right) \tag{4.23}$$

where, γ is the forgetting factor coefficient which takes a value between 0 and 1.

Since R is the covariance matrix of the measurement noises, it is possible to estimate its entries by taking numerical samples. Following this idea, in the case of visual servoing, one possible task is to get the data from the visual system whenever the robot is in a stationary status and estimate R as $\hat{R}$. However, it has been observed that R entries vary by the end-effector moves from one point to another or with different velocities caused by delay, blur, and vibration during image acquisition. To cope with this problem, the following tuning method for R was suggested by Wu et al. [37],

$$\widehat{\mathbf{R}}_k = \left| \widehat{\mathbf{R}}_{s_k} + \widehat{\mathbf{R}}_{v_k} \right| \tag{4.24}$$

where $\widehat{\mathbf{R}}_s$ and $\widehat{\mathbf{R}}_v$ are the covariances of noise measurement when the robot is stationary and moving respectively. $\widehat{\mathbf{R}}_s$ and $\widehat{\mathbf{R}}_v$ are evaluated utilizing the following relations,

$$\widehat{\mathbf{R}}_{s_{k_{i,i}}} = \mathbf{C}_i \times \eta_{k_{(1:6)}} \tag{4.25}$$

$$\widehat{\mathbf{R}}_{v_{k_{i,i}}} = \mu_i \times \left| \eta_{k_{(6+i)}} \right| \tag{4.26}$$

where, μ_1 to μ_6 are positive constant weights and $\mathbf{C}_i$ is the regressor vector whose entries are computed by applying the least square error (LSE) identification method [142] based on the collected data from several tests on the robot. μ_i is considered to depend on the position and orientation variables as follows [37]:

$$\mu_i = \mathbf{D}_i \times q_{k_{(1:6)}} \tag{4.27}$$

In the relation above, $\mathbf{D}_i$ is the regressor vector, whose entries are calculated by using the same method employed for $\mathbf{C}_i$, and using the collected data from several tests on the robot when it is moving with constant speed. Both $\widehat{\mathbf{R}}_s$ and $\widehat{\mathbf{R}}_v$ are diagonal matrices [37]. The existing uncertainties in the robot model may result in in accurate estimation of P. To cope with this issue, an adaptive robust correction method is suggested [27]. In this method, the estimation of P and the theoretical evaluated $\overline{\mathbf{P}}$ are compared. A correction factor α is adopted to compensate the inaccuracy of P. The compensated P, i.e. $\overline{\mathbf{P}}$ is obtained as follows [27],

$$\widehat{\mathbf{P}}_k = \mathbf{P}_k / \hat{\alpha}_k \tag{4.28}$$

where $\hat{\alpha}_k$ is obtained using the following switching mechanism:

$$\hat{\alpha}_k = \beta\left(\hat{\alpha}_{k-1}\right) + (1-\beta)\left(\alpha_k\right) \tag{4.29}$$

where $\hat{\alpha}_k$ is computed by Eq. 3.14 and β is the forgetting factor coefficient which valued between 0 and 1.

$$\alpha_k = \begin{cases} 1 & \text{tr}\left(\overline{\mathbf{P}}_k\right) < \text{tr}\left(\mathbf{P}_k\right) \\ \text{tr}\left(\mathbf{P}_k\right) / \text{tr}\left(\bar{P}_k\right) & \text{otherwise} \end{cases} \tag{4.30}$$

In Eq. 4.30, $\overline{\mathbf{P}}$ is obtained as follows [37],

$$\overline{\mathbf{P}}_k = \omega\left(d_{k-1}d_{k-1}^{\mathrm{T}}\right) + (1-\omega)\left(d_k d_k^{\mathrm{T}}\right) \tag{4.31}$$

where ω is the filter coefficient which takes a value between 0 and 1.

4.2.2 Chattering-free Digital Fast Sliding Mode Control Method

The objective of the designing a PBVS is to steers the error of the robot's pose to zero. The error of the robot's pose e_X is:

$$e_{X_k} = \hat{X}_k - X_{d_k} \tag{4.32}$$

where X_d is the desired pose. Based on Eq. 4.14, the first and second derivative of Eq. 4.32 are as follows:

$$\frac{\left(e_{X_k} - e_{X_{k-1}}\right)}{T} = \frac{\left(\hat{X}_k - \hat{X}_{k-1}\right)}{T} - \frac{\left(X_{d_k} - X_{d_{k-1}}\right)}{T} \tag{4.33}$$

$$\frac{\left(e_{X_{k+1}-2e_{X_k}+e_{X_{k-1}}}\right)}{T^2} = \frac{\left(\hat{X}_{k+1} - 2\hat{X}_k + \hat{X}_{k-1}\right)}{T^2} - \frac{\left(X_{d_{k+1}} - 2X_{d_k} + X_{d_{k-1}}\right)}{T^2} \tag{4.34}$$

In order to design and SMC, first a sliding variable must be defined. In this study, the sliding variable considered to be a nonlinear one as follows:

$$\sigma_k = \frac{\left(e_{X_k} - e_{X_{k-1}}\right)}{T} + \Lambda_1 \times \tanh\left(\Lambda_2 \times e_{X_{k-1}}\right) \tag{4.35}$$

In the relation above, Λ_1 and Λ_2 are 6×6 diagonal positive definite matrices of the sliding surface coefficients. Note that $\sigma = 0$ is the sliding surface and it must be asymptotically stable. This issue is investigated in Theorem 1. In discrete time domain, the control processes of SMC comprises of two: reaching phase, and Quasi -sliding motion [149]. The SMC law should be defined in a way that the sliding variable converges towards zero, i.e. sliding surface. This is the reaching phase. Once it reaches the vicinity of the sliding surface, it is trapped in a boundary layer, and cannot escape out. This is the Quasi-motion phase. the two phases of an SMC in discrete time domain is shown in Fig. 4.2. In order to let the robot system present as Eq. 4.15 to comply with the above-mentioned conditions of SMC, the following chattering-free fast control law is considered.

$$\begin{aligned}\tau_k = \left(\mathrm{J_n}\left(q_k\right)\mathbf{g}\left(q_k, q_{k-1}\right)\right)^{-1}\Big(-\left(\mathrm{f}_\sigma\left(\sigma_k\right)\right) - \left(\tfrac{\mathrm{J_n}(q_k)_k - \mathrm{J_n}(q_k)_{k-1}}{T}\right)\left(\tfrac{q_k - q_{k-1}}{T}\right) - \\ \mathrm{J_n}\left(q_k\right) f_n\left(q_k, q_{k-1}\right) + \tfrac{x_{d_{k+1}} - 2X_{d_k} + X_d}{T^2} - \tfrac{\Lambda_1(\tanh(\Lambda_2 e_k) - \tanh(\Lambda_2 e_{k-1}))}{T}\Big)\end{aligned} \tag{4.36}$$

with,

$$\mathrm{f}_\sigma\left(\sigma_k\right) = \mathrm{sat}\left(K_1\sigma_k + K_2\left|\sigma_k\right|^\alpha \mathrm{sign}\left(\sigma_k\right) + K_3\left|\sigma_k\right|^\beta \mathrm{sign}\left(\sigma_k\right)\right) \tag{4.37}$$

In the relation above, K_1 to K_1 are 6×6 diagonal positive definite matrices of the reaching law, α and β are positive constant powers of the nonlinear functions. The influence of each term is stated in Remark-1. Note that α is higher than 0 and lower than 1, whereas, beta is higher than 1. Therefore, the second term take effects when the error is rather low and the

third term takes effect when the error is rather high. $sat(.)$ is the saturating linear transfer function with the following relation:

$$\text{sat}(x) = \begin{cases} K_0, & x \geq K_0 \\ x, & -K_0 < x < K_0 \\ -K_0, & x \leq -K_0 \end{cases} \tag{4.38}$$

where, K_0 is the threshold of the saturation. The idea behind adopting $sat(.)$ is to prevent the generation of excessive value of controller output at the beginning of the reaching phase [117]. The block diagram of the proposed robust visual servoing controller is shown in Figure 4.2. Also, the stability proof of the closed-loop system of the robot under the control law of Eq. 4.36 is investigated in Theorem 2. However, Assumption 1 must be held beforehand. The block diagram of the proposed robust visual servoing controller is shown in Fig 4.2.

Assumption 1. *δ_L is bounded as follows,*

$$|\Delta_{\mathrm{L}}| < \delta_{\mathrm{L}} \tag{4.39}$$

where, σ_L is a 6×1 vector with positive elements and δ_L is:

$$\Delta_{\mathrm{L}} = \Delta_{q_k} + \mathrm{J_n}\left(q_k\right) \dot{\Delta}_{X_k} \tag{4.40}$$

Theorem 1 (Stability of the nonlinear sliding surface) Considering the sliding variable as given in Eq. 4.35, the sliding surface, i.e., $\sigma_k = 0$ is asymptotically stable if the following

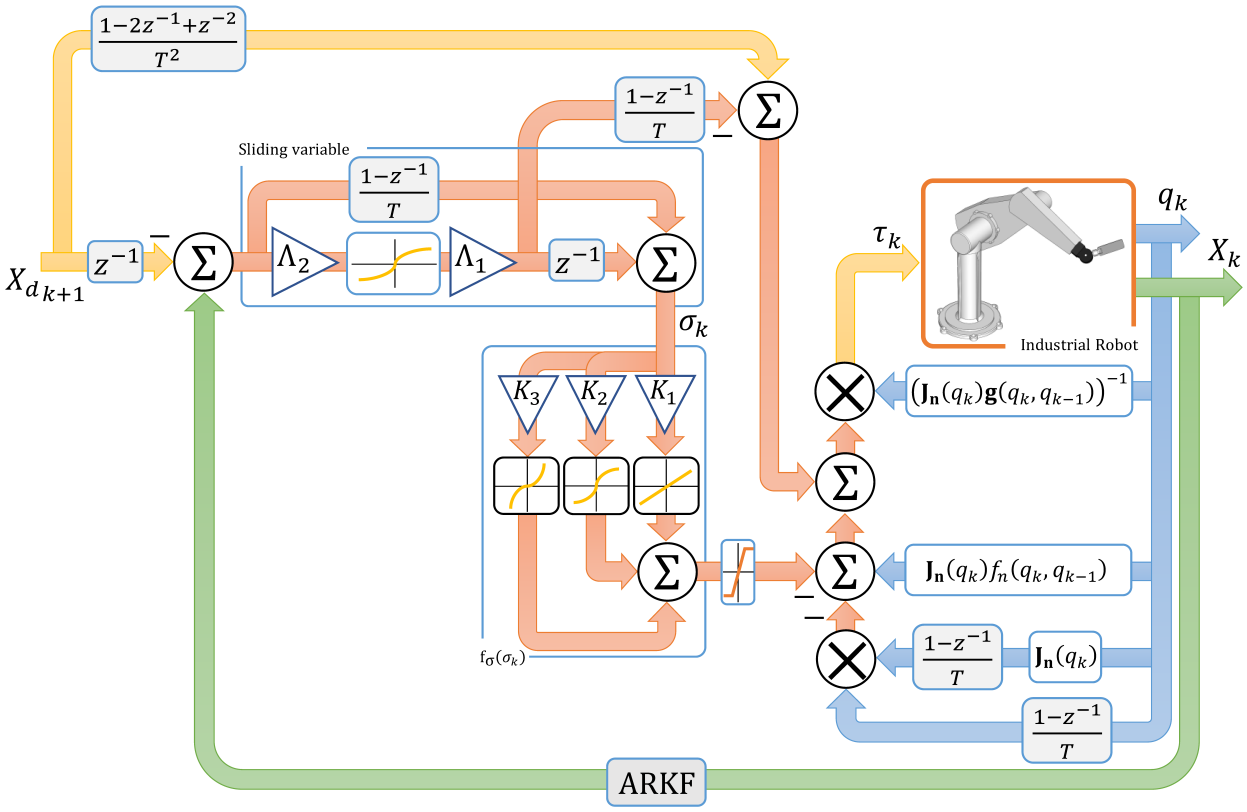

Figure 4.2: Schematic of the proposed controllers.

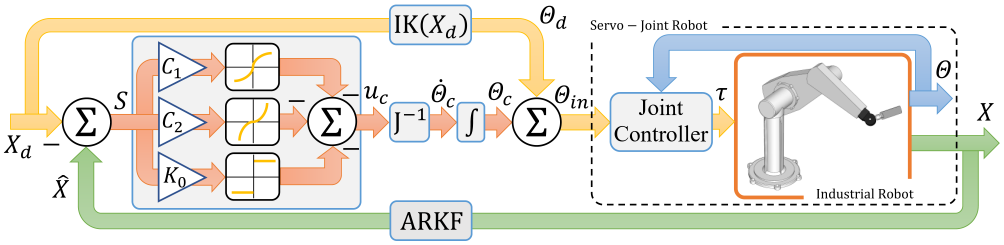

Figure 4.3: Schematic of the proposed controllers: a) FSMC.

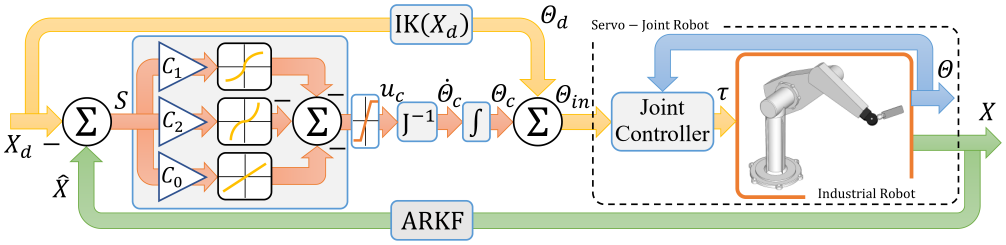

Figure 4.4: Schematic of the proposed controllers:b) chattering-free FSMC.

condition is satisfied.

$$\Lambda_1 < \frac{2}{T}\Lambda_2^{-1} \tag{4.41}$$

Proof. Let the candidate Lyapunov function $V_e\left(e_{X_{k-1}}\right)$ and its time difference $\Delta \mathrm{V}\left(e_{X_k}\right)$ for the system error be as Eq. 4.40.

$$\begin{aligned} &V_e\left(e_{X_{k-1}}\right) = e_{X_{k-1}}^{\mathrm{T}} e_{X_{k-1}} \\ &\Delta V_e\left(e_{X_k}\right) = V_e\left(e_{X_k}\right) - V\left(e_{X_{k-1}}\right) = e_{X_k}^{\mathrm{T}} e_{X_k} - e_X^{\mathrm{T}} e_{k-1} e_{X_{k-1}} \end{aligned} \tag{4.42}$$

By putting$\sigma_K = 0$ in Eq. 4.35, the following relation yields:

$$e_{X_k} = -T\left(\Lambda_1 \times \tanh\left(\Lambda_2 \times e_{X_{k-1}}\right)\right) + e_{X_{k-1}} \tag{4.43}$$

Substituting the relation above into Eq. 4.42 results in:

$$\begin{aligned} \Delta V_e\left(e_{X_k}\right) = &\left(-T\left(\Lambda_1 \times \tanh\left(\Lambda_2 \times e_{X_{k-1}}\right)\right) + e_{X_{k-1}}\right)^{\mathrm{T}} \left(-T\left(\Lambda_1 \times \tanh\left(\Lambda_2 \times\right.\right.\right. \\ &\left.\left.\left. e_{X_{k-1}}\right)\right) + e_{X_{k-1}}\right) - e_{X_{k-1}^{\mathrm{T}}} e_{X_{k-1}} \end{aligned} \tag{4.44}$$

Referring to the relation above, when $e_{x_k} = 0, \Delta V_e\left(e_{x_k}\right) = 0$. For $e_{X_k} \neq 0$, from inequality of Eq. 4.39, the following relation is concluded:

$$\left|-T\left(\Lambda_1 \times \tanh\left(\Lambda_2 \times e_{X_{k-1}}\right)\right)\right| < 2\left|e_{k-1}\right| \tag{4.45}$$

Accordingly, since $-T\left(\Lambda_1 \times \tanh\left(\Lambda_2 \times e_{X_{k-1}}\right)\right)$ and e_{k-1} have the opposite signs. Therefore, $\left|-T\left(\Lambda_1 \times \tanh\left(\Lambda_2 \times e_{X_{k-1}}\right)\right) + e_{X_{k-1}}\right| < \left|e_{X_{k-1}}\right|$ and thus,$\Delta V_e\left(e_{X_k}\right) < 0$. □

This proves that the defined sliding surface is asymptotically stable [150].

Theorem 2 (Stability of chattering-free DFSMC) If the conditions in Eq. 4.46 and

Assumption 1 are satisfied, the control law of Eq.4.36 makes the system of Eq.4.15 stable as an sliding mode with quasi-motion.

$$\begin{aligned} &K_0 > \mathrm{f}_\sigma\left(C_0\right), \mathrm{f}_\sigma\left(C_0\right) > \delta_{\mathrm{L}}, \quad C_0, K_1, K_2, K_3 > 0, \quad 0 < \alpha < 1, \beta > 1 \\ &\left|2\sigma_k\right| > \left|T\left(\mathrm{f}_\sigma\left(\sigma_k\right) + \mathrm{f}_\sigma\left(C_0\right)\right)\right| \end{aligned} \tag{4.46}$$

$$\Lambda_1 < \frac{2}{T}\Lambda_2^{-1} \tag{4.47}$$

$$\begin{aligned} &V\left(\sigma_k\right) = \sigma_k^{\mathrm{T}}\sigma_k \\ &\Delta V\left(\sigma_{k+1}\right) = V\left(\sigma_{k+1}\right) - V\left(\sigma_k\right) = \sigma_{k+1}^{\mathrm{T}}\sigma_{k+1} - \sigma_k^{\mathrm{T}}\sigma_k \end{aligned} \tag{4.48}$$

Proof. Let the candidate Lyapunov function $V_e\left(e_{X_{k-1}}\right)$ and its time difference $\Delta \mathrm{V}\left(e_{X_k}\right)$ for the sliding variable of Eq. 4.35 be as Eq. 4.48.

Based on Eq. 4.35, the following can be obtained:

$$\sigma_{k+1} = T\left(\frac{X_{k+1} - 2X_k + X_{k-1}}{T^2} - \frac{X_{d_{k+1}} - 2X_{d_k} + X_{d_{k-1}}}{T^2} + \frac{\Lambda_1\left(\tanh\left(\Lambda_2 e_k\right) - \tanh\left(\Lambda_2 e_{k-1}\right)\right)}{T}\right) + \sigma_k \tag{4.49}$$

which can be rewritten as:

$$\sigma_{k+1} = T\left(\frac{X_{k+1} - 2X_k + X_{k-1}}{T^2} - \frac{X_{d_{k+1}} - 2X_{d_k} + X_{d_{k-1}}}{T^2} + \frac{\Lambda_1\left(\tanh\left(\Lambda_2 e_k\right) - \tanh\left(\Lambda_2 e_{k-1}\right)\right)}{T}\right) + \sigma_k \tag{4.50}$$

Substituting Eq. 4.15 into Eq. 4.50 yields:

$$\begin{aligned} \sigma_{k+1} = T\Bigg(&\left(\frac{\mathrm{J_n}(q_k) - \mathrm{J_n}(q_{k-1})}{T}\right)\left(\frac{q_k - q_{k-1}}{T}\right) + \mathrm{J_n}\left(q_k\right)\left(\frac{q_{k+1} - 2q_k + q_{k-1}}{T^2}\right) + \dot{\Delta}_{X_k}\Bigg) - \\ &\frac{X_{d_{k+1}} - 2X_{d_k} + X_{d_{k-1}}}{T^2} + \frac{\Lambda_1(\tanh(\Lambda_2 e_k) - \tanh(\Lambda_2 e_{k-1}))}{T}\Bigg) + \sigma_k \end{aligned} \tag{4.51}$$

Substituting Eq. 4.15 into Eq. 4.51 yields:

$$\sigma_{k+1} = T\left(\left(\frac{\ln(q_k)-\mathrm{J_n}(q_{k-1})}{T}\right)\left(\frac{q_k-q_{k-1}}{T}\right) + \mathbf{J_n}\left(q_k\right)\left(f_n\left(q_k,q_{k-1}\right) + \mathbf{g_n}\left(q_k,q_{k-1}\right)\tau_k + \Delta_{q_k}\right) + \dot{\Delta}_{X_k}\right) - \frac{X_{d_{k+1}}-2X_{d_k}+X_{d_{k-1}}}{T^2} + \frac{\Lambda_1(\tanh(\Lambda_2 e_k)-\tanh(\Lambda_2 e_{k-1}))}{T}\Bigg) + \sigma_k \tag{4.52}$$

Then, substituting Eq. 4.36 into Eq. 4.52 results in:

$$\sigma_{k+1} = T\left(-f_\sigma\left(\sigma_k\right) + \Delta_{q_k} + J_n\left(q_k\right)\dot{\Delta}_{X_k}\right) + \sigma_k \tag{4.53}$$

Substituting relation above in Eq.4.48 yields:

$$\Delta V\left(\sigma_{k+1}\right) = \left(T\left(-\mathrm{f}_\sigma\left(\sigma_k\right) + \Delta_{q_k} + \mathrm{J_n}\left(q_k\right)\dot{\Delta}_{X_k}\right) + \sigma_k\right)^{\mathrm{T}}\left(T\left(-\mathrm{f}_\sigma\left(\sigma_k\right) + \Delta_{q_k} + \mathrm{J_n}\left(q_k\right)\dot{\Delta}_{X_k}\right) + \sigma_k\right) - \sigma_k^{\mathrm{T}}\sigma_k \tag{4.54}$$

□

Considering the above-mentioned conditions and Assumption 1, Lemma 1 can be applied to Eq.4.54. Based on Lemma 1, when $|\sigma_k| > C_0, \Delta V\left(\sigma_{k+1}\right)$ in Eq. 4.54 is negative. It is the reaching phase. It means that σ_k would be converging towards the sliding surface until $|\sigma_k| \leq C_0$. Thereafter, $|\sigma_k| \leq C_0$ holds, and as a result σ_k performs a Quasi motion in the boundary layer.

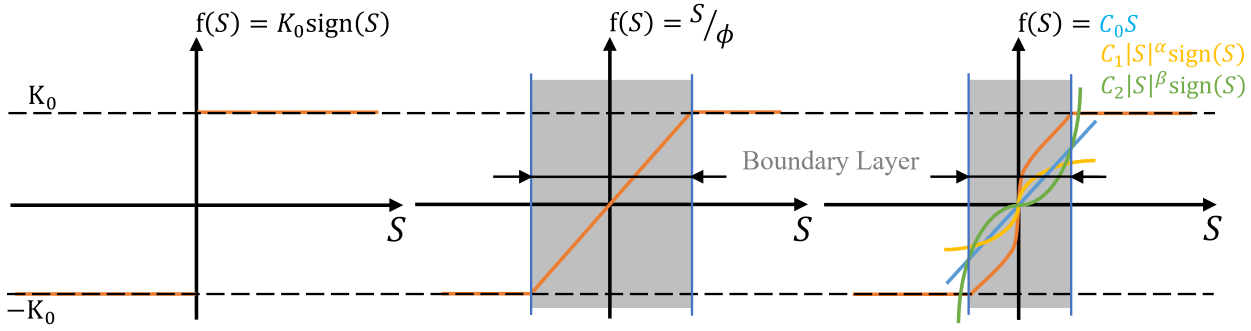

Figure 4.5: Different types of reaching laws for SMC

Lemma 1. *Assume that* $|\Delta| < \Delta_A, \Delta_\mathrm{A} < |f_A\left(x_A\right)|$, *and* $|2x| > |t\left(|f_A(x)| + f_A\left(x_A\right)\right)|$ *where*

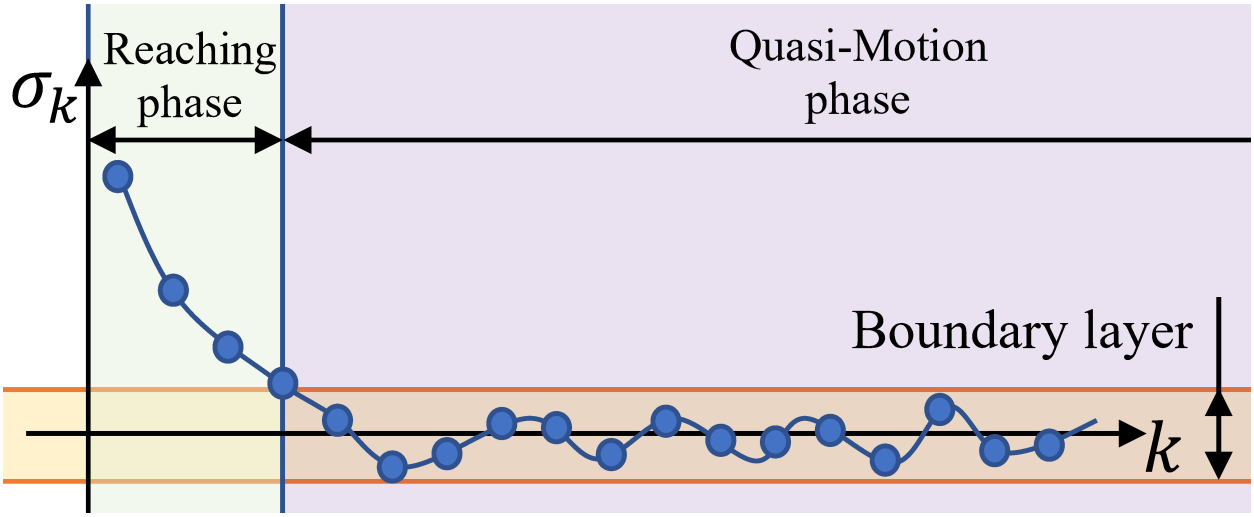

Figure 4.6: Reaching phase and Quasi-motion phase in DSMC

$f_A(x_A)$ is an ascendant and odd function, $x_A > 0, t > 0$, and $\delta_A > 0$. Then, for $|x| > x_A$ the following relation holds.

$$\left(t\left(-f_A(x)+\Delta\right)+x\right)^{\mathrm{T}}\left(t\left(-f_A(x)+\Delta\right)+x\right)-x^{\mathrm{T}}x<0 \tag{4.55}$$

Proof. Since $f_A(.)$ is ascendant and odd, for $|x| > x_A, \Delta_{\mathrm{A}} < |f_A(x)|$. Also, $|\Delta| \leq \Delta_A$. Accordingly, $|\Delta| < |f_A(x)|$. Therefore, $-f_{A(x)}$ dominates δ and thus signs of $t(-f_{A(x)}+\delta)$ and x are always the opposite of each other, i.e.

$$\operatorname{sign}\left(-f_A(x)+\Delta\right)=-\operatorname{sign}(x) \tag{4.56}$$

Additionally, since$|\Delta| < |f_A(x_A)| \leq |f_A(x)|$, then one has:

$$t\left|-f_A(x)+\Delta\right|<t\left(\left|f_A(x)\right|+f_A\left(x_A\right)\right) \tag{4.57}$$

Based on Eq. 4.56 and Eq. 4.57 and given that $|2x| > |t(|f_A(x)|+f_A(x_A))|$, it can be deduced

that $t\,|-f_A(x)+\Delta| < |2x|$ and thus $|t\,(-f_A(x)+\Delta)+x| < |x|$. Accordingly inequality Eq. 4.55 holds [144].

□

4.3 Summary

In this chapter, a robust PBVS approach for industrial robots based on FSMC and ARKF is suggested. ARKF filters out the noise of the robot's pose that is detected by the C-track. The FSMC takes advantage of a nonlinear reaching law which results in faster and more accurate trajectory tracking compared to standard SMC. Substituting the switching function with a linear function and a saturate function to the overall reaching law also leads to a continuous output and thus eliminating the chattering. In the next chapter, a simulation of applying the proposed method to a PUMA 560 robot will be carried out to validate the superiority of the proposed method over standard SMC and SMC with saturated output in terms of chattering level, precision, and convergence speed.

Chapter 5

Matlab Simulation of Vision Servoing System

In this chapter, we aim at evaluating the performance of the proposed method. A PUMA 560 robot is therefore modeled in the SimScape toolbox (formerly known as SimMechanics) of MATLAB software. The physical parameters of the robot are taken from Ref. [151]. The robot's pose contaminated with additive noise is assumed to be the given pose detected by the visual system C-track. Note that the additive noise is structured by identifying the experimental data as in Ref. [37]. Also, to have a comparative study, standard SMC and saturated-line SMC (SMC-SAT) are applied to the system. The desired pose is considered to be a circular trajectory as:

5.1 Schemes of PBVS Control Strategies

The block diagram of different PBVS methods are declared as follows Fig. 5.4, 5.5, 5.6, 5.7, 5.8.

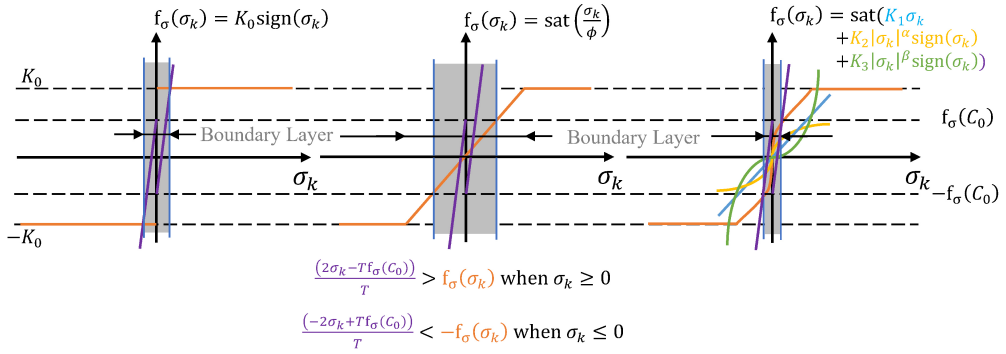

Figure 5.1: Different types of reaching laws for DSMC

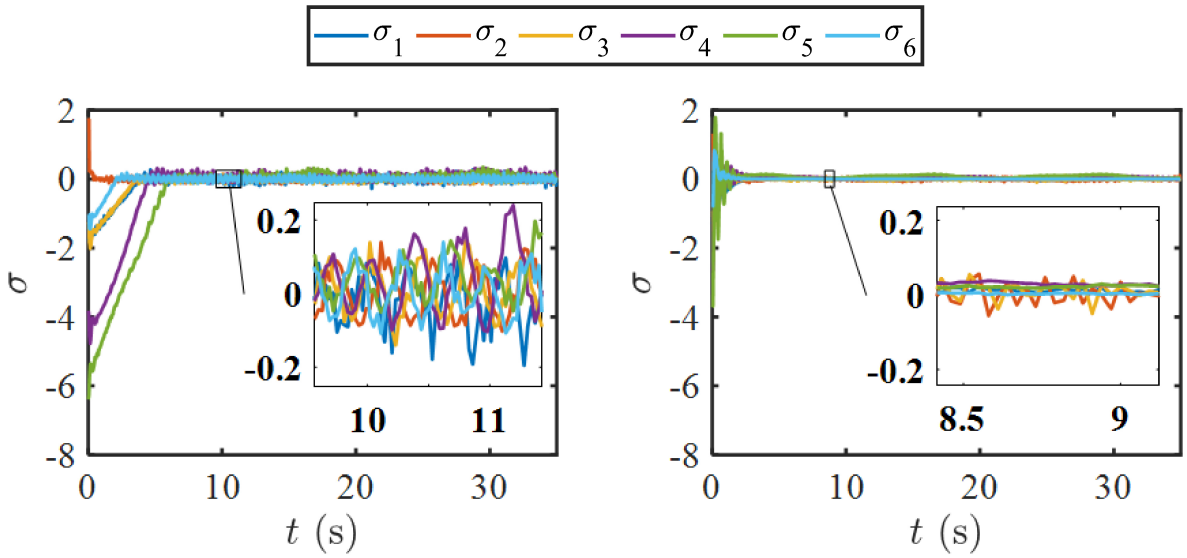

Figure 5.2: Sliding variable; a) DSMC; b) FDSMC

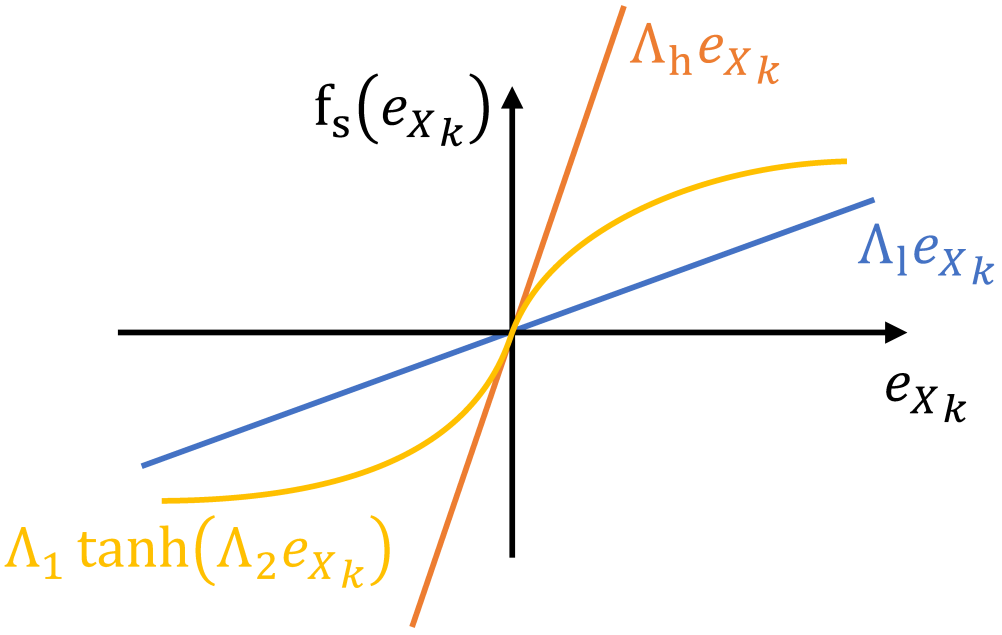

Figure 5.3: Linear and nonlinear sliding surface using tanh(.)

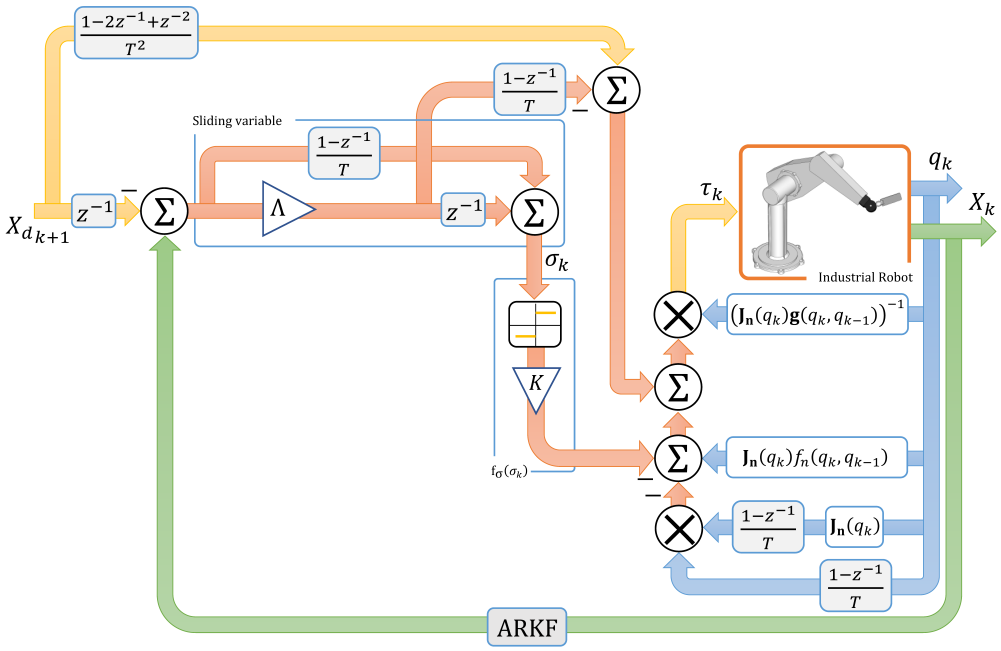

Figure 5.4: Schematic of digital Sliding mode control method

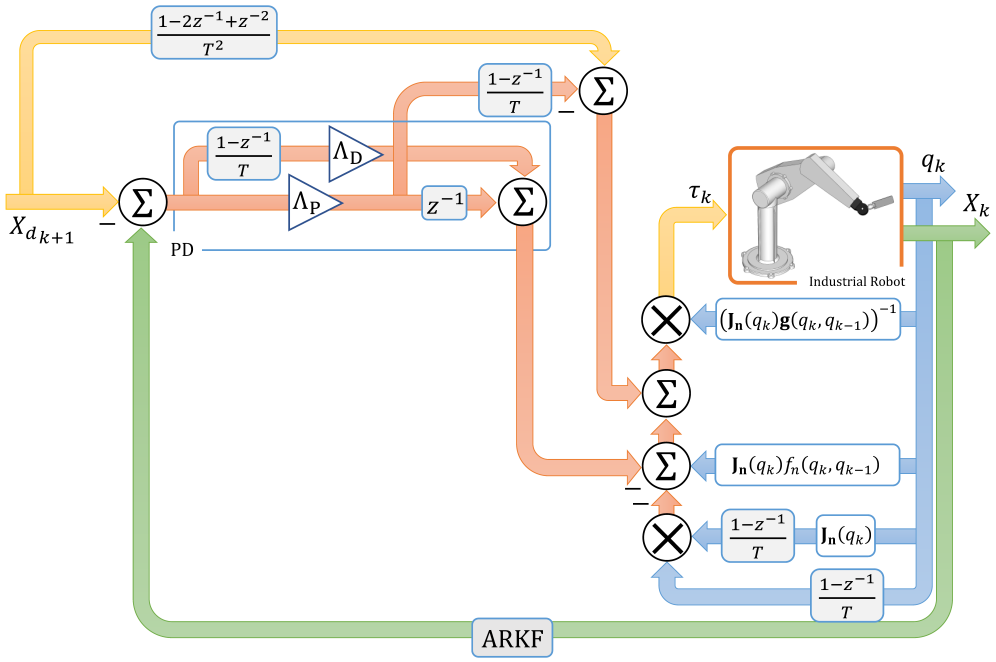

Figure 5.5: Schematic of torque computing-proportional derivative (TC-PD) control method

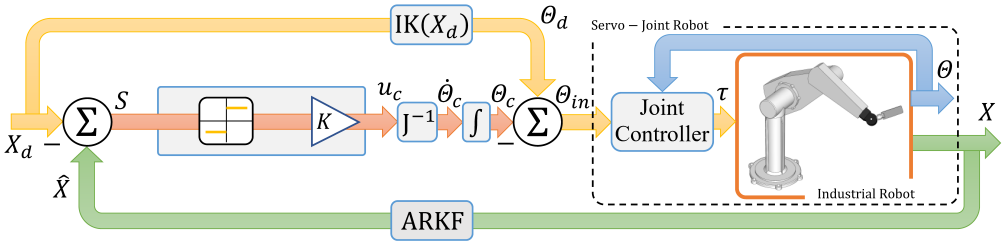

Figure 5.6: Schematic of sliding mode control method

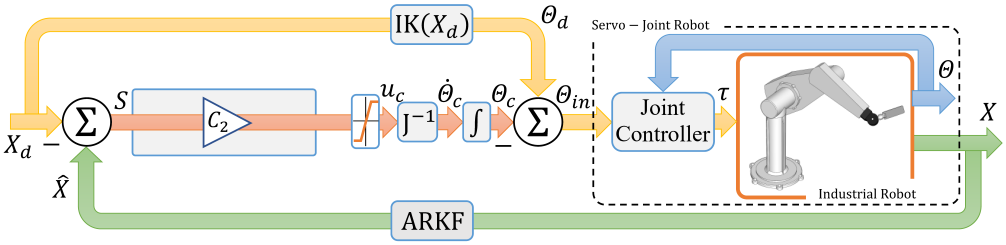

Figure 5.7: Schematic of chattering-free fast sliding mode method

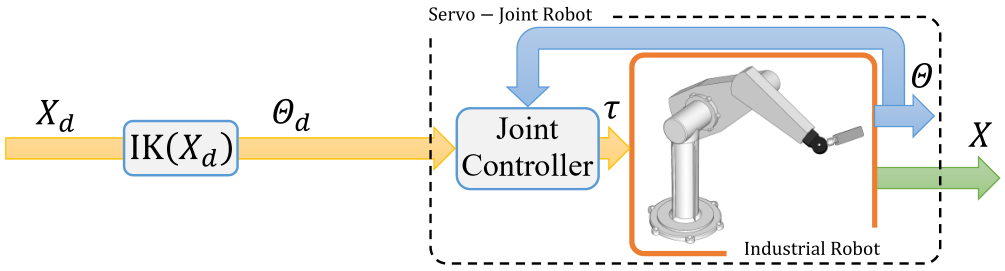

Figure 5.8: Schematic of open-loop control using invers kinematics

$$X_d = \begin{bmatrix} 0.5 & 0.33 + 0.15\sin(0.5t) & 0.15\cos(0.5t) & -\frac{\pi}{2} & 0 & 0 \end{bmatrix}^{\mathrm{T}} \tag{5.1}$$

where t is the simulation time.

5.2 Simulation Configuration

In this project, MATLAB 2018a is used as the main modeling and programming software. All simulations are performed in the Simulink, which is a block diagram environment for Model-Based Design. For modeling the robot, however, first, the mechanical and physical components were designed by SOLIDWORKS-2019 software (see Figure 5.9). Then, the model exported as an XML file. Finally, the generated files, including physical parameters such as mass and moment of inertia of the links, center of mass of each link, their frames, and graphical parts were imported in SimScape Toolbox of MATLAB/Simulink SimScape toolbox, which formerly known as SimMechanics, is a multibody modeling software for mechanical systems, which sets the stage for modeling of a robot as well (see Figure 5.10). Therefore, the model includes dynamics and kinematics of the robot. The input of the robot is vector of joint torques and its outputs in the vector of end-effector's pose variables. Note that to model the estimated robot's pose by C-Track vision system, a variable noise vector

added to the robot's pose, the structure of which was identified based on the collected experimental data of C-track and Fanuc robot in the real application.

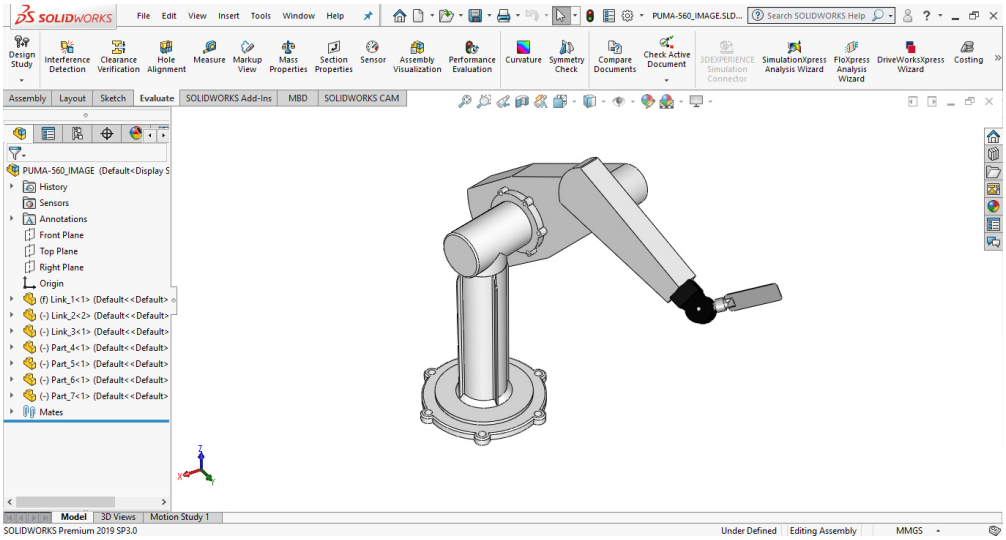

Figure 5.9: Figure A: Modeling the robot in SOLIDWORKS-2019 software.

The simulation of each Simulink file includes two separated parts: Simulation of the robot, and simulation of the vision system. For the first part, the solver type considered to be Runge-Kutta 4th-order with the sampling time interval of 0.001s, while for the second part, the discrete-time solver is chosen with the sampling time interval of 1/29 s.

5.2.1 Comparison among Aforementioned Control Strategies

Fig. 5.13 shows the results of the pose control highlights the superiority of CFSMC to other methods. CFSMC converges towards the desired signals faster than SMC and SMC-SAT. It also tracks the desired signals more accurately without chattering. The results, however, demonstrate a high level of chattering for SMC and a high level of filtering error for SMC-SAT. Noticeable level of offset error also appears when the compensators are not applied which emphasizes the necessity of providing a proper PBVS method. Fig. 5.11 shows Θ_d

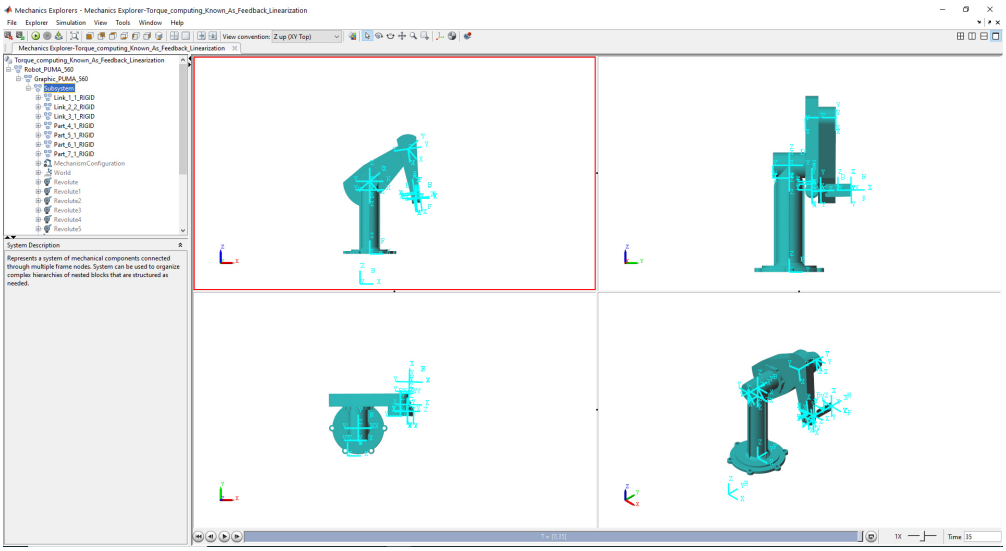

Figure 5.10: Figure B: SimScape Toolbox.

and Θ_{in} generated by SMC, SMC-SAT, and CFSMC. The results reveal the high level of chattering generated by SMC and relatively smooth output for FSMC and SMC-SAT. These plots also demonstrate that Θ_{in} deviated from Θ_d, which means the compensators are capable of modifying the desired joint angles so as to correct the robot pose.

To perform a numerical comparison, root mean square (RMS) and standard deviation (STA) indexes for error of the robot pose are also evaluated and tabulated in Table 5.2. The results show that these values are the lowest for CFSMC and definitely superior to other methods. The dramatic difference between these values is evident for non-compensated and compensated robot pose control. It further shows the necessity of a proper compensator to address the offset error emanated from uncertain kinematics.

5.3 Simulation Results

The performance of a DSMC depends on a) the reaching law, and b) the dynamics of the sliding surface. Generally, DSMC with the relative order of one has the following form [123]:

$$\frac{\sigma_{k+1}-\sigma_k}{T} = -\mathrm{f}_\sigma(\sigma_k) + \Delta_\mathrm{L} \tag{5.2}$$

$$\begin{aligned}
&\mathrm{f}_\sigma(\sigma_k) = K_0 \operatorname{sign}(\sigma_k) \\
&\mathrm{f}_\sigma(\sigma_k) = \operatorname{sat}\left(\tfrac{\sigma_k}{\phi}\right) \\
&\mathrm{f}_\sigma(\sigma_k) = \operatorname{sat}\left(K_1\sigma_k + K_2|\sigma_k|^\alpha \operatorname{sign}(\sigma_k) + K_3|\sigma_k|^\beta \operatorname{sign}(\sigma_k)\right)
\end{aligned} \tag{5.3}$$

In the relation above, f_{σ_S}, i.e. the reaching law of DSMC, has the switching form of Eq.5.3. Continuous forms of reaching laws are also suggested such as saturating linear reaching law of Eq.5.3. As mentioned before, the proposed reaching law in this paper is a continuous and a fast one as presented in Eq.5.3.

5.3.1 Analysis of the Tracking Performance of the Chattering-free DFSMC

For the above-mentioned reaching laws, the relationship between $\mathrm{f}_\sigma(\sigma_k)$ and σ_k, along with the thickness of bandar layer are plotted in 5.3. Unlike the continuous SMC, in DSMC, the boundary layer always exists [120] which directly results in increasing the filtering error. The thicker the boundary layer is, the higher the filtering error is. Even, adopting a switching function cannot prevent generating the boundary layer in DSMC. This is because the required stability condition presented in 4.46, i.e. $|2\sigma_k| > |T(\mathrm{f}_\sigma(\sigma_k) + \mathrm{f}_\sigma(C_0))|$ This inequality can be rewritten as two separated inequalities as follows:

$$\begin{aligned}
&\tfrac{(2\sigma_k - T\mathrm{f}_\sigma(C_0))}{T} > \mathrm{f}_\sigma(\sigma_k) \ \text{ when } \sigma_k \geq 0 \\
&\tfrac{(-2\sigma_k + T\mathrm{f}_\sigma(c_0))}{T} < -\mathrm{f}_\sigma(\sigma_k) \ \text{ when } \sigma_k < 0
\end{aligned} \tag{5.4}$$

Based on Theorem 2, simultaneous satisfaction of the relation above and uncertainty condition, i.e. Assumption 1, is required for the DSMC to be convergent. However, in the vicinity of the sliding surface, those conditions cannot be satisfied, and hence, boundary layer appears. The switching function has just one tunable parameter, i.e. K_0, which is adjusted based on the bound of the uncertainty. It means minimum flexibility. Besides, its switching essence results in an intense chattering in the boundary layer. Therefore, it is not a good choice for reaching law and usually is not employed. Saturating linear transfer function Eq. 5.3 is an alternative solution. It has two parameters to tune, i.e. ϕ and K_0. Therefore, it is more flexible than the switching function.

Additionally, it is continuous and thus results in alleviating the chattering issue. However, since its flexibility is not high enough, a trade-off between the chattering reduction and the boundary layer thickness exist. The fast reaching law proposed in this paper, i.e. Eq. 5.3 has some advantageous features compared to the previously discussed. Employing this reaching law, the boundary layer thickness depends on three terms including five parameters. It means that this reaching law is more flexible than the others. Therefore, tuning the controller gains properly may lead to increasing the tracking precision, convergence speed, and continuous output, simultaneously.

Remark 1. *The fast reaching law of Eq.5.3 comprises three linear and nonlinear terms. The first term is a sloping line which is responsible for converge with medium rate when the sliding variable error is medium. The two next nonlinear terms lead to increasing the convergence speed and tracking precision. These terms take effect when the filtering error is low and rather high, respectively Fig. 5.3.*

As mentioned earlier, dynamics of the sliding surface affects the precision of the filtering

error. The general form of the sliding dynamics for a second-order system is:

$$\frac{\left(e_{X_{k+1}} - e_{X_k}\right)}{T} = -\mathrm{f_s}\left(e_{x_k}\right) \tag{5.5}$$

For the conventional DSMC a linear surface is considered as Eq. 5.6. The problem with this linear function is its low flexibility. When λ is set to a high value, the convergence speed of the system increases. However, when the error is relatively high, it may enlarge the value of the sliding value which not only reduces the stability of the range of system, but also results in generating excessive value of controller output. In this study, a nonlinear sliding surface dynamic based on $tanh(.)$ function is proposed Eq. 5.6 to tackle the mentioned issues. Its parameters can be adjusted in a way that for the low error values it has the maximum admissible slop, while for high error values it has a rather low value. The comparison of the proposed nonlinear sliding surface dynamics and the linear one is presented in Fig. 5.3.

$$\begin{aligned} \mathrm{f_s}\left(e_{X_k}\right) &= \Lambda e_{X_{k-1}} \\ \mathrm{f_s}\left(e_{X_k}\right) &= \Lambda_1 \tanh\left(\Lambda_2 e_{X_{k-1}}\right) \end{aligned} \tag{5.6}$$

5.3.2 Circular Trajectory Tracking Results and Discussion

Also, to have performed a comparative study, a torque computing technique based on proportional-derivative controller (TC-PD), standard DSMC (as in Eq.5.3). In the simulations (experimental test), the sampling interval T is determined to be $0.03s$. The desired pose is considered to be a circular trajectory as:

$$X_d = \begin{bmatrix} 0.5 & 0.33 + 0.15\sin(0.5t) & 0.15\cos(0.5t) & -\frac{\pi}{2} & 0 & 0 \end{bmatrix}^{\mathrm{T}} \tag{5.7}$$

where t is the simulation time. 5.13, Referring to 5.13, it can be seen that FDSMC track the desired signals with higher precision and faster rate than those of the other methods.

Table 5.1: Computed indicators for the simulation result.

Indicator	PBVS			
	...	SMC	SMC-SAT	FSMC-SAT
RMS	0.02396	0.00347	0.00385	0.00251
STD	0.00582	0.00338	0.00370	0.00247

Table 5.2: Computed indicators for the robot's pose control

Indicator	Control method		
	TC-PD	SMC	CFSMC
RMS	0.02646	0.00712	0.00467
STD	0.01394	0.00605	0.00275

DSMC also tracks the desired signals relatively with high precision. However, it suffers from a high level of chattering. Besides, compared to TC-PD and FDSMC, its convergence speed is rather low. TC-PD tracks the desired signals smoothly, although its precision is very low due to the existing uncertainties in the robot parameters. TC-PD is not robust against them. As a result, high level of filtering error appears. The extent of the chattering in FDSMC is close that in TC-PD, while DFSMC suffers from a very high extent of chattering. This is because, in FDSMC the switching function is replaced with a smooth reaching law, which reduces resultant chattering significantly.

The generated chattering of the FDSMC in the controller output is lower than that of the DSMC to a high extend. The existing chattering in the controller outputs is associated with two terms: a) camera noise in the pose feedback signals and b) variable structure within the sliding mode controllers. In the TC-PD controller, the chattering is only associated with the feedback noise, and since ARKF is used to smooth the camera noise, its output is relatively smooth. It is obvious that the sliding variables in FDSMC converge towards the sliding surfaces faster and smoother those in the DSMC. It shows that employing the fast reaching law is practically effective.

To perform a quantitative comparison, root mean square (RMS) and standard deviation

Table 5.3: Computed indicators for controller

Indicator	Control method		
	TC-PD	SMC	CFSMC
RMS	4.88603	5.36198	4.80922
STD	1.54765	2.24383	1.58708

Table 5.4: Indicators for sliding variable

Indicator	Control method		
	TC-PD	SMC	CFSMC
RMS	–	0.09395	0.03848
STD	–	0.08505	0.02488

(STA) indexes for error of the robot's pose, control effort, and sliding variable are evaluated and tabulated in Table 5.2, Table 5.3, and Table 5.4, respectively. The results of Table 5.2 show that the lowest values of RMS and SDT are attributed to FDSMC with 82% and 80% reductions compared to DSMC, and 34% and 54% reductions compared to TC-PD. These dramatic reductions show that the adopted controller has been significantly effective in increasing precision of the robot's pose in tracking the desired signals. Referring to Table 5.3, RMS and STD indicators of the control efforts for TC-PD and FDSMC are almost in the same level. However, due to the high level of chattering in the controller output of the DSMC, its RMS and STD values are about 10% and 30% higher than the FDSMC. Since TC-PD is not an SMC controller, it has not any sliding variable. Therefore, Table 5.4 only contains RMS and STD values of sliding variables of FDSMC and DSMC. The numerical results of this table show high reductions by FDSMC compared to DSMC: 59% reduction of RMS and 70% of STD. All of these numerical results confirm the results of simulation plots, that FDSMC is superior to other methods in terms of filtering error precision, chattering level, control effort, and convergence speed.

5.4 Summary

In this chapter, we analyzed the performance of the proposed CFSMC method. First a PUMA 560 robot is modeled in the SimScape toolbox of MATLAB2018a. The robot's pose contaminated with additive noise is assumed to be the given pose detected by the visual system C-track. Then, root mean square (RMS) and standard deviation (STA) indexes for error of the robot's pose, control effort, and sliding variable are evaluated and tabulated for quantitative comparison. The results show that the adopted controller is very effective in increasing precision of the robot's pose in tracking the desired signals. RMS and STD indicators of the control efforts for TC-PD and FDSMC are almost in the same level. The RMS and STD values of DSMC are higher than those of FDSMC due to the high level chattering of DSMC. The numerical results of this table show high indicators reductions by FDSMC compared to DSMC. The FDSMC is demonstrated to be superior to other aforementioned methods in terms of filtering error precision, chattering level, control effort, and convergence speed.

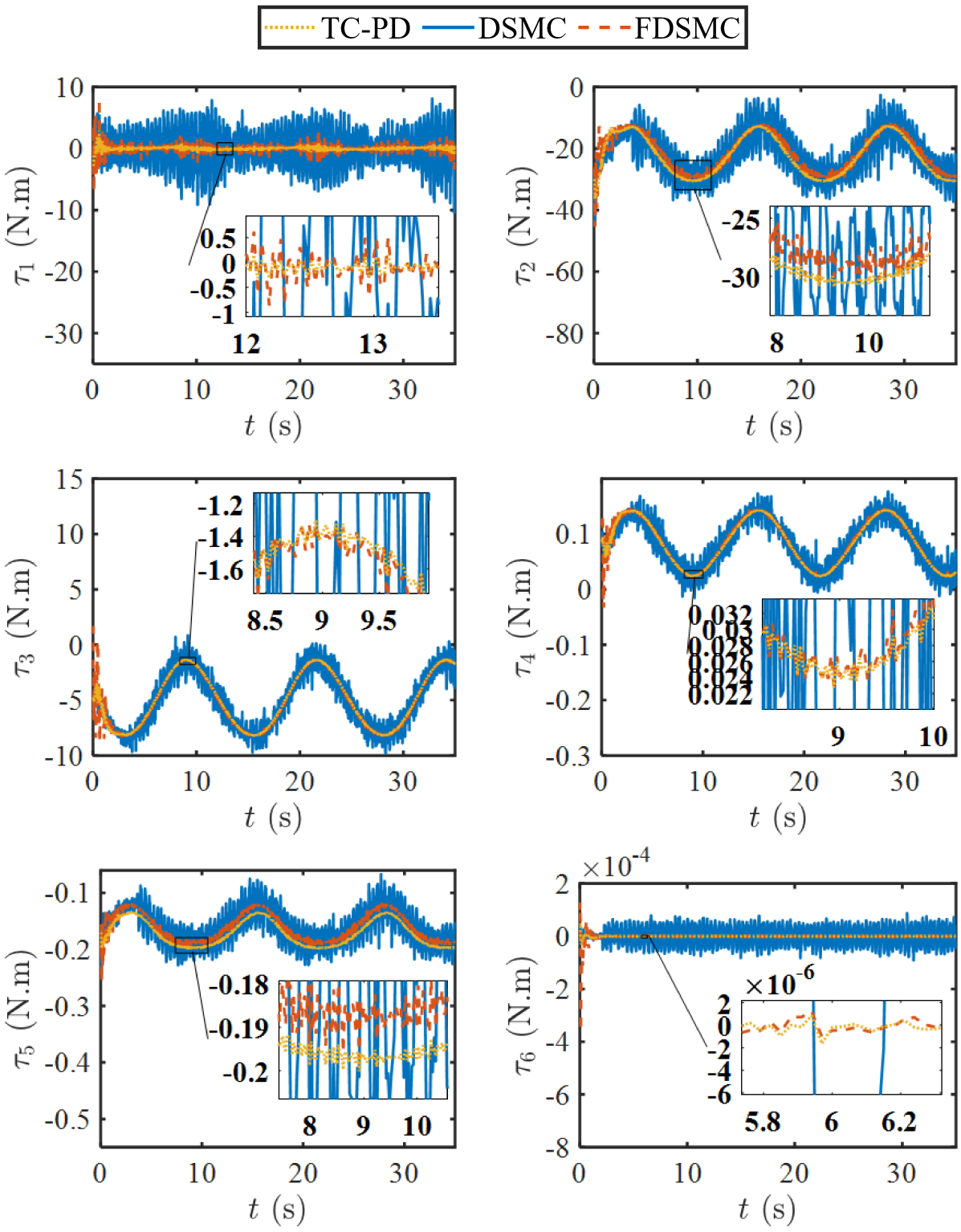

Figure 5.11: Controller output; a)τ_1; b)τ_2; c) τ_3; d)τ_4; e)τ_5; f) τ_6

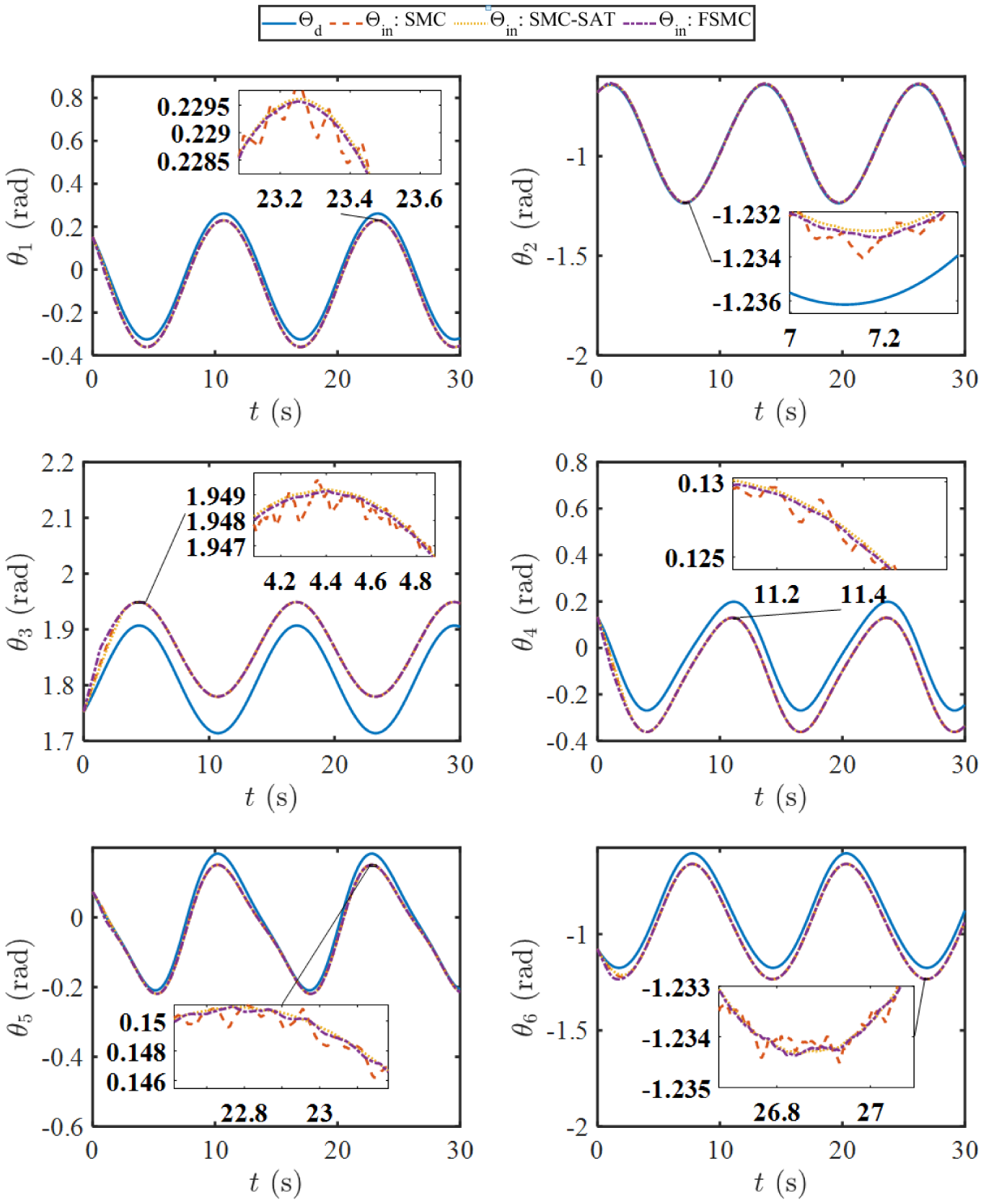

Figure 5.12: Simulation result of the joints desired and compensated signals.

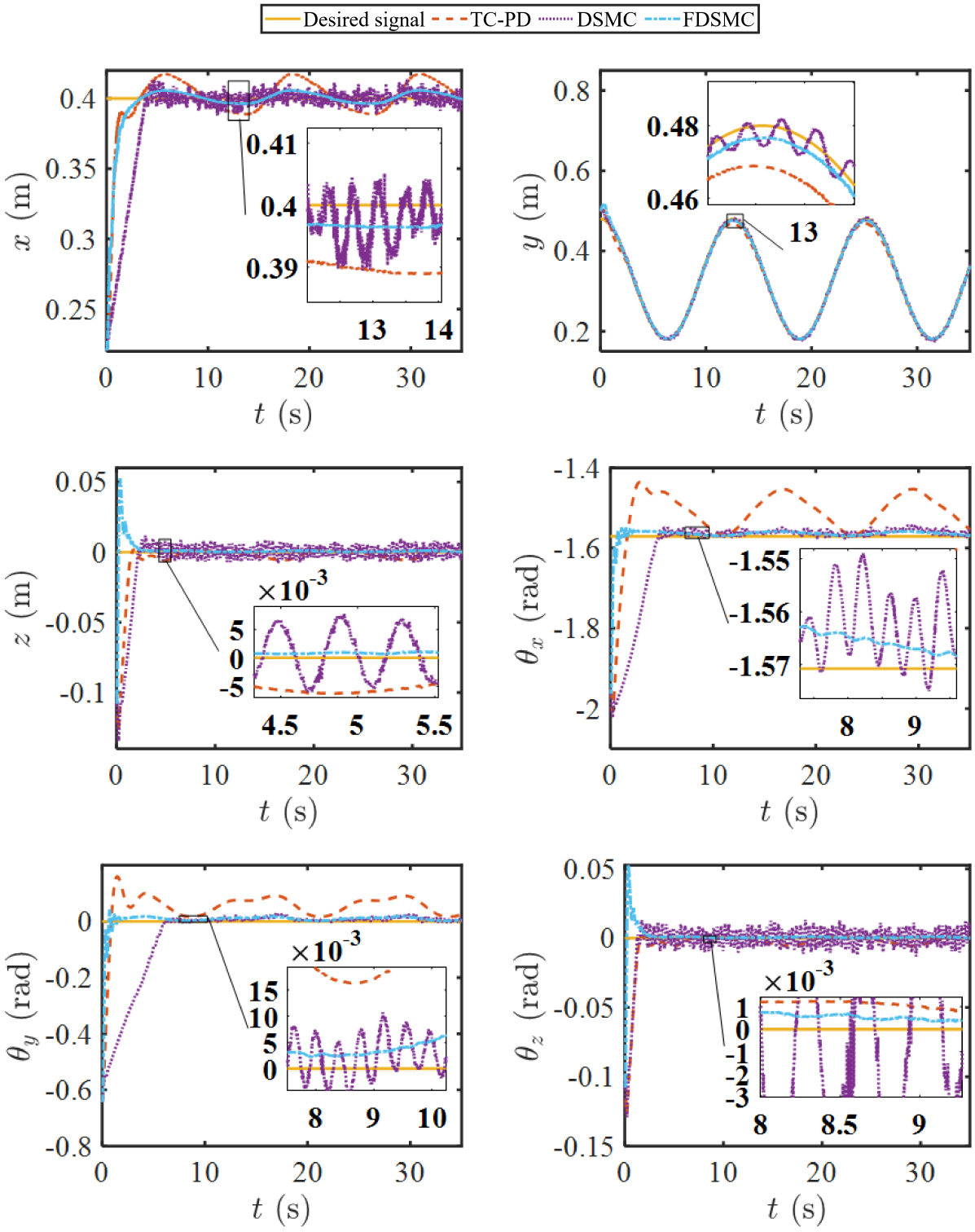

Figure 5.13: The end-effector's pose control a) x; b) y; c) z; d)θ_x; e)θ_y; f)θ_z

Chapter 6

Conclusion and Future Work

In this chapter, the main conclusions of this thesis are summarized according to the obtained results. Some extra extensions and future works are suggested as well.

6.1 Research Summary

In this research, a novel robust position-based visual servoing (PBVS) approach for industrial robots is presented. This method combines a chattering-free sliding mode controller (CF-SMC) with an adaptive robust Kalman filter (ARKF) to exploit their beneficial features. The main contributions of this thesis are as follows:

- The proposed ARKF exploits the advantages of adaptive estimation method for states noise covariance (Q), least square identification for measurement noise covariance (R) and a robust mechanism for state variables error covariance (P).
- In simulation on PUMA 560, the comparison between the proposed ARKF and other well-known version of Kalman filter such as adaptive Kalman filter (AKF) and standard Kalman filter (SKF) shows the superiority of the ARKF in terms of root mean square

(RMS) and Variance (Var) of filtered errors.

- The simulation tests demonstrate that the proposed ARKF is able to reduce the effects of noise on the pose estimation signal effectively and has a superior performance to the other KF methods in terms of smoothness and tracking errors for all state variables.

- This PBVS control scheme results in improving the robustness and tracking performance of the robot. An eye-to-hand vision system (C-track) is used to detect the pose of the robot and ARKF is applied to filter out the noises in the detected pose signals which exploit a fast-nonlinear reaching law and nonlinear sliding surface.

- The CFSMC provide not only robustness against uncertainties in dynamics and kinematics of the robot, but also high tracking accuracy and fast convergence speed.

- The stability proof of the CFSMC in the discrete time domain is investigated and the quasi-motion in the generated boundary layer is also analyzed.

- The simulation results of applying the proposed PBVS method to PUMA 560 robot demonstrate superiority of the proposed CFSMC with ARKF to other controllers in terms of tracking accuracy, convergence speed, control effort, and chattering level.

- The CFSMC takes advantage of a nonlinear reaching law which results in faster and more accurate trajectory tracking compared to the standard SMC. Substituting the switching function with a continuous nonlinear reaching law to eliminating the chattering.

- Since the sliding surface dynamics is considered to be a nonlinear one, the convergence speed and accuracy are improved. The simulation results of applying the proposed method to a PUMA 560 robot showed the superiority of the proposed method over

standard SMC and TC-PD in terms of chattering level, precision, control effort, and convergence speed.

6.2 Future Works

The future work includes applying the ARKF to the experimental test of pose estimation of industrial robots and implemented the CFSMC control scheme via communicating with the industrial robot's controller to improve the tracking accuracy for the industrial robots. Analyzing the corresponding experimental results also are suggested.

Bibliography

[1] E. Zakeri, S. A. Moezi, M. Zare, and M. P. Rad, "Control of puma-560 robot using feedback linearization control method and kalman filter estimator for regulation and tracking purpose," *J. Math. Comput. Sci*, vol. 11, pp. 264–276, 2014.

[2] J. Mozaryn and J. E. Kurek, "Design of the sliding mode control for the puma 560 robot," 2003.

[3] B. Siciliano, L. Sciavicco, L. Villani, and G. Oriolo, "Robotics: modelling, planning and control," 2010.

[4] H. Kochekali, A. Nowrouzi, Y. Kavina, and R. Whitaker, "Factors affecting robot performance," *Industrial robot*, vol. 18, no. 1, pp. 9–13, 1991.

[5] R. Kumar and A. R. Hanson, "Robust methods for estimating pose and a sensitivity analysis," pp. 313–342, 1994.

[6] N. Peterfreund, "Robust tracking of position and velocity with kalman snakes," *IEEE transactions on pattern analysis and machine intelligence*, vol. 21, no. 6, pp. 564–569, 1999.

[7] K. M. Hangos, J. Bokor, and G. Szederkényi, *Analysis and control of nonlinear process systems*. Springer Science & Business Media, 2006.

[8] E. Malis and F. Chaumette, "Theoretical improvements in the stability analysis of a new class of model-free visual servoing methods," *IEEE Transactions on robotics and automation*, vol. 18, no. 2, pp. 176–186, 2002.

[9] M. Marey and F. Chaumette, "Analysis of classical and new visual servoing control laws," in *2008 IEEE International Conference on Robotics and Automation*. IEEE, 2008, pp. 3244–3249.

[10] A. Mittal, L. Zhao, and L. S. Davis, "Human body pose estimation using silhouette shape analysis," in *Proceedings of the IEEE Conference on Advanced Video and Signal Based Surveillance, 2003.* IEEE, 2003, pp. 263–270.

[11] B. M. Haralick, C.-N. Lee, K. Ottenberg, and M. Nölle, "Review and analysis of solutions of the three point perspective pose estimation problem," *International journal of computer vision*, vol. 13, no. 3, pp. 331–356, 1994.

[12] A. Nubiola and I. A. Bonev, "Absolute calibration of an abb irb 1600 robot using a laser tracker," *Robotics and Computer-Integrated Manufacturing*, vol. 29, no. 1, pp. 236–245, 2013.

[13] A. Nubiola, M. Slamani, A. Joubair, and I. A. Bonev, "Comparison of two calibration methods for a small industrial robot based on an optical cmm and a laser tracker," *Robotica*, vol. 32, no. 3, p. 447, 2014.

[14] T. Chang, T. Hong, M. Shneier, G. Holguin, J. Park, and R. D. Eastman, "Dynamic 6dof metrology for evaluating a visual servoing system," in *Proceedings of the 8th Workshop on Performance Metrics for Intelligent Systems*, 2008, pp. 173–180.

[15] S. Rathjen and C. Richardson, "High path accuracy, high process force articulated robot," SAE Technical Paper, Tech. Rep., 2013.

[16] T. Shu, S. Gharaaty, W. Xie, A. Joubair, and I. A. Bonev, "Dynamic path tracking of industrial robots with high accuracy using photogrammetry sensor," *IEEE/ASME Transactions on Mechatronics*, vol. 23, no. 3, pp. 1159–1170, 2018.

[17] P. Zanne, G. Morel, and F. Piestan, "Robust vision based 3d trajectory tracking using sliding mode control," in *Proceedings 2000 ICRA. Millennium Conference. IEEE International Conference on Robotics and Automation. Symposia Proceedings (Cat. No. 00CH37065)*, vol. 3. IEEE, 2000, pp. 2088–2093.

[18] J.-J. Slotine and S. S. Sastry, "Tracking control of non-linear systems using sliding surfaces, with application to robot manipulators," *International journal of control*, vol. 38, no. 2, pp. 465–492, 1983.

[19] G. Morel, P. Zanne, and F. Plestan, "Robust visual servoing: Bounding the task function tracking errors," *IEEE Transactions on Control Systems Technology*, vol. 13, no. 6, pp. 998–1009, 2005.

[20] S. Gharaaty, T. Shu, A. Joubair, W. F. Xie, and I. A. Bonev, "Online pose correction of an industrial robot using an optical coordinate measure machine system," *International Journal of Advanced Robotic Systems*, vol. 15, no. 4, p. 1729881418787915, 2018.

[21] M. Z. Huang and O. Masory, "A simple method of accuracy enhancement for industrial manipulators," *The International Journal of Advanced Manufacturing Technology*, vol. 8, no. 2, pp. 114–122, 1993.

[22] L. J. Everett and T.-W. Hsu, "The theory of kinematic parameter identification for industrial robots," 1988.

[23] Z. Zhang, "A flexible new technique for camera calibration," *IEEE Transactions on pattern analysis and machine intelligence*, vol. 22, no. 11, pp. 1330–1334, 2000.

[24] S. B. Clay and P. M. Knoth, "Experimental results of quasi-static testing for calibration and validation of composite progressive damage analysis methods," *Journal of Composite Materials*, vol. 51, no. 10, pp. 1333–1353, 2017.

[25] R. C. DeVlieg, "Robotic manufacturing system with accurate control," Mar. 24 2015, uS Patent 8,989,898.

[26] R. Devlieg, "Expanding the use of robotics in airframe assembly via accurate robot technology," *SAE International Journal of Aerospace*, vol. 3, no. 2010-01-1846, pp. 198–203, 2010.

[27] Y. Yang and W. Gao, "An optimal adaptive kalman filter," *Journal of Geodesy*, vol. 80, no. 4, pp. 177–183, 2006.

[28] E. Zakeri, S. A. Moezi, and M. Eghtesad, "Optimal interval type-2 fuzzy fractional order super twisting algorithm: A second order sliding mode controller for fully-actuated and under-actuated nonlinear systems," *ISA transactions*, vol. 85, pp. 13–32, 2019.

[29] S. Hutchinson, G. D. Hager, and P. I. Corke, "A tutorial on visual servo control," *IEEE transactions on robotics and automation*, vol. 12, no. 5, pp. 651–670, 1996.

[30] Y. Zeng, "Recursive object model (ROM) – Modelling of linguistic information in engineering design," *Computers in Industry*, vol. 59, no. 6, pp. 612–625, Aug. 2008. [Online]. Available: http://www.sciencedirect.com/science/article/pii/S0166361508000249

[31] M. Wang and Y. Zeng, "Asking the right questions to elicit product requirements," *International Journal of Computer Integrated Manufacturing*, vol. 22, no. 4, pp. 283–298, Apr. 2009. [Online]. Available: http://dx.doi.org/10.1080/09511920802232902

[32] P. Corke, "Robotics," *Vision and Control*, 2011.

[33] P. I. Corke and S. A. Hutchinson, "Real-time vision, tracking and control," in *Proceedings 2000 ICRA. Millennium Conference. IEEE International Conference on Robotics and Automation. Symposia Proceedings (Cat. No. 00CH37065)*, vol. 1. IEEE, 2000, pp. 622–629.

[34] P. I. Corke *et al.*, *Visual Control of Robots: high-performance visual servoing*. Research Studies Press Taunton, UK, 1996.

[35] G. Palmieri, M. Palpacelli, M. Battistelli, and M. Callegari, "A comparison between position-based and image-based dynamic visual servoings in the control of a translating parallel manipulator," 2012.

[36] J. S. Goddard and M. A. Abidi, "Pose and motion estimation using dual quaternion-based extended kalman filtering," in *Three-Dimensional Image Capture and Applications*, vol. 3313. International Society for Optics and Photonics, 1998, pp. 189–200.

[37] X. Wu, E. Zakeri, and W.-F. Xie, "Adaptive robust kalman filter for vision-based pose estimation of industrial robots," in *2019 IEEE 5th International Conference on Computer and Communications (ICCC)*. IEEE, 2019, pp. 298–302.

[38] W. J. Wilson, C. W. Hulls, and G. S. Bell, "Relative end-effector control using cartesian position based visual servoing," *IEEE Transactions on Robotics and Automation*, vol. 12, no. 5, pp. 684–696, 1996.

[39] H. Sinoquet, S. Thanisawanyangkura, H. Mabrouk, and P. Kasemsap, "Characterization of the light environment in canopies using 3d digitising and image processing," *Annals of Botany*, vol. 82, no. 2, pp. 203–212, 1998.

[40] M. Parsapour, S. RayatDoost, and H. Taghirad, "Position based sliding mode control for visual servoing system," in *2013 First RSI/ISM International Conference on Robotics and Mechatronics (ICRoM)*. IEEE, 2013, pp. 337–342.

[41] M. Parsapour, S. RayatDoost, and H. D. Taghirad, "A 3d sliding mode control approach for position based visual servoing system," *Scientia Iranica*, vol. 22, no. 3, pp. 844–853, 2015.

[42] W. Wilson, "Visual servo control of robots using kalman filter estimates of relative pose," *IFAC Proceedings Volumes*, vol. 26, no. 2, pp. 633–638, 1993.

[43] J. Swevers, C. Ganseman, D. B. Tukel, J. de Schutter, and H. Van Brussel, "Optimal robot excitation and identification," *IEEE Transactions on Robotics and Automation*, vol. 13, no. 5, pp. 730–740, 1997.

[44] H.-J. Kim, Y.-D. Kim, and D.-H. Lee, "Scheduling for an arc-welding robot considering heat-caused distortion," *Journal of the Operational Research Society*, vol. 56, no. 1, pp. 39–50, 2005.

[45] J. Davis, R. Ramamoorthi, and S. Rusinkiewicz, "Spacetime stereo: A unifying framework for depth from triangulation," in *2003 IEEE Computer Society Conference on Computer Vision and Pattern Recognition, 2003. Proceedings.*, vol. 2. IEEE, 2003, pp. II–359.

[46] D. DeMenthon and L. S. Davis, "Exact and approximate solutions of the perspective-three-point problem," pp. 1100–1105, 1992.

[47] R. Horaud, B. Conio, O. Leboulleux, and B. Lacolle, "An analytic solution for the perspective 4-point problem," IEEE, pp. 500–507, 1989.

[48] A. Gelb, "Applied optimal estimation," 1974.

[49] S. Akhlaghi, N. Zhou, and Z. Huang, "Adaptive adjustment of noise covariance in kalman filter for dynamic state estimation," in *2017 IEEE Power & Energy Society General Meeting*. IEEE, 2017, pp. 1–5.

[50] P. I. Corke, "Visual control of robot manipulators–a review," in *Visual Servoing: Real-Time Control of Robot Manipulators Based on Visual Sensory Feedback*. World Scientific, 1993, pp. 1–31.

[51] K. Sabe, M. Fukuchi, J.-S. Gutmann, T. Ohashi, K. Kawamoto, and T. Yoshigahara, "Obstacle avoidance and path planning for humanoid robots using stereo vision," in *IEEE International Conference on Robotics and Automation, 2004. Proceedings. ICRA'04. 2004*, vol. 1. IEEE, 2004, pp. 592–597.

[52] G. D. Hager, W.-C. Chang, and A. S. Morse, "Robot feedback control based on stereo vision: Towards calibration-free hand-eye coordination," in *Proceedings of the 1994 IEEE International Conference on Robotics and Automation*. IEEE, 1994, pp. 2850–2856.

[53] D. Murray and J. J. Little, "Using real-time stereo vision for mobile robot navigation," *autonomous robots*, vol. 8, no. 2, pp. 161–171, 2000.

[54] R. R. Goldberg, "Constrained pose refinement of parametric objects," pp. 181–211, 1994.

[55] S. Ganapathy, "Decomposition of transformation matrices for robot vision," pp. 401–412, 1984.

[56] B. P. Larouche, Z. H. Zhu, and S. A. Meguid, "Development of autonomous robot for space servicing," in *2010 IEEE International Conference on Mechatronics and Automation*. IEEE, 2010, pp. 1558–1562.

[57] C.-Y. Tsai, K.-T. Song, X. Dutoit, H. Van Brussel, and M. Nuttin, "Robust visual tracking control system of a mobile robot based on a dual-jacobian visual interaction model," *Robotics and Autonomous Systems*, vol. 57, no. 6-7, pp. 652–664, 2009.

[58] S. Li and P. Ni, "Square-root unscented kalman filter based simultaneous localization and mapping," in *The 2010 IEEE International Conference on Information and Automation*. IEEE, 2010, pp. 2384–2388.

[59] F. Janabi-Sharifi and M. Marey, "A kalman-filter-based method for pose estimation in visual servoing," *IEEE transactions on Robotics*, vol. 26, no. 5, pp. 939–947, 2010.

[60] E. A. Wan and R. Van Der Merwe, "The unscented kalman filter for nonlinear estimation," in *Proceedings of the IEEE 2000 Adaptive Systems for Signal Processing, Communications, and Control Symposium (Cat. No. 00EX373)*. Ieee, 2000, pp. 153–158.

[61] E. Ivanjko and I. Petrovic, "Extended kalman filter based mobile robot pose tracking using occupancy grid maps," in *Proceedings of the 12th IEEE Mediterranean Electrotechnical Conference (IEEE Cat. No. 04CH37521)*, vol. 1. IEEE, 2004, pp. 311–314.

[62] M. Alatise and G. Hancke, "Pose estimation of a mobile robot based on fusion of imu data and vision data using an extended kalman filter," *Sensors*, vol. 17, no. 10, p. 2164, 2017.

[63] S. J. Julier and J. K. Uhlmann, "Reduced sigma point filters for the propagation of means and covariances through nonlinear transformations," in *Proceedings of the 2002 American Control Conference (IEEE Cat. No. CH37301)*, vol. 2. IEEE, 2002, pp. 887–892.

[64] J. L. Crassidis, F. L. Markley, and Y. Cheng, "Survey of nonlinear attitude estimation methods," *Journal of guidance, control, and dynamics*, vol. 30, no. 1, pp. 12–28, 2007.

[65] M. Ficocelli and F. Janabi-Sharifi, "Adaptive filtering for pose estimation in visual servoing," in *Proceedings 2001 IEEE/RSJ International Conference on Intelligent Robots and Systems. Expanding the Societal Role of Robotics in the the Next Millennium (Cat. No. 01CH37180)*, vol. 1. IEEE, 2001, pp. 19–24.

[66] P. Wunsch and G. Hirzinger, "Real-time visual tracking of 3d objects with dynamic handling of occlusion," in *Proceedings of International Conference on Robotics and Automation*, vol. 4. IEEE, 1997, pp. 2868–2873.

[67] D. G. Lowe, "Three-dimensional object recognition from single two-dimensional images," *Artificial intelligence*, vol. 31, no. 3, pp. 355–395, 1987.

[68] F. Janabi-Sharifi, "Visual servoing: theory and applications," *Opto-Mechatronic Systems Handbook*, pp. 15–1, 2002.

[69] E. Malis and F. Chaumette, "2 1/2 d visual servoing with respect to unknown objects through a new estimation scheme of camera displacement," *International Journal of Computer Vision*, vol. 37, no. 1, pp. 79–97, 2000.

[70] G. Chesi and K. Hashimoto, "A simple technique for improving camera displacement estimation in eye-in-hand visual servoing," *IEEE Transactions on Pattern Analysis and Machine Intelligence*, vol. 26, no. 9, pp. 1239–1242, 2004.

[71] S. Hutchinson and F. Chaumette, "Visual servo control, part i: Basic approaches," *IEEE Robotics and Automation Magazine*, vol. 13, no. 4, pp. 82–90, 2006.

[72] ——, "Visual servo control, part ii: Advanced approaches," *IEEE Robotics and Automation Magazine*, vol. 14, no. 1, pp. 109–118, 2007.

[73] J. T. Feddema and O. R. Mitchell, "Vision-guided servoing with feature-based trajectory generation (for robots)," *IEEE Transactions on Robotics and Automation*, vol. 5, no. 5, pp. 691–700, 1989.

[74] E. Malis, F. Chaumette, and S. Boudet, "2 1/2 d visual servoing," *IEEE Transactions on Robotics and Automation*, vol. 15, no. 2, pp. 238–250, 1999.

[75] M. Vincze and G. D. Hager, "Robust image processing and positionbased visual servoing," 2000.

[76] F. Janabi-Sharifi and W. J. Wilson, "Automatic selection of image features for visual servoing," *IEEE Transactions on Robotics and Automation*, vol. 13, no. 6, pp. 890–903, 1997.

[77] Y. Shirai, *Three-dimensional computer vision*. Springer Science & Business Media, 2012.

[78] X. Wan and G. Xu, "Camera parameters estimation and evaluation in active vision system," *Pattern Recognition*, vol. 29, no. 3, pp. 439–447, 1996.

[79] R. M. Haralick, H. Joo, C.-N. Lee, X. Zhuang, V. G. Vaidya, and M. B. Kim, "Pose estimation from corresponding point data," *IEEE Transactions on Systems, Man, and Cybernetics*, vol. 19, no. 6, pp. 1426–1446, 1989.

[80] Q. Ji, M. S. Costa, R. M. Haralick, and L. G. Shapiro, "An integrated linear technique for pose estimation from different geometric features," *International Journal of Pattern Recognition and Artificial Intelligence*, vol. 13, no. 05, pp. 705–733, 1999.

[81] D. F. Dementhon and L. S. Davis, "Model-based object pose in 25 lines of code," *International journal of computer vision*, vol. 15, no. 1-2, pp. 123–141, 1995.

[82] R. K. Lenz and R. Y. Tsai, "Techniques for calibration of the scale factor and image center for high accuracy 3-d machine vision metrology," *IEEE Transactions on pattern analysis and machine intelligence*, vol. 10, no. 5, pp. 713–720, 1988.

[83] C.-P. Lu, G. D. Hager, and E. Mjolsness, "Fast and globally convergent pose estimation from video images," *IEEE transactions on pattern analysis and machine intelligence*, vol. 22, no. 6, pp. 610–622, 2000.

[84] J. Wang and W. J. Wilson, "3d relative position and orientation estimation using kalman filter for robot control," in *Proceedings 1992 IEEE International Conference on Robotics and Automation*. IEEE, 1992, pp. 2638–2645.

[85] J. Carpenter, P. Clifford, and P. Fearnhead, "Improved particle filter for nonlinear problems," *IEE Proceedings-Radar, Sonar and Navigation*, vol. 146, no. 1, pp. 2–7, 1999.

[86] Q.-T. Luong and O. D. Faugeras, "The fundamental matrix: Theory, algorithms, and stability analysis," *International journal of computer vision*, vol. 17, no. 1, pp. 43–75, 1996.

[87] É. Marchand and F. Chaumette, "Virtual visual servoing: a framework for real-time augmented reality," in *Computer Graphics Forum*, vol. 21, no. 3. Wiley Online Library, 2002, pp. 289–297.

[88] L. Deng, W. J. Wilson, and F. Janabi-Sharifi, "Combined target model estimation and position-based visual servoing," in *2004 IEEE/RSJ International Conference on Intelligent Robots and Systems (IROS)(IEEE Cat. No. 04CH37566)*, vol. 2. IEEE, 2004, pp. 1395–1400.

[89] L. Deng, W. Wilson, and F. Janabi-Sharifi, "Decoupled ekf for simultaneous target model and relative pose estimation using feature points," in *Proceedings of 2005 IEEE Conference on Control Applications, 2005. CCA 2005.* IEEE, 2005, pp. 749–754.

[90] S. J. Julier and J. K. Uhlmann, "Unscented filtering and nonlinear estimation," *Proceedings of the IEEE*, vol. 92, no. 3, pp. 401–422, 2004.

[91] V. Lippiello, B. Siciliano, and L. Villani, "Adaptive extended kalman filtering for visual motion estimation of 3d objects," *Control Engineering Practice*, vol. 15, no. 1, pp. 123–134, 2007.

[92] A. Shademan and F. Janabi-Sharifi, "Sensitivity analysis of ekf and iterated ekf pose estimation for position-based visual servoing," in *Proceedings of 2005 IEEE Conference on Control Applications, 2005. CCA 2005.* IEEE, 2005, pp. 755–760.

[93] T. Lefebvre*, H. Bruyninckx, and J. De Schutter, "Kalman filters for non-linear systems: a comparison of performance," *International journal of Control*, vol. 77, no. 7, pp. 639–653, 2004.

[94] J. Hill, "Real time control of a robot with a mobile camera," in *9th Int. Symp. on Industrial Robots, 1979*, 1979, pp. 233–246.

[95] D. B. Zhang, L. Van Gool, and A. Oosterlinck, "Stochastic predictive control of robot tracking systems with dynamic visual feedback," in *Proceedings., IEEE International Conference on Robotics and Automation*, 1990, pp. 610–615 vol.1.

[96] P. Li, A. Ghasemi, W. Xie, and W. Tian, "Visual closed-loop dynamic model identification of parallel robots based on optical cmm sensor," *Electronics*, vol. 8, p. 836, 07 2019.

[97] A. Tayebi, S. Abdul, M. B. Zaremba, and Y. Ye, "Robust iterative learning control design: Application to a robot manipulator," *IEEE/ASME Transactions on Mechatronics*, vol. 13, no. 5, pp. 608–613, 2008.

[98] A. Tayebi and S. Islam, "Adaptive iterative learning control for robot manipulators: Experimental results," *Control Engineering Practice*, vol. 14, no. 7, pp. 843–851, 2006.

[99] ——, "Experimental evaluation of an adaptive iterative learning control scheme on a 5-dof robot manipulator," in *Proceedings of the 2004 IEEE International Conference on Control Applications, 2004.*, vol. 2. IEEE, 2004, pp. 1007–1011.

[100] M. Takegaki and S. Arimoto, "A new feedback method for dynamic control of manipulators," 1981.

[101] M. W. Spong and M. Vidyasagar, *Robot dynamics and control*. John Wiley & Sons, 2008.

[102] P. Tomei, "Adaptive pd controller for robot manipulators," *IEEE Transactions on Robotics and Automation*, vol. 7, no. 4, pp. 565–570, 1991.

[103] R. Kelly, "Comments on" adaptive pd controller for robot manipulators," *IEEE Transactions on Robotics and Automation*, vol. 9, no. 1, pp. 117–119, 1993.

[104] J. T. Wen and S. H. Murphy, *PID control for robot manipulators*. Rensselaer Polytechnic Institute, 1990.

[105] R. Kelly, "A tuning procedure for stable pid control of robot manipulators," *Robotica*, vol. 13, no. 2, pp. 141–148, 1995.

[106] S. Arimoto, "Stability and robustness of pid feedback control for robot manipulators of sensory capability," in *Robotics Research: First Int. Symp.* MIT Press, Cambridge, Massachusetts, 1984, pp. 783–799.

[107] R. Ortega, A. Loria, and R. Kelly, "A semiglobally stable output feedback pid regulator for robot manipulator, automatic control," *IEEE Transaction August*, vol. 40, 1995.

[108] R. Kelly, "Global positioning of robot manipulators via pd control plus a class of nonlinear integral actions," *IEEE Transactions on Automatic Control*, vol. 43, no. 7, pp. 934–938, 1998.

[109] S. Arimoto, "A quasi-natural potential and its role in design of hyper-stable pid servo-loop for robotic systems," in *Proc. of CAI Pacific Symposium'94 on Control and Industrial Automation Applications*, 1994, pp. 110–117.

[110] P. Rocco, "Stability of pid control for industrial robot arms," *IEEE transactions on robotics and automation*, vol. 12, no. 4, pp. 606–614, 1996.

[111] S. Islam and P. X. Liu, "Pd output feedback control design for industrial robotic manipulators," *IEEE/ASME Transactions on mechatronics*, vol. 16, no. 1, pp. 187–197, 2010.

[112] P. B. Sistu and B. W. Bequette, "Nonlinear predictive control of uncertain processes: Application to a cstr," *AIChE Journal*, vol. 37, no. 11, pp. 1711–1723, 1991.

[113] E. M. Wolff, U. Topcu, and R. M. Murray, "Robust control of uncertain markov decision processes with temporal logic specifications," in *2012 IEEE 51st IEEE Conference on Decision and Control (CDC)*. IEEE, 2012, pp. 3372–3379.

[114] W. Burger, E. Dean-Leon, and G. Cheng, "Robust second order sliding mode control for 6d position based visual servoing with a redundant mobile manipulator," in *2015 IEEE-RAS 15th International Conference on Humanoid Robots (Humanoids)*. IEEE, 2015, pp. 1127–1132.

[115] E. Zakeri, S. Farahat, S. A. Moezi, and A. Zare, "Robust sliding mode control of a mini unmanned underwater vehicle equipped with a new arrangement of water jet propulsions: Simulation and experimental study," *Applied Ocean Research*, vol. 59, pp. 521–542, 2016.

[116] C.-B. Feng, T.-P. Zhang, and Y.-Q. Wu, "Fuzzy sliding mode control for uncertain dynamic systems via output feedback," *IFAC Proceedings Volumes*, vol. 29, no. 1, pp. 3496–3501, 1996, 13th World Congress of IFAC, 1996, San Francisco USA, 30 June–5 July. [Online]. Available: http://www.sciencedirect.com/science/article/pii/S1474667017582191

[117] J. Liu and X. Wang, *Advanced sliding mode control for mechanical systems*. Springer, 2012.

[118] N. Ullah, S. Han, and M. Khattak, "Adaptive fuzzy fractional-order sliding mode controller for a class of dynamical systems with uncertainty," *Transactions of the Institute of Measurement and Control*, vol. 38, no. 4, pp. 402–413, 2016.

[119] G. Bartolini, A. Pisano, E. Punta, and E. Usai, "A survey of applications of second-order sliding mode control to mechanical systems," *International Journal of control*, vol. 76, no. 9-10, pp. 875–892, 2003.

[120] W.-C. Su, S. V. Drakunov, and U. Ozguner, "An o (t/sup 2/) boundary layer in sliding

mode for sampled-data systems," *IEEE Transactions on Automatic Control*, vol. 45, no. 3, pp. 482–485, 2000.

[121] W. Wang and J. Lee, "Hitting time reduction and chattering attenuation in multiinput variable-structure systems," pp. 491–499, 1993.

[122] D. Zhang and S. Panda, "Chattering-free and fast-response sliding mode controller," *IEE Proceedings-Control Theory and Applications*, vol. 146, no. 2, pp. 171–177, 1999.

[123] H. Du, X. Yu, M. Z. Chen, and S. Li, "Chattering-free discrete-time sliding mode control," *Automatica*, vol. 68, pp. 87–91, 2016.

[124] G. F. Franklin, J. D. Powell, and M. L. Workman, "Digital control of dynamic systems, 1990," *Addison and Wesley*.

[125] L. Fridman, Y. Shtessel, C. Edwards, and X.-G. Yan, "Higher-order sliding-mode observer for state estimation and input reconstruction in nonlinear systems," *International Journal of Robust and Nonlinear Control: IFAC-Affiliated Journal*, vol. 18, no. 4-5, pp. 399–412, 2008.

[126] Y. B. Shtessel, I. A. Shkolnikov, and M. D. Brown, "An asymptotic second-order smooth sliding mode control," *Asian journal of control*, vol. 5, no. 4, pp. 498–504, 2003.

[127] A. Levant, "Higher order sliding modes and arbitrary-order exact robust differentiation," in *2001 European Control Conference (ECC)*, 2001, pp. 996–1001.

[128] M. Zhihong, A. P. Paplinski, and H. R. Wu, "A robust mimo terminal sliding mode control scheme for rigid robotic manipulators," *IEEE transactions on automatic control*, vol. 39, no. 12, pp. 2464–2469, 1994.

[129] X. Yu and Z. Man, "Model reference adaptive control systems with terminal sliding modes," *International Journal of Control*, vol. 64, no. 6, pp. 1165–1176, 1996.

[130] A. Isidori, "A tool for semi-global stabilization of uncertain non-minimum-phase nonlinear systems via output feedback," *IEEE transactions on automatic control*, vol. 45, no. 10, pp. 1817–1827, 2000.

[131] S. V. Emel'yanov, S. K. Korovin, and L. Levantovskii, "Higher-order sliding regimes in binary control systems," in *Doklady Akademii Nauk*, vol. 287, no. 6. Russian Academy of Sciences, 1986, pp. 1338–1342.

[132] J.-J. E. Slotine, W. Li *et al.*, *Applied nonlinear control*. Prentice hall Englewood Cliffs, NJ, 1991, vol. 199, no. 1.

[133] J.-J. E. Slotine, "Sliding controller design for non-linear systems," *International Journal of control*, vol. 40, no. 2, pp. 421–434, 1984.

[134] K. S. Yeung and Y. P. Chen, "A new controller design for manipulators using the theory of variable structure systems," *IEEE Transactions on Automatic Control*, vol. 33, no. 2, pp. 200–206, 1988.

[135] G.-C. Hwang and S.-C. Lin, "A stability approach to fuzzy control design for nonlinear systems," *Fuzzy sets and Systems*, vol. 48, no. 3, pp. 279–287, 1992.

[136] J. Y. Hung, W. Gao, and J. C. Hung, "Variable structure control: A survey," *IEEE transactions on industrial electronics*, vol. 40, no. 1, pp. 2–22, 1993.

[137] X. Yu, B. Wang, and X. Li, "Computer-controlled variable structure systems: The state-of-the-art," *IEEE Transactions on Industrial Informatics*, vol. 8, no. 2, pp. 197–205, 2011.

[138] B. Draženović, "The invariance conditions in variable structure systems," *Automatica*, vol. 5, no. 3, pp. 287–295, 1969.

[139] S. P. Bhat and D. S. Bernstein, "Finite-time stability of continuous autonomous systems," *SIAM Journal on Control and Optimization*, vol. 38, no. 3, pp. 751–766, 2000.

[140] R. G. Brown, P. Y. Hwang *et al.*, *Introduction to random signals and applied Kalman filtering*. Wiley New York, 1992, vol. 3.

[141] A. Mohamed and K. Schwarz, "Adaptive kalman filtering for ins/gps," *Journal of geodesy*, vol. 73, no. 4, pp. 193–203, 1999.

[142] L. Ljung, "System identification," *Wiley Encyclopedia of Electrical and Electronics Engineering*, 2001.

[143] K. S. Fu, R. Gonzalez, and C. G. Lee, *Robotics: Control Sensing. Vis.* Tata McGraw-Hill Education, 1987.

[144] J. J. Craig, *Introduction to robotics: mechanics and control, 3/E*. Pearson Education India, 2009.

[145] B. Armstrong, O. Khatib, and J. Burdick, "The explicit dynamic model and inertial parameters of the puma 560 arm," in *Proceedings. 1986 IEEE international conference on robotics and automation*, vol. 3. IEEE, 1986, pp. 510–518.

[146] C. G. Lee, "Robot arm kinematics, dynamics, and control," *Computer*, vol. 15, no. 12, pp. 62–80, 1982.

[147] P. I. Corke and B. Armstrong-Hélouvry, "A meta-study of puma 560 dynamics: A critical appraisal of literature data," *Robotica*, vol. 13, no. 3, pp. 253–258, 1995.

[148] O. Kaynak and A. Denker, "Discrete-time sliding mode control in the presence of system uncertainty," *International Journal of Control*, vol. 57, no. 5, pp. 1177–1189, 1993.

[149] A. Bartoszewicz, "Discrete-time quasi-sliding-mode control strategies," *IEEE Transactions on Industrial Electronics*, vol. 45, no. 4, pp. 633–637, 1998.

[150] N. Bof, R. Carli, and L. Schenato, "Lyapunov theory for discrete time systems," *arXiv preprint arXiv:1809.05289*, 2018.

[151] P. I. Corke and B. Armstrong-Helouvry, "A search for consensus among model parameters reported for the puma 560 robot," in *Proceedings of the 1994 IEEE International Conference on Robotics and Automation*. IEEE, 1994, pp. 1608–1613.